

Kernel Mode Decomposition and programmable/interpretable regression networks

Houman Owhadi* Clint Scovel† Gene Ryan Yoo‡

July 27, 2022

Abstract

Mode decomposition is a prototypical pattern recognition problem that can be addressed from the (a priori distinct) perspectives of numerical approximation, statistical inference and deep learning. Could its analysis through these combined perspectives be used as a Rosetta stone for deciphering mechanisms at play in deep learning? Motivated by this question we introduce programmable and interpretable regression networks for pattern recognition and address mode decomposition as a prototypical problem. The programming of these networks is achieved by assembling elementary modules decomposing and recomposing kernels and data. These elementary steps are repeated across levels of abstraction and interpreted from the equivalent perspectives of optimal recovery, game theory and Gaussian process regression (GPR). The prototypical mode/kernel decomposition module produces an approximation (w_1, w_2, \dots, w_m) of an element $(v_1, v_2, \dots, v_m) \in V_1 \times \dots \times V_m$ of a product of Hilbert subspaces $(V_i, \|\cdot\|_{V_i})$ of a common Hilbert space from the observation of the sum $v := v_1 + \dots + v_m \in V_1 + \dots + V_m$. This approximation is minmax optimal with respect to the relative error in the product norm $\sum_{i=1}^m \|\cdot\|_{V_i}^2$ and obtained as $w_i = Q_i(\sum_j Q_j)^{-1}v = \mathbb{E}[\xi_i | \sum_j \xi_j = v]$ where Q_i and $\xi_i \sim \mathcal{N}(0, Q_i)$ are the covariance operator and the Gaussian process defined by the norm $\|\cdot\|_{V_i}$. The prototypical mode/kernel recomposition module performs partial sums of the recovered modes w_i and covariance operators Q_i based on the alignment between each recovered mode w_i and the data v with respect to the inner product defined by S^{-1} with $S := \sum_i Q_i$ (which has a natural interpretation as model/data alignment $\langle w_i, v \rangle_{S^{-1}} = \mathbb{E}[\langle \xi_i, v \rangle_{S^{-1}}^2]$ and variance decomposition in the GPR setting). We illustrate the proposed framework by programming regression networks approximating the modes $v_i = a_i(t)y_i(\theta_i(t))$ of a (possibly noisy) signal $\sum_i v_i$ when the amplitudes a_i , instantaneous phases θ_i and periodic waveforms y_i may all be unknown and show near machine precision recovery under regularity and separation assumptions on the instantaneous amplitudes a_i and frequencies θ_i . The structure of some of these networks share intriguing similarities with convolutional neural networks while being interpretable, programmable and amenable to theoretical analysis.

*Corresponding author. Caltech, MC 9-94, Pasadena, CA 91125, USA, owhadi@caltech.edu

†Caltech, MC 9-94, Pasadena, CA 91125, USA, clintscovel@gmail.com

‡Caltech, MC 253-37, Pasadena, CA 91125, USA, gyoo@caltech.edu

1 Introduction

The purpose of the *Empirical Mode Decomposition* (EMD) algorithm [16] can be loosely expressed as solving a (usually noiseless) version of the following problem, illustrated in Figure 1.

Problem 1. For $m \in \mathbb{N}^*$, let a_1, \dots, a_m be piecewise smooth functions on $[0, 1]$ and let $\theta_1, \dots, \theta_m$ be strictly increasing functions on $[0, 1]$. Assume that m and the a_i, θ_i are unknown. Given the (possibly noisy) observation of $v(t) = \sum_{i=1}^m a_i(t) \cos(\theta_i(t))$, $t \in [0, 1]$, recover the modes $v_i := a_i(t) \cos(\theta_i(t))$.

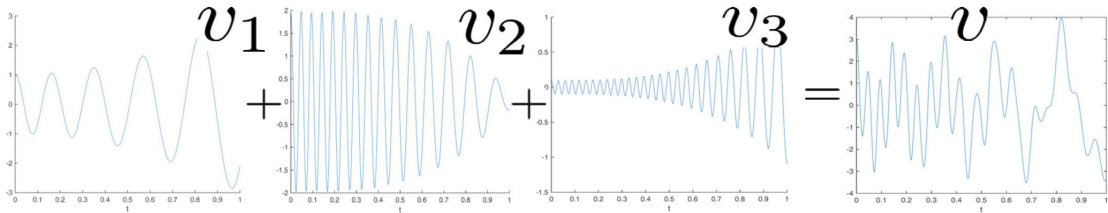


Figure 1: A prototypical mode decomposition problem: given $v = v_1 + v_2 + v_3$ recover v_1, v_2, v_3 .

In practical applications, generally the *instantaneous frequencies* $\omega_i = \frac{d\theta_i}{dt}$ are assumed to be smooth and well separated. Furthermore the ω_i and the *instantaneous amplitudes* are assumed to be varying at a slower rate than the *instantaneous phases* θ_i so that near $\tau \in [0, 1]$ the *intrinsic mode function* v_i can be approximated by a trigonometric function, i.e.

$$v_i(t) \approx a_i(\tau) \cos(\omega_i(\tau)(t - \tau) + \theta_i(\tau)) \text{ for } t \approx \tau. \quad (1.1)$$

The difficulty of analyzing and generalizing the EMD approach and its popularity in practical applications [15] have stimulated the design of alternative methods aimed at solving Problem 1. Methods that are amenable to a greater degree of analysis include synchrosqueezing [3, 20], variational-mode decomposition [4] and non-linear L_1 minimization with sparse time-frequency representations [13, 14].

A Rosetta stone for deep learning? Since Problem 1 can be seen as prototypical pattern recognition problem that can be addressed from the perspectives of numerical approximation, statistical inference and machine learning, one may wonder if its analysis, from the combined approaches of numerical approximation and statistical inference, could be used as a Rosetta stone for deciphering deep learning.

Indeed, although successful industrial applications [19] have consolidated the recognition of artificial neural networks (ANNs) as powerful pattern recognition tools, their

utilization has recently been compared to “operating on an alien technology” [17] due to the challenges brought by a lag in theoretical understanding: (1) because ANNs are not easily interpretable the resulting models may not be interpretable (and identifying causes of success or failure may be challenging) (2) because ANNs rely on the resolution of non-convex (possibly stochastic) optimization problems, they are not easily amenable to a complete uncertainty quantification analysis (3) because the architecture design of ANNs essentially relies on trial and error, the design of architectures with good generalization properties may involve a significant amount of experimentation.

Since elementary operations performed by ANNs can be interpreted [29] as stacking Gaussian process regression steps with nonlinear thresholding and pooling operations across levels of abstractions, it is natural to wonder whether interpretable Gaussian process regression (GPR) based networks could be conceived for mode decomposition/pattern recognition. Could such networks (1) be programmable based on rational and modular (object oriented) design? (2) be amenable to analysis and convergence results? (3) help our understanding of fundamental mechanisms that might be at play in pattern recognition and thereby help elaborate a rigorous theory for Deep Learning? This paper is an attempt to address these questions, while using mode decomposition [16] as a prototypical pattern recognition problem. As an application of the programmable and interpretable regression networks introduced in this paper, we will also address the following generalization of Problem 1, where the periodic waveforms may all be non-trigonometric, distinct, and unknown and present an algorithm producing near machine precision (10^{-7} to 10^{-4}) recoveries of the modes.

Problem 2. For $m \in \mathbb{N}^*$, let a_1, \dots, a_m be piecewise smooth functions on $[-1, 1]$, let $\theta_1, \dots, \theta_m$ be piecewise smooth functions on $[-1, 1]$ such that the instantaneous frequencies θ_i are strictly positive and well separated, and let y_1, \dots, y_m be square-integrable 2π -periodic functions. Assume that m and the a_i, θ_i, y_i are all unknown. Given the observation $v(t) = \sum_{i=1}^m a_i(t)y_i(\theta_i(t))$ (for $t \in [-1, 1]$) recover the modes $v_i := a_i(t)y_i(\theta_i(t))$.

One fundamental idea is that although Problems 1 and 2 are nonlinear, they can be, to some degree, linearized by recovering the modes v_i as aggregates of sufficiently fine modes living in linear spaces (which, as suggested by the approximation (1.1), can be chosen as linear spans of functions $t \rightarrow \cos(\omega(t - \tau) + \theta)$ windowed around τ , i.e. Gabor wavelets). The first part of the resulting network recovers those finer modes through a linear optimal recovery operation. Its second part recovers the modes v_i through a hierarchy of (linear) aggregation steps sandwiched between (nonlinear) ancestor/descendant identification steps. These identification steps are obtained by composing the alignments between v and the aggregates of the fine modes with simple and interpretable nonlinearities (such as thresholding, graph-cuts, etc...), as presented in Section 3.

2 The mode decomposition problem

To begin the general (abstract) formulation of the *mode decomposition problem*, let V be a separable Hilbert space with inner product $\langle \cdot, \cdot \rangle$ and corresponding norm $\|\cdot\|$. Also

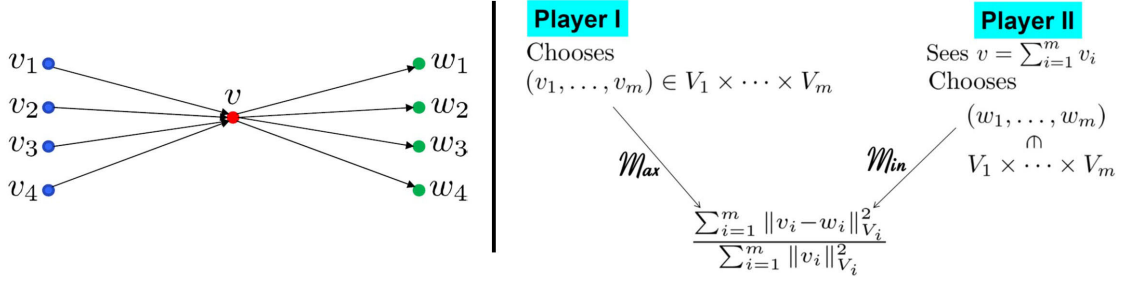


Figure 2: Left: The mode decomposition problem. Right: The game theoretic approach.

let \mathcal{I} be a finite set of indices and let $(V_i)_{i \in \mathcal{I}}$ be linear subspaces $V_i \subset V$ such that

$$V = \sum_{i \in \mathcal{I}} V_i. \quad (2.1)$$

The mode decomposition problem can be informally formulated as follows

Problem 3. *Given $v \in V$ recover $v_i \in V_i, i \in \mathcal{I}$, such that $v = \sum_{i \in \mathcal{I}} v_i$.*

Our solution to Problem 3 will use the interface between numerical approximation, inference and learning (as presented in [26, 27]), which although traditionally seen as entirely separate subjects, are intimately connected through the common purpose of making estimations with partial information [27]. Since the study of this interface has been shown to help automate the process of discovery in numerical analysis and the design of fast solvers [25, 26, 32], this paper is also motivated by the idea it might, in a similar manner and to some degree, also help the process of discovery in machine learning. Here, these interplays will be exploited to address the general formulation 3 of the mode recovery problem from the three perspectives of optimal recovery, game theory and Gaussian process regression. The corresponding minmax recovery framework (illustrated in Figure 2 and presented below) will then be used as a building block for the proposed programmable networks.

2.1 Optimal recovery setting

Problem 3 is ill-posed if the subspaces $(V_i)_{i \in \mathcal{I}}$ are not linearly independent, in the sense that such a recovery will not be unique. Nevertheless, optimal solutions can be defined in the optimal recovery setting of Micchelli and Rivlin [24]. To this end, let $\|\cdot\|_{\mathcal{B}}$ be a quadratic norm on the product space

$$\mathcal{B} = \prod_{i \in \mathcal{I}} V_i, \quad (2.2)$$

making \mathcal{B} a Hilbert space, and let

$$\Phi : \mathcal{B} \rightarrow V$$

be the information map defined by

$$\Phi(u) := \sum_{i \in \mathcal{I}} u_i, \quad u = (u_i)_{i \in \mathcal{I}} \in \mathcal{B}. \quad (2.3)$$

An optimal recovery solution mapping

$$\Psi : V \rightarrow \mathcal{B}$$

for the mode decomposition problem is defined as follows: for given $v \in V$, we define $\Psi(v)$ to be the minimizer of

$$\min_{w \in \mathcal{B} | \Phi(w) = v} \max_{u \in \mathcal{B} | \Phi(u) = v} \frac{\|u - w\|_{\mathcal{B}}}{\|u\|_{\mathcal{B}}}. \quad (2.4)$$

Lemma 2.1. *Let $\Phi : \mathcal{B} \rightarrow V$ be surjective. For $v \in V$, the solution w of the convex optimization problem*

$$\begin{cases} \text{Minimize } \|w\|_{\mathcal{B}} \\ \text{Subject to } w \in \mathcal{B} \text{ and } \Phi(w) = v. \end{cases} \quad (2.5)$$

determines the unique optimal minmax solution $w = \Psi(v)$ to (2.4). Moreover,

$$\Psi(v) = \Phi^- v,$$

where the Moore-Penrose inverse $\Phi^- : V \rightarrow \mathcal{B}$ of Φ is defined by

$$\Phi^- := \Phi^T (\Phi \Phi^T)^{-1}.$$

Now let us be more specific about the structure of \mathcal{B} that we will assume. Indeed, let the subspaces $(V_i)_{i \in \mathcal{I}}$ be equipped with quadratic norms $(\|\cdot\|_{V_i})_{i \in \mathcal{I}}$ making each

$$(V_i, \|\cdot\|_{V_i})$$

a Hilbert space, and equip their product $\mathcal{B} = \prod_{i \in \mathcal{I}} V_i$ with the product norm

$$\|u\|_{\mathcal{B}}^2 := \sum_{i \in \mathcal{I}} \|u_i\|_{V_i}^2, \quad u = (u_i)_{i \in \mathcal{I}} \in \mathcal{B}. \quad (2.6)$$

We use the notation $[\cdot, \cdot]$ for the duality product between V^* on the left and V on the right, and also for the duality product between V_i^* and V_i for all i . The norm $\|\cdot\|_{V_i}$ makes V_i into a Hilbert space if and only if

$$\|v_i\|_{V_i}^2 = [Q_i^{-1} v_i, v_i], \quad v_i \in V_i, \quad (2.7)$$

for some positive symmetric linear bijection

$$Q_i : V_i^* \rightarrow V_i,$$

where by positive and symmetric we mean $[\phi, Q_i\phi] \geq 0$ and $[\phi, Q_i\varphi] = [\varphi, Q_i\phi]$ for all $\varphi, \phi \in V_i^*$. For each $i \in \mathcal{I}$, the dual space V_i^* to $(V_i, \|\cdot\|_{V_i})$ is also a Hilbert space with norm

$$\|\phi_i\|_{V_i^*}^2 := [\phi_i, Q_i\phi_i], \quad \phi_i \in V_i^*, \quad (2.8)$$

and therefore the dual space \mathcal{B}^* of \mathcal{B} can be identified with the product of the dual spaces

$$\mathcal{B}^* = \prod_{i \in \mathcal{I}} V_i^* \quad (2.9)$$

with (product) duality product

$$[\phi, u] = \sum_{i \in \mathcal{I}} [\phi_i, u_i], \quad \phi = (\phi_i)_{i \in \mathcal{I}} \in \mathcal{B}^*, \quad u = (u_i)_{i \in \mathcal{I}} \in \mathcal{B}, \quad (2.10)$$

and that the symmetric positive linear bijection

$$Q : \mathcal{B}^* \rightarrow \mathcal{B} \quad (2.11)$$

defining the quadratic norm $\|\cdot\|_{\mathcal{B}}$ is the block-diagonal operator

$$Q := \text{diag}(Q_i)_{i \in \mathcal{I}}$$

defined by its action $Q\phi = (Q_i\phi_i)_{i \in \mathcal{I}}$, $\phi \in \mathcal{B}^*$.

Let

$$e_i : V_i \rightarrow V$$

be the subset inclusion and let its adjoint

$$e_i^* : V^* \rightarrow V_i^*$$

be defined through $[e_i^*\phi, v_i] = [\phi, e_iv_i]$ for $\phi \in V^*$, $v_i \in V_i$. These operations naturally transform the family of operators

$$Q_i : V_i^* \rightarrow V_i, \quad i \in \mathcal{I},$$

into a family of operators

$$e_i Q_i e_i^* : V^* \rightarrow V, \quad i \in \mathcal{I},$$

all defined on the same space, so that we can define their sum $S : V^* \rightarrow V$ by

$$S = \sum_{i \in \mathcal{I}} e_i Q_i e_i^*. \quad (2.12)$$

The following proposition demonstrates that S is invertible and that S^{-1} and S naturally generate dual Hilbert space norms on V and V^* respectively.

Lemma 2.2. *The operator $S : V^* \rightarrow V$, defined in (2.12), is invertible. Moreover,*

$$\|v\|_{S^{-1}}^2 := [S^{-1}v, v], \quad v \in V, \quad (2.13)$$

defines a Hilbert space norm on V and

$$\|\phi\|_S^2 := [\phi, S\phi] = \sum_{i \in \mathcal{I}} \|e_i^* \phi\|_{V_i^*}^2, \quad \phi \in V^*. \quad (2.14)$$

defines a Hilbert space norm on V^ which is dual to that on V .*

The following theorem determines the optimal recovery map Ψ .

Theorem 2.3. *For $v \in V$, the minimizer of (2.5) and therefore the minmax solution of (2.4) is*

$$\Psi(v) = (Q_i e_i^* S^{-1}v)_{i \in \mathcal{I}}. \quad (2.15)$$

Furthermore

$$\Phi(\Psi(v)) = v, \quad v \in V,$$

and

$$\Psi : (V, \|\cdot\|_{S^{-1}}) \rightarrow (\mathcal{B}, \|\cdot\|_{\mathcal{B}})$$

and

$$\Phi^* : (V^*, \|\cdot\|_S) \rightarrow (\mathcal{B}^*, \|\cdot\|_{\mathcal{B}^*})$$

are isometries. In particular, writing $\Psi_i(v) := Q_i e_i^ S^{-1}v$, we have*

$$\|v\|_{S^{-1}}^2 = \|\Psi(v)\|_{\mathcal{B}}^2 = \sum_{i \in \mathcal{I}} \|\Psi_i(v)\|_{V_i}^2 \quad v \in V. \quad (2.16)$$

Observe that the adjoint

$$\Phi^* : V^* \rightarrow \mathcal{B}^*$$

of $\Phi : \mathcal{B} \rightarrow V$, defined by $[\varphi, \Phi(u)] = [\Phi^*(\varphi), u]$ for $\varphi \in V^*$ and $u \in \mathcal{B}$, is computed to be

$$\Phi^*(\varphi) = (e_i^* \varphi)_{i \in \mathcal{I}}, \quad \varphi \in V^*. \quad (2.17)$$

The following theorem presents optimality results in terms of Φ^* .

Theorem 2.4. *We have*

$$\|u - \Psi(\Phi(u))\|_{\mathcal{B}}^2 = \inf_{\phi \in V^*} \|u - Q\Phi^*(\phi)\|_{\mathcal{B}}^2 = \inf_{\phi \in V^*} \sum_{i \in \mathcal{I}} \|u_i - Q_i e_i^* \phi\|_{V_i}^2. \quad (2.18)$$

2.2 Game/decision theoretic setting

Optimal solutions to Problem 3 can also be defined in the setting of the game/decision theoretic approach to numerical approximation presented in [26]. In this setting the minmax problem (2.4) is interpreted as an adversarial zero sum game (illustrated in Figure 2) between two players and lifted to mixed strategies to identify a saddle point. Let $\mathcal{P}_2(\mathcal{B})$ be the set of Borel probability measures μ on \mathcal{B} such that $\mathbb{E}_{u \sim \mu}[\|u\|_{\mathcal{B}}^2] < \infty$, and let $L(V, \mathcal{B})$ be the set of Borel measurable functions $\psi : V \rightarrow \mathcal{B}$. Let $\mathcal{E} : \mathcal{P}_2(\mathcal{B}) \times L(V, \mathcal{B}) \rightarrow \mathbb{R}$ be the loss function defined by

$$\mathcal{E}(\mu, \psi) = \frac{\mathbb{E}_{u \sim \mu}[\|u - \psi(\Phi(u))\|_{\mathcal{B}}^2]}{\mathbb{E}_{u \sim \mu}[\|u\|_{\mathcal{B}}^2]}, \quad \mu \in \mathcal{P}_2(\mathcal{B}), \psi \in L(V, \mathcal{B}). \quad (2.19)$$

Let us also recall the more general notion of a Gaussian field as described in [26, Chap. 17]. To that end, a Gaussian space \mathbf{H} is a linear subspace $\mathbf{H} \subset L^2(\Omega, \Sigma, \mathbb{P})$ of the L^2 space of a probability space consisting of centered Gaussian random variables. A centered Gaussian field ξ on \mathcal{B} with covariance operator $Q : \mathcal{B}^* \rightarrow \mathcal{B}$, written $\xi \sim \mathcal{N}(0, Q)$, is an isometry

$$\xi : \mathcal{B}^* \rightarrow \mathbf{H}$$

from \mathcal{B}^* to a Gaussian space \mathbf{H} , in that

$$[\phi, \xi] \sim \mathcal{N}(0, [\phi, Q\phi]), \quad \phi \in \mathcal{B}^*,$$

where we use the notation $[\phi, \xi]$ to denote the action $\xi(\phi)$ of ξ on the element $\phi \in \mathcal{B}^*$, thus indicating that ξ is a weak \mathcal{B} -valued Gaussian random variable. As discussed in [26, Chap. 17], there is a one to one correspondence between Gaussian cylinder measures and Gaussian fields¹. Let ξ denote the Gaussian field

$$\xi \sim \mathcal{N}(0, Q)$$

on \mathcal{B} where $Q : \mathcal{B}^* \rightarrow \mathcal{B}$ is the block diagonal operator $Q := \text{diag}(Q_i)_{i \in \mathcal{I}}$. Theorem 2.5 shows that the optimal strategy of Player I is the Gaussian field $\xi - \mathbb{E}[\xi|\Phi(\xi)]$ and the optimal strategy of Player II is the conditional expectation

$$\Psi(v) = \mathbb{E}[\xi|\Phi(\xi) = v], \quad (2.20)$$

that is also equal to (2.15). Write μ^\dagger for the cylinder measure defined by the Gaussian field $\xi - \mathbb{E}[\xi|\Phi(\xi)]$, or the corresponding Gaussian measure in finite dimensions.

¹ The *cylinder sets* of \mathcal{B} consists of all sets of the form $F^{-1}(B)$ where $B \in \mathbb{R}^n$ is a Borel set and $F : \mathcal{B} \rightarrow \mathbb{R}^n$ is a continuous linear map, over all integers n . A *cylinder measure* μ , see also [26, Chap. 17], on \mathcal{B} , is a collection of measures μ_F indexed by $F : \mathcal{B} \rightarrow \mathbb{R}^n$ over all n such that each μ_F is a Borel measure on \mathbb{R}^n and such that for $F_1 : \mathcal{B} \rightarrow \mathbb{R}^{n_1}$ and $F_2 : \mathcal{B} \rightarrow \mathbb{R}^{n_2}$ and $G : \mathbb{R}^{n_1} \rightarrow \mathbb{R}^{n_2}$ linear and continuous with $F_2 = GF_1$, we have $G_*\mu_{F_1} = \mu_{F_2}$, where G_* is the pushforward operator on measures corresponding to the map G , defined by $(G_*\nu)(B) := \nu(G^{-1}B)$. When each measure μ_F is Gaussian, the cylinder measure is said to be a Gaussian cylinder measure. A sequence μ_n of cylinder measures such that the sequence $(\mu_n)_F$ converges in the weak topology for each F , is said to converge in the *weak cylinder measure topology*.

We say that a tuple (μ', ψ') is a saddle point of the loss function $\mathcal{E} : \mathcal{P}_2(\mathcal{B}) \times L(V, \mathcal{B}) \rightarrow \mathbb{R}$ if

$$\mathcal{E}(\mu, \psi') \leq \mathcal{E}(\mu', \psi') \leq \mathcal{E}(\mu', \psi), \quad \mu \in \mathcal{P}_2(\mathcal{B}), \quad \psi \in L(V, \mathcal{B}).$$

Theorem 2.5. *Let \mathcal{E} be defined as in (2.19). It holds true that*

$$\max_{\mu \in \mathcal{P}_2(\mathcal{B})} \min_{\psi \in L(V, \mathcal{B})} \mathcal{E}(\mu, \psi) = \min_{\psi \in L(V, \mathcal{B})} \max_{\mu \in \mathcal{P}_2(\mathcal{B})} \mathcal{E}(\mu, \psi). \quad (2.21)$$

Furthermore,

- If $\dim(V) < \infty$ then (μ^\dagger, Ψ) is a saddle point for the loss (2.19), where Ψ is as in (2.15) and (2.20).
- If $\dim(V) = \infty$, then the loss (2.19) admits a sequence of saddle points $(\mu_n, \Psi) \in \mathcal{P}_2(\mathcal{B}) \times L(V, \mathcal{B})$ where Ψ is as in (2.15) and (2.20), and the μ_n are Gaussian measures, with finite dimensional support, converging towards μ^\dagger in the weak cylinder measure topology.

Proof. The proof is similar to that of [26, Thm. 18.2] □

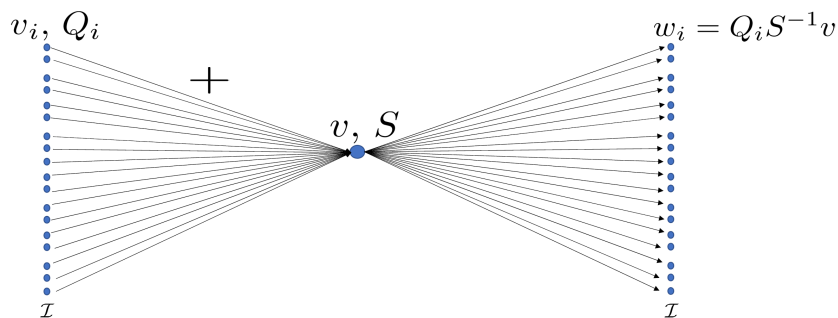


Figure 3: The minmax solution of the mode decomposition problem.

2.3 Gaussian process regression setting

It follows from Theorem 2.5 that the minmax optimal solution to Problem 3 with loss measured as the relative error in the norm (2.6) can be obtained via Gaussian process regression as follows. For $i \in \mathcal{I}$, let $\xi_i \sim \mathcal{N}(0, Q_i)$ be independent V_i -valued Gaussian fields defined by the norms $\|\cdot\|_{V_i}$. Recall that Q_i is defined in (2.7) and that ξ_i is an isometry from $(V_i^*, \|\cdot\|_{V_i^*})$ onto a Gaussian space mapping $\phi \in V_i^*$ to $[\phi, \xi_i] \sim \mathcal{N}(0, [\phi, Q_i \phi])$. Theorem 2.5 asserts that the minmax estimator is (2.20), which, written componentwise, makes the optimal reconstruction of each mode v_j of $v = \sum_{i \in \mathcal{I}} v_i$ to be

$$\mathbb{E}[\xi_j | \sum_{i \in \mathcal{I}} \xi_i = v] = Q_j (\sum_{i \in \mathcal{I}} Q_i)^{-1} v. \quad (2.22)$$

where the right hand side of (2.22) is obtained from (2.15) and $\sum_{i \in \mathcal{I}} Q_i$ is a shorthand notation for $\sum_i e_i Q_i e_i^*$ obtained by dropping the indications of the injections e_i and their adjoint projections e_i^* . From now on, we will use such simplified notations whenever there is no risk of confusion. In summary, the minmax the minmax solution of the abstract mode decomposition problem is obtained as illustrated in Figure 3 based on the specification of the operators $Q_i : V_i^* \rightarrow V_i$ which can be interpreted as quadratic norm defining operators or as covariance operators. Table 1 illustrates the three equivalent interpretations -optimal recovery/operator kernel/Gaussian process regression of our methodology.

Norm	Operator/Kernel	GP
$\ v_i\ _{V_i}^2 := \langle Q_i^{-1} v_i, v_i \rangle$	$Q_i : V_i^* \rightarrow V_i$	$\xi_i \sim \mathcal{N}(0, Q_i)$
$\arg \min \left\{ \begin{array}{l} \text{minimize } \sum_i \ w_i\ _{V_i}^2 \\ \sum_i w_i = v \end{array} \right.$	$Q_i (\sum_j Q_j)^{-1} v$	$\mathbb{E}[\xi_i \mid \sum_j \xi_j = v]$

Table 1: Three equivalent interpretations -optimal recovery/operator kernel/Gaussian process regression of our methodology.

Example 2.6. Consider the problem of recovering the modes v_1, v_2, v_3, v_4 from the observation of the signal $v = v_1 + v_2 + v_3 + v_4$ illustrated in Fig. 4. In this example all modes are defined on the interval $[0, 1]$, $v_1(t) = (1 + 2t^2) \cos(\theta_1(t)) - 0.5t \sin(\theta_1(t))$, $v_2(t) = 2(1 - t^3) \cos(\theta_2(t)) + (-t + 0.5t^2) \sin(\theta_2(t))$, $v_3(t) = 2 + t - 0.2t^2$, and v_4 is white-noise (the instantiation of a centered GP with covariance function $\delta(s - t)$). $\theta_1(t) = \int_0^t \omega_1(s) ds$ and $\theta_2(t) = \int_0^t \omega_2(s) ds$ are defined by the instantaneous frequencies $\omega_1(t) = 16\pi(1 + t)$ and $\omega_2(t) = 30\pi(1 + t^2/2)$. In this recovery problem $\omega_1(t)$ and $\omega_2(t)$ are known, v_3 and the amplitudes of the oscillations of v_1, v_2 are unknown smooth functions of time, only the distribution of v_4 is known. To define optimal recovery solutions one can either define the normed subspaces $(V_i, \|\cdot\|_{V_i})$ or (equivalently via (2.7)) define the covariance functions/operators of the Gaussian Processes ξ_i . In this example it is simpler to use the latter. To define the covariance function of the GP ξ_1 we assume that $\xi_1(t) = \zeta_{1,c}(t) \cos(\theta_1(t)) + \zeta_{1,s}(t) \sin(\theta_1(t))$, where $\zeta_{1,c}$ and $\zeta_{1,s}$ are independent identically distributed centered Gaussian processes with covariance function $\mathbb{E}[\zeta_{1,c}(s)\zeta_{1,c}(t)] = \mathbb{E}[\zeta_{1,s}(s)\zeta_{1,s}(t)] = e^{-\frac{(s-t)^2}{\gamma^2}}$ (chosen with $\gamma = 0.2$ as a prior regularity assumption). Note that under this choice ξ_1 is a centered GP with covariance function $K_1(s, t) = e^{-\frac{(s-t)^2}{\gamma^2}} (\cos(\theta_1(s)) \cos(\theta_1(t)) + \sin(\theta_1(s)) \sin(\theta_1(t)))$. Note that the trigonometric identities $\cos(a+b) = \cos a \cos b - \sin a \sin b$ and $\sin(a+b) = \sin a \cos b + \cos a \sin b$ imply that translating θ_1 by an arbitrary phase b leaves K_1 invariant (knowing θ_1 up to a phase shift is sufficient to construct that kernel). Similarly we select the covariance func-

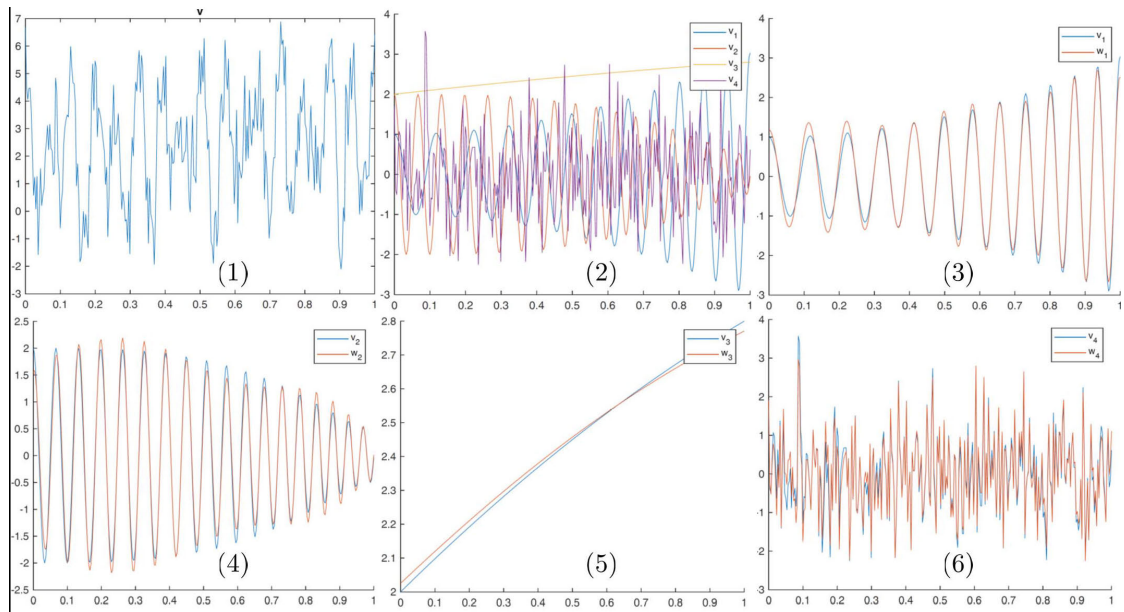


Figure 4: (1) The signal $v = v_1 + v_2 + v_3 + v_4$ (2) The modes v_1, v_2, v_3, v_4 (3) v_1 and its approximation w_1 (4) v_2 and its approximation w_2 (5) v_3 and its approximation w_3 (6) v_4 and its approximation w_4 .

tion of the independent centered GP ξ_2 to be $K_2(s, t) = e^{-\frac{(s-t)^2}{\gamma^2}} (\cos(\theta_2(s)) \cos(\theta_2(t)) + \sin(\theta_2(s)) \sin(\theta_2(t)))$. To enforce the regularity of ξ_3 we select its covariance function to be $K_3(s, t) = 1 + st + e^{-\frac{(s-t)^2}{4}}$. Finally since v_4 is white noise we represent it with a centered GP with covariance function $K_4(s, t) = \delta(s - t)$. Fig. 4 shows the recovered modes using (2.22) (or equivalently defined as (2.15) and the minimizer of (2.5)). In this numerical implementation the interval $[0, 1]$ is discretized with 302 points (with uniform time steps between points), ξ_4 is a discretized centered Gaussian vector of dimension 302 and of identity covariance matrix and ξ_1, ξ_2, ξ_3 are discretized as centered Gaussian vectors with covariance matrices corresponding to the kernel matrices $(K(t_i, t_j))_{i,j=1}^{302}$ corresponding to K_1, K_2 and K_3 determined by the sample points $t_i, i = 1, \dots, 302$.

Table 2 provides a summary of the approach of Example 2.6, illustrating the connection between the assumed mode structure and corresponding Gaussian process structure and its corresponding reproducing kernel structure.

On additive models. The recovery approach of Example 2.6 is based on the design of an appropriate additive regression model. Additive regression models are not new. They were introduced in [34] for approximating multivariate functions with sums of uni-

Mode	GP	Kernel
$v_1(t) = a_1(t) \cos(\theta_1(t))$ θ_1 known a_1 unknown smooth	$\xi_1(t) = \zeta_1(t) \cos(\theta_1(t))$ $\mathbb{E}[\zeta_1(s)\zeta_1(t)] = e^{-\frac{ s-t ^2}{\gamma^2}}$	$K_1(s, t) = e^{-\frac{ s-t ^2}{\gamma^2}} \cos(\theta_1(s)) \cos(\theta_1(t))$
$v_2(t) = a_2(t) \cos(\theta_2(t))$ θ_2 known a_2 unknown smooth	$\xi_2(t) = \zeta_2(t) \cos(\theta_2(t))$ $\mathbb{E}[\zeta_2(s)\zeta_2(t)] = e^{-\frac{ s-t ^2}{\gamma^2}}$	$K_2(s, t) = e^{-\frac{ s-t ^2}{\gamma^2}} \cos(\theta_2(s)) \cos(\theta_2(t))$
v_3 unknown smooth	$\mathbb{E}[\xi_3(s)\xi_3(t)] = e^{-\frac{ s-t ^2}{\gamma^2}}$	$K_3(s, t) = e^{-\frac{ s-t ^2}{\gamma^2}}$
v_4 unknown white noise	$\mathbb{E}[\xi_4(s)\xi_4(t)] = \sigma^2\delta(s-t)$	$K_4(s, t) = \sigma^2\delta(s-t)$
$v = v_1 + v_2 + v_3 + v_4$	$\xi = \xi_1 + \xi_2 + \xi_3 + \xi_4$	$K = K_1 + K_2 + K_3 + K_4$

Table 2: A summary of the approach of Example 2.6, illustrating the connection between the assumed mode structure and corresponding Gaussian process structure and its corresponding reproducing kernel structure. Note that, for clarity of presentation, this summary does not exactly match that of Example 2.6.

variate functions. Generalized additive models (GAMs) [11] replace a linear regression model $\sum_i \alpha_i X_i$ with an additive regression model $\sum_i f_i(X_i)$ where the f_i are unspecified (smooth) functions estimated from the data. Since their inception GAMs have become increasingly popular because they are both easy to interpret and easy to fit [30]. This popularity has motivated the introduction of additive Gaussian processes [8, 6] defined as Gaussian processes whose high dimensional covariance kernels are obtained from sums of low dimensional ones (such kernels are expected to overcome the curse of dimensionality by exploiting additive non-local effects when such effects are present [8]). Of course, performing regression or mode decomposition with Gaussian processes (GPs) obtained as sums of independent GPs (i.e. performing kriging with kernels obtained as sums of simpler kernels) is much older since Tikhonov regularization (for signal/noise separation) has a natural interpretation as a conditional expectation $\mathbb{E}[\xi_s | \xi_s + \xi_\sigma]$ where ξ_s is a GP with a smooth prior (for the signal) and ξ_σ is a white noise GP independent from ξ_s . More recent applications include classification [22], source separation [28, 21], and the detection of the periodic part of a function from partial point evaluations [7, 1]. For that latter application, the approach of [7] is to (1) consider the RKHS $(H, \langle \cdot, \cdot \rangle_H)$ defined by a Matérn kernel K (2) interpolate the data with the kernel K and (3) recover the periodic

part by projecting the interpolator (using a projection that is orthogonal with respect to the RKHS scalar product $\langle \cdot, \cdot \rangle_H$) onto $H_p := \text{span}\{\cos(2\pi kt/\lambda), \sin(2\pi kt/\lambda) \mid 1 \leq k \leq q\}$ (the parameters of the Matérn kernel and the period λ are obtained via maximum likelihood estimation). Defining K_p and K_{np} as the kernels induced on H_p and its orthogonal complement in H , we have $K = K_p + K_{np}$ and the recovery (after MLE estimation of the parameters) can also be identified as the conditional expectation of the GP induced by K_p conditioned on the GP induced by $K_p + K_{np}$.

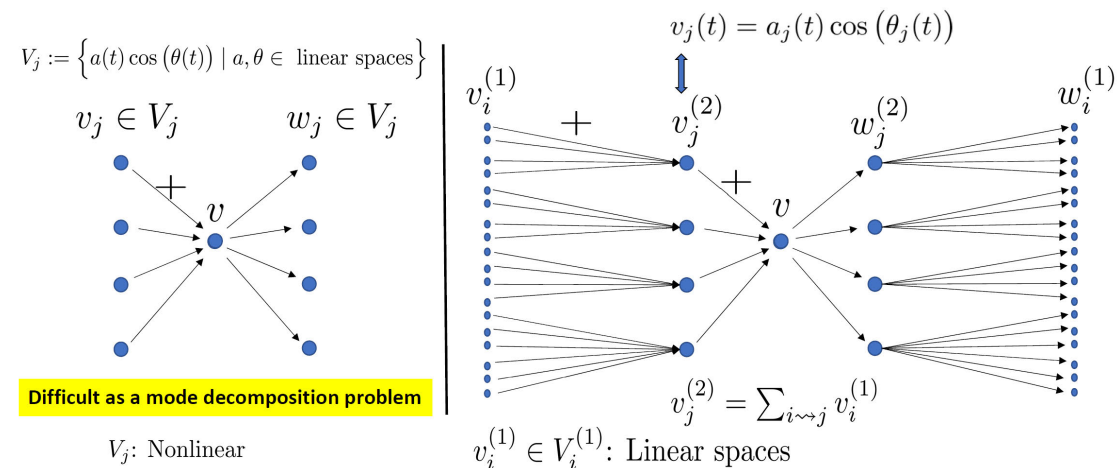


Figure 5: Left: Problem 1 is hard as a mode decomposition problem because the modes $v_j = a_j(t) \cos(\theta_j(t))$ live in non-linear functional spaces. Right: One fundamental idea is to recover those modes as aggregates of finer modes v_i living in linear spaces.

3 Kernel Mode Decomposition Networks

The recovery approach described in Example 2.6 is based on the prior knowledge of (1) the number of quasi-periodic modes (2) their instantaneous frequencies and (3) their base periodic waveform (which need not be a cosine function). In most applications (1) and (2) are not available and the base waveform may not be trigonometric and may not be known. Even when the periodic waveforms are known and trigonometric (as in Problem 1), the recovery of the modes is still significantly harder because, as illustrated in Figure 5, the functional spaces defined by the modes $a_j(t) \cos(\theta_j(t))$ (under regularity assumptions on the a_j and θ_j) are no longer linear spaces and the simple calculus of Section 2 requires the spaces V_j to be linear. One fundamental idea is to recover those modes v_j as aggregates of finer modes v_i living in linear spaces V_i (see Figure 5). For Problem 1 we will identify i with time-frequency-phase triples (τ, ω, θ) and the spaces V_i with one dimensional spaces spanned by functions that are maximally localized in

the time-frequency-phase domain (i.e. by Gabor wavelets as suggested by the approximation (1.1)) and recover the modes $a_j(t) \cos(\theta_j(t))$ by aggregating the finer recovered modes. The implementation of this idea will therefore transform the nonlinear mode

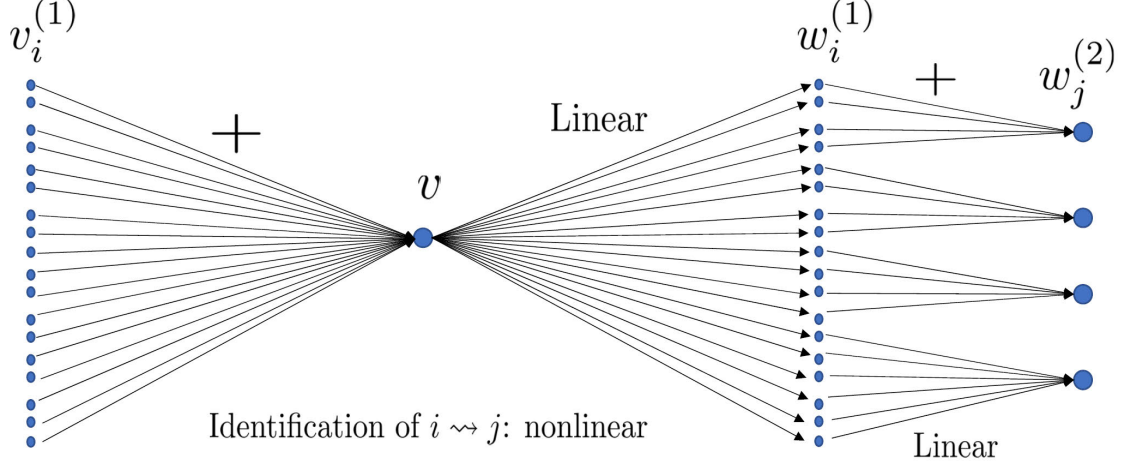


Figure 6: Mode decomposition/recomposition problem.

decomposition problem illustrated on the left hand side of Figure 5 into the mode decomposition/recomposition problem illustrated in Figure 6 and transfer its nonlinearity to the identification of ancestor/descendant relationships $i \rightsquigarrow j$.

To identify these ancestor/descendant relations we will compute the energy $E(i) := \|w_i\|_{V_i}^2$ for each recovered mode w_i , which as illustrated in Figure 7 and discussed in Section 3.1, can also be identify as the alignment $\langle w_i, v \rangle_{S^{-1}}$ between recovered mode w_i and the signal v or as the alignment $\mathbb{E}[\text{Var}[\langle \xi_i, v \rangle_{S^{-1}}]]$ between the model ξ_i and the data v . Furthermore E satisfy an energy preservation identity $\sum_i E(i) = \|v\|_{S^{-1}}^2 =$ which leads to its variance decomposition interpretation. Although alignment calculations are linear, the calculations of the resulting child-ancestor relations may involve a nonlinearity (such as thresholding, graph-cut, computation of a maximizer) and the resulting network can be seen as a sequence of sandwiched linear operations and simple non-linear steps having striking similarities with artificial neural networks.

Of course this strategy can be repeated across levels of abstractions and its complete deployment will also require the generalization of the setting of Section 2 (illustrated in Figure 3) to a hierarchical setting (illustrated in Figure 10 and described in Section 3.3).

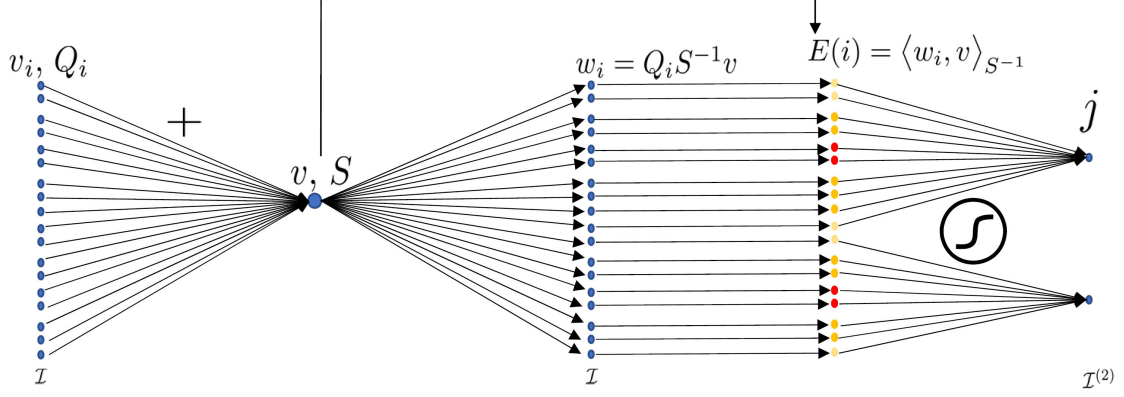


Figure 7: Derivation of ancestor/descendant relations from energy calculations.

3.1 Model/data alignment and energy/variance decomposition

Using the setting and notations of Section 2 and fixing the observed data $v \in V$, let $E : \mathcal{I} \rightarrow \mathbb{R}_+$ be the function defined by

$$E(i) := \|\Psi_i(v)\|_{V_i}^2, \quad i \in \mathcal{I}. \quad (3.1)$$

We will refer to $E(i)$ as the energy of the mode i in reference to its numerical analysis interpretation (motivated by $E(i) = [Q_i^{-1}\Psi_i(v), \Psi_i(v)]$ and the interpretation of Q_i^{-1} as an elliptic operator) and our general approach will be based on using its local and/or global maximizers to decompose/recompose kernels.

Writing $E_{\text{tot}} := \|v\|_{S^{-1}}^2$, note that (2.16) implies that

$$E_{\text{tot}} = \sum_{i \in \mathcal{I}} E(i). \quad (3.2)$$

Let $\langle \cdot, \cdot \rangle_{S^{-1}}$ be the scalar product on V defined by the norm $\|\cdot\|_{S^{-1}}$. Let $\xi \sim \mathcal{N}(0, Q)$ and let $\phi = S^{-1}v$.

Proposition 3.1. *It holds true that for $i \in \mathcal{I}$,*

$$E(i) = \langle \Psi_i(v), v \rangle_{S^{-1}} = \text{Var}([\phi, \xi_i]) = \text{Var}(\langle \xi_i, v \rangle_{S^{-1}}). \quad (3.3)$$

Observe that $E(i) = \text{Var}(\langle \xi_i, v \rangle_{S^{-1}})$ implies that $E(i)$ is a measure of the alignment between the Gaussian process (GP) model ξ_i and the data v in V and (3.2) corresponds to the variance decomposition

$$\text{Var}(\langle \sum_{i \in \mathcal{I}} \xi_i, v \rangle_{S^{-1}}) = \sum_{i \in \mathcal{I}} \text{Var}(\langle \xi_i, v \rangle_{S^{-1}}). \quad (3.4)$$

Therefore, the stronger this alignment $E(i)$ is, the better the model ξ_i is at explaining/representing the data. Consequently, we refer to the energy $E(i)$ as the *alignment energy*. Observe also that the identity $E(i) = \langle w_i, v \rangle_{S^{-1}}$ with $w_i = \Psi_i(v)$ implies that $E(i)$ is also a measure of the alignment between the optimal approximation w_i of v_i and the signal v . Table 3 illustrates the relations between the conservation of alignment energies and the variance decomposition derived from Theorem 2.3 and Proposition 3.1.

	Norm	Operator/Kernel	GP
$E(i)$	$\ \Psi_i(v)\ _{V_i}^2 = \langle \Psi_i(v), v \rangle_{S^{-1}}$	$[S^{-1}v, Q_i S^{-1}v]$	$\text{Var}(\langle \xi_i, v \rangle_{S^{-1}})$
$\sum_i E(i)$	$\ v\ _{S^{-1}}^2$	$[S^{-1}v, v]$	$\text{Var}(\langle \sum_i \xi_i, v \rangle_{S^{-1}})$

Table 3: Identities for $E(i)$ and $\sum_i E(i)$

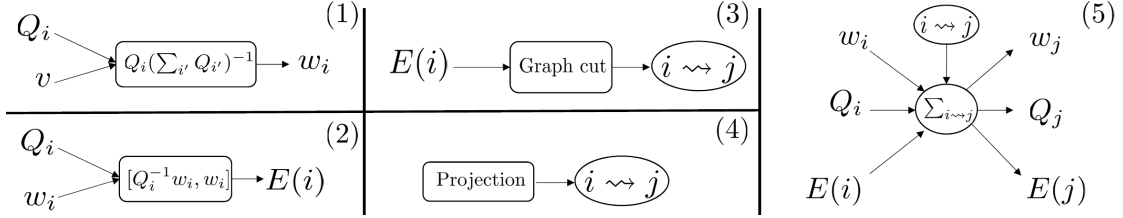


Figure 8: Elementary programming modules for Kernel Mode Decomposition.

3.2 Programming modules and feedforward network

We will now combine the alignment energies of Section 3.1 with the mode decomposition approach of Section 2 to design elementary programming modules (illustrated in Figure 8) for kernel mode decomposition networks (KMDNets). These will be introduced in this section and developed in the following ones. Per Section 2 and Theorem 2.3, the optimal recoveries of the modes $(v_i)_{i \in \mathcal{I}}$ given the covariance operators $(Q_i)_{i \in \mathcal{I}}$ and the observation of $\sum_{i \in \mathcal{I}} v_i$ are the elements $Q_i(\sum_{i'} Q_{i'})^{-1}v$ in V_i . This operation is illustrated in module (1) of Figure 8. An important quantity derived from this recovery is the energy function $E : \mathcal{I} \rightarrow \mathbb{R}_+$, defined in (3.1) by $E(i) := [Q_i^{-1}w_i, w_i]$ with $w_i := \Psi_i(v)$, and illustrated in module (2). Since, per (3.2), $E_{tot} = \sum_{i \in \mathcal{I}} E(i)$, where $E_{tot} := \|v\|_{S^{-1}}^2$ is the total energy (3.1), the function E can be interpreted as performing a decomposition of the total energy over the set of labels \mathcal{I} . When \mathcal{I} can be identified with the set of vertices of a graph, the values of the $E(i)$ can be used to cut that graph into subgraphs indexed by labels $j \in \mathcal{J}$ and define a relation $i \rightsquigarrow j$ mapping $i \in \mathcal{I}$ to its subgraph j . This graph-cut operation is illustrated in module (3). Since, per Section 3.1, $E(i)$ is also the mean squared

alignment between the model ξ_i and the data v , and (3.4) is a variance decomposition, this clustering operation combines variance/model alignment information (as done with PCA) with the geometric information (as done with mixture models [23]) provided by the graph to assign a class $j \in \mathcal{J}$ to each element $i \in \mathcal{I}$. However, the $i \rightsquigarrow j$ relation may also be obtained through a projection step, possibly ignoring the values of $E(i)$, as illustrated in module (4) (e.g. when i is an r -tuple (i_1, i_2, \dots, i_r) then the truncation/projection map naturally defines a \rightsquigarrow relation via $(i_1, \dots, i_r) \rightsquigarrow (i_1, \dots, i_{r-1})$). As illustrated in module (5), combining the \rightsquigarrow relation with a sum $\sum_{i \rightsquigarrow j}$ produces aggregated covariance operators $Q_j := \sum_{i \rightsquigarrow j} Q_i$, modes $w_j := \sum_{i \rightsquigarrow j} w_i$ and energies $E(j) := \sum_{i \rightsquigarrow j} E(i)$ such that for $V_j := \sum_{i \rightsquigarrow j} V_i$, the modes $(w_i)_{i \rightsquigarrow j}$ are optimal recovery modes in $\prod_{i \rightsquigarrow j} V_i$ given the covariance operators $(Q_i)_{i \rightsquigarrow j}$ and the observation of $w_j = \sum_{i \rightsquigarrow j} w_i$ in V_j . Furthermore, we have $E(j) = [Q_j^{-1} w_j, w_j]$. Naturally, combining these elementary modules leads to more complex secondary modules (illustrated in Figure 9) whose nesting produces a network aggregating the fine modes w_i into increasingly coarse modes with the last node corresponding to v .

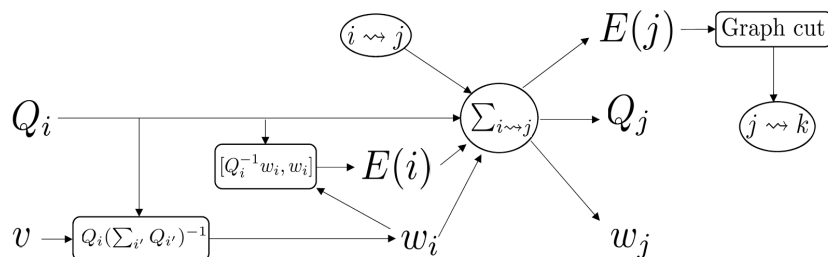


Figure 9: Programming modules derived from the elementary modules of Figure 8.

3.3 Hierarchical mode decomposition

The hierarchy of mode decomposition/recomposition steps discussed in Section 3.2 naturally produces a hierarchy of labels, covariance operators, subspaces and recoveries (illustrated in Figure 10) whose geometries and relationships will now be described. This description will lead to the meta-algorithm 1, presented in Section 3.4, aimed at the production of a KMDNet such as the one illustrated in Figure 9. Section 3.5 will present a practical application to Problem 1.

Our first step is to generalize the recovery approach of Section 2 to the case where V is the sum of a hierarchy of linear nested subspaces labeled by a hierarchy of indices, as defined below.

Definition 3.2. For $q \in \mathbb{N}^*$, let $\mathcal{I}^{(1)}, \dots, \mathcal{I}^{(q)}$ be finite sets of indices such that $\mathcal{I}^{(q)} = \{1\}$ has only one element. Let $\cup_{l=1}^q \mathcal{I}^{(l)}$ be endowed with a relation \rightsquigarrow that is (1) transitive, i.e., $i \rightsquigarrow j$ and $j \rightsquigarrow k$ implies $i \rightsquigarrow k$ (2) directed, i.e., $i \in \mathcal{I}^{(s)}$ and $j \in \mathcal{I}^{(r)}$ with $r \leq s$

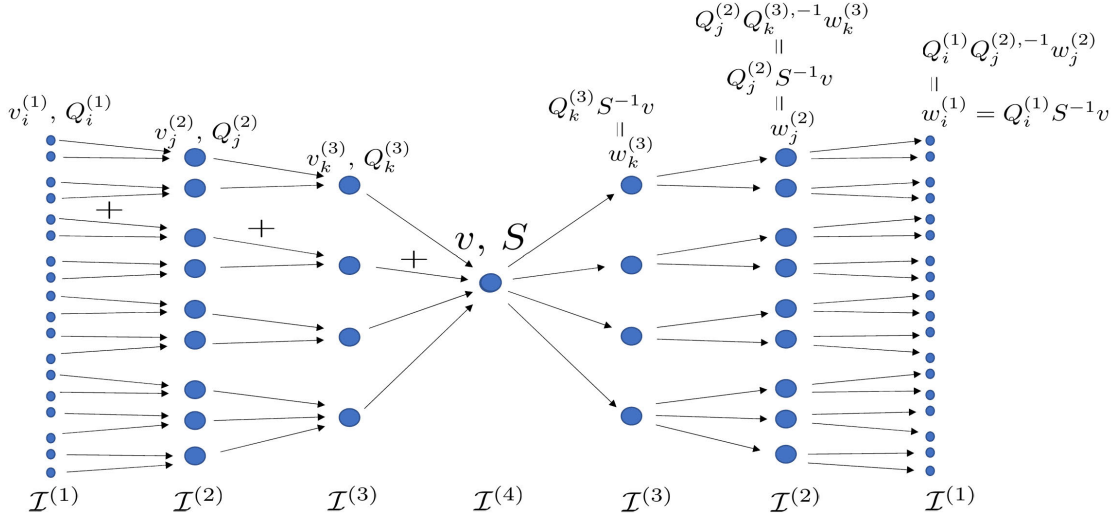


Figure 10: The generalization of abstract mode decomposition problem of Figure 3 to a hierarchy as described in Section 3.3.

implies $i \not\rightsquigarrow j$ (that is, i does not lead to j) and (3) such that for $r > 1$ any element $j \in \mathcal{I}^{(r)}$ has at least one $i \in \mathcal{I}^{(r-1)}$ such that $i \rightsquigarrow j$. For $1 \leq k < r \leq q$ and an element $i \in \mathcal{I}^{(r)}$, write $i^{(k)} := \{j \in \mathcal{I}^{(k)} \mid j \rightsquigarrow i\}$ for the level k ancestors of i .

Let $V_i^{(k)}$, $i \in \mathcal{I}^{(k)}$, $k \in \{1, \dots, q\}$ be a hierarchy of nested linear subspaces of a separable Hilbert space V such that

$$V_1^{(q)} = V$$

and, for each level in the hierarchy $k \in \{1, \dots, q-1\}$,

$$V_i^{(k+1)} = \sum_{j \in i^{(k)}} V_j^{(k)}, \quad i \in \mathcal{I}^{(k+1)}. \quad (3.5)$$

Let $\mathcal{B}^{(q)} = V$ and for $k \in \{1, \dots, q-1\}$, let $\mathcal{B}^{(k)}$ be the product space

$$\mathcal{B}^{(k)} := \prod_{i \in \mathcal{I}^{(k)}} V_i^{(k)}. \quad (3.6)$$

For $j \in \mathcal{I}^{(r)}$ with $r > k$, let

$$\mathcal{B}_j^{(k)} := \prod_{i \in j^{(k)}} V_i^{(k)}, \quad (3.7)$$

and let

$$\Phi_j^{(r,k)} : \mathcal{B}_j^{(k)} \rightarrow V_j^{(r)}$$

be defined by

$$\Phi_j^{(r,k)}(u) := \sum_{i \in j^{(k)}} u_i, \quad u \in \mathcal{B}_j^{(k)}. \quad (3.8)$$

Putting these components together as $\Phi^{(r,k)} = (\Phi_j^{(r,k)})_{j \in \mathcal{I}^{(r)}}$, we obtain the multi-linear map

$$\Phi^{(r,k)} : \mathcal{B}^{(k)} \rightarrow \mathcal{B}^{(r)}, \quad 1 \leq k < r \leq q,$$

defined by

$$\Phi^{(r,k)}(u) := \left(\sum_{i \in j^{(k)}} u_i \right)_{j \in \mathcal{I}^{(r)}}, \quad u = (u_i)_{i \in \mathcal{I}^{(k)}} \in \mathcal{B}^{(k)}. \quad (3.9)$$

To put hierarchical metric structure on these spaces, for $k \in \{1, \dots, q\}$ and $i \in \mathcal{I}^{(k)}$, let

$$Q_i^{(k)} : V_i^{(k),*} \rightarrow V_i^{(k)}$$

be positive symmetric linear bijections determining the quadratic norms

$$\|v\|_{V_i^{(k)}}^2 = [Q_i^{(k),-1} v, v], \quad v \in V_i^{(k)}, \quad (3.10)$$

on the $V_i^{(k)}$. For $k \in \{1, \dots, q\}$, let $\mathcal{B}^{(k)}$ be endowed with the quadratic norm defined by

$$\|u\|_{\mathcal{B}^{(k)}}^2 = \sum_{i \in \mathcal{I}^{(k)}} \|u_i\|_{V_i^{(k)}}^2, \quad u \in \mathcal{B}^{(k)}, \quad (3.11)$$

and for $k < r \leq q$ and $j \in \mathcal{I}^{(r)}$, let $\mathcal{B}_j^{(k)} := \prod_{i \in j^{(k)}} V_i^{(k)}$ be endowed with the quadratic norm defined by

$$\|u\|_{\mathcal{B}_j^{(k)}}^2 = \sum_{i \in j^{(k)}} \|u_i\|_{V_i^{(k)}}^2, \quad u \in \mathcal{B}_j^{(k)}.$$

For $1 \leq k < r \leq q$, the nesting relations (3.5) imply that

$$V_i^{(k)} \subset V_j^{(r)}, \quad i \in j^{(k)}, \quad j \in \mathcal{I}^{(r)},$$

so that the subset injection

$$e_{j,i}^{(r,k)} : V_i^{(k)} \rightarrow V_j^{(r)} \quad (3.12)$$

is well defined for all $i \in j^{(k)}$, $j \in \mathcal{I}^{(r)}$, and since all spaces are complete, they have well-defined adjoints, which we write

$$e_{i,j}^{(k,r)} : V_j^{(r),*} \rightarrow V_i^{(k),*}. \quad (3.13)$$

For $1 \leq k < r \leq q$, $i \in \mathcal{I}^{(k)}$ and $j \in \mathcal{I}^{(r)}$, let $\Psi_{i,j}^{(k,r)} : V_j^{(r)} \rightarrow V_i^{(k)}$ be defined by

$$\Psi_{i,j}^{(k,r)}(v_j) = Q_i^{(k)} e_{i,j}^{(k,r)} Q_j^{(r),-1} v_j, \quad v_j \in V_j^{(r)}, \quad (3.14)$$

that, when putting the components together as

$$\Psi_j^{(k,r)} := (\Psi_{i,j}^{(k,r)})_{i \in j^{(k)}}, \quad (3.15)$$

determines the multi-linear map

$$\Psi_j^{(k,r)} : V_j^{(r)} \rightarrow \mathcal{B}_j^{(k)}.$$

Further collecting components simultaneously over the range and domain as

$$\Psi^{(k,r)} = (\Psi_j^{(k,r)})_{j \in \mathcal{I}^{(r)}}$$

we obtain the multi-linear map

$$\Psi^{(k,r)} : \mathcal{B}^{(r)} \rightarrow \prod_{j \in \mathcal{I}^{(r)}} \mathcal{B}_j^{(k)}$$

defined by

$$\Psi^{(k,r)}(v) = (Q_i^{(k)} e_{i,j}^{(k,r)} Q_j^{(r,-1)} v_j)_{i \in j^{(k)}}, \quad v = (v_j)_{j \in \mathcal{I}^{(r)}} \in \mathcal{B}^{(r)}. \quad (3.16)$$

The following condition assumes that the relation \rightsquigarrow determines a mapping $\rightsquigarrow : \mathcal{I}^{(k)} \rightarrow \mathcal{I}^{(k+1)}$ for all $k = 1, \dots, q-1$.

Condition 3.3. *For $k \in \{1, \dots, q-1\}$, every $i \in \mathcal{I}^{(k)}$ has a unique descendant in $\mathcal{I}^{(k+1)}$. That is, there exists a $j \in \mathcal{I}^{(k+1)}$ with $i \rightsquigarrow j$ and there is no other $j' \in \mathcal{I}^{(k+1)}$ such that $i \rightsquigarrow j'$.*

Condition 3.3 simplifies the previous results as follows: the subsets $(\{i \in j^{(k)}\})_{j \in \mathcal{I}^{(k+1)}}$ form a partition of $\mathcal{I}^{(k)}$, so that we obtain the simultaneous product structure

$$\begin{aligned} \mathcal{B}^{(k)} &= \prod_{j \in \mathcal{I}^{(r)}} \mathcal{B}_j^{(k)} \\ \mathcal{B}^{(r)} &= \prod_{j \in \mathcal{I}^{(r)}} V_j^{(r)} \end{aligned} \quad (3.17)$$

so that both

$$\Phi^{(k,r)} : \mathcal{B}^{(k)} \rightarrow \mathcal{B}^{(r)}$$

and

$$\Psi^{(k,r)} : \mathcal{B}^{(r)} \rightarrow \mathcal{B}^{(k)}$$

are diagonal multi-linear maps with components

$$\Phi_j^{(r,k)} : \mathcal{B}_j^{(k)} \rightarrow V_j^{(r)}$$

and

$$\Psi_j^{(k,r)} : V_j^{(r)} \rightarrow \mathcal{B}_j^{(k)}$$

respectively. Moreover, both maps are *linear* under the isomorphism between products and external direct sums of vector spaces. For $r > k$, we have the following connections between $\mathcal{B}^{(k)}, \mathcal{B}^{(r)}, V_i^{(k)}$ and $V_j^{(r)}$.

$$\begin{array}{ccc}
\mathcal{B}^{(k)} & \xleftarrow{\quad \prod_{i \in \mathcal{I}^{(k)}} \quad} & V_i^{(k)} \\
\uparrow \Psi^{(k,r)} & & \downarrow \sum_{i \in \mathcal{I}^{(k)}} \\
\mathcal{B}^{(r)} & \xleftarrow{\quad \prod_{j \in \mathcal{I}^{(r)}} \quad} & V_j^{(r)}
\end{array}
\quad \text{with } \Phi^{(r,k)} \text{ between } \mathcal{B}^{(k)} \text{ and } \mathcal{B}^{(r)}
\tag{3.18}$$

The following theorem is a consequence of Theorem 2.3.

Theorem 3.4. *Assume that Condition 3.3 holds and that the $Q_i^{(k)} : V_i^{(k),*} \rightarrow V_i^{(k)}$ satisfy the nesting relations*

$$Q_j^{(k+1)} = \sum_{i \in \mathcal{I}^{(k)}} e_{j,i}^{(k+1,k)} Q_i^{(k)} e_{i,j}^{(k,k+1)}, \quad j \in \mathcal{I}^{(k+1)}, \tag{3.19}$$

for $k \in \{1, \dots, q-1\}$. Then for $1 \leq k < r \leq q$,

- $\Psi^{(k,r)} \circ \Phi^{(r,k)}(u)$ is the minmax recovery of $u \in \mathcal{B}^{(k)}$ given the observation of $\Phi^{(r,k)}(u) \in \mathcal{B}^{(r)}$ using the relative error in $\|\cdot\|_{\mathcal{B}^{(k)}}$ norm as a loss.
- $\Phi^{(r,k)} \circ \Psi^{(k,r)}$ is the identity map on $\mathcal{B}^{(r)}$
- $\Psi^{(k,r)} : (\mathcal{B}^{(r)}, \|\cdot\|_{\mathcal{B}^{(r)}}) \rightarrow (\mathcal{B}^{(k)}, \|\cdot\|_{\mathcal{B}^{(k)}})$ is an isometry.
- $\Phi^{(k,r),*} : (\mathcal{B}^{(r),*}, \|\cdot\|_{\mathcal{B}^{(r),*}}) \rightarrow (\mathcal{B}^{(k),*}, \|\cdot\|_{\mathcal{B}^{(k),*}})$ is an isometry.

Moreover we have the following semigroup properties for $1 \leq k < r < s \leq q$:

- $\Phi^{(s,k)} = \Phi^{(s,r)} \circ \Phi^{(r,k)}$
- $\Psi^{(k,s)} = \Psi^{(k,r)} \circ \Psi^{(r,s)}$
- $\Psi^{(r,s)} = \Phi^{(r,k)} \circ \Psi^{(k,s)}$

Remark 3.5. *The proof of Theorem 3.4 also demonstrates that, under its assumptions, for $1 \leq k < r \leq q$ and $j \in \mathcal{I}^{(r)}$, $\Psi_j^{(k,r)} \circ \Phi_j^{(r,k)}(u)$ is the minmax recovery of $u \in \mathcal{B}_j^{(k)}$ given the observation of $\Phi_j^{(r,k)}(u) \in V_j^{(r)}$ using the relative error in $\|\cdot\|_{\mathcal{B}_j^{(k)}}$ norm as a loss. Furthermore, $\Phi_j^{(r,k)} \circ \Psi_j^{(k,r)}$ is the identity map on $V_j^{(r)}$ and $\Psi_j^{(k,r)} : (V_j^{(r)}, \|\cdot\|_{V_j^{(r)}}) \rightarrow (\mathcal{B}_j^{(k)}, \|\cdot\|_{\mathcal{B}_j^{(k)}})$ and $\Phi_j^{(k,r),*} : (V_j^{(r),*}, \|\cdot\|_{V_j^{(r),*}}) \rightarrow (\mathcal{B}_j^{(k),*}, \|\cdot\|_{\mathcal{B}_j^{(k),*}})$ are isometries.*

Gaussian process regression interpretation As in the setting of Section 3.3, for $k \in \{1, \dots, q\}$, let

$$Q^{(k)} : \mathcal{B}^{(k),*} \rightarrow \mathcal{B}^{(k)}$$

be the block-diagonal operator

$$Q^{(k)} := \text{diag}(Q_i^{(k)})_{i \in \mathcal{I}^{(k)}}$$

defined by its action $Q^{(k)}\phi := (Q_i^{(k)}\phi_i)_{i \in \mathcal{I}^{(k)}}$, $\phi \in \mathcal{B}^{(k),*}$, and, as discussed in Section 2.2, write

$$\xi^{(k)} \sim \mathcal{N}(0, Q^{(k)})$$

for the centered Gaussian field on $\mathcal{B}^{(k)}$ with covariance operator $Q^{(k)}$.

Theorem 3.6. *Under the assumptions of Theorem 3.4, for $1 < k \leq q$, the distribution of $\xi^{(k)}$ is that of $\Phi^{(k,1)}(\xi^{(1)})$. Furthermore $\xi^{(1)}$ conditioned on $\Phi^{(k,1)}(\xi^{(1)})$ is a time reverse martingale in k and, for $1 \leq k < r \leq q$, we have*

$$\Psi^{(k,r)}(v) = \mathbb{E}[\xi^{(k)} \mid \Phi^{(r,k)}(\xi^{(k)}) = v], \quad v \in \mathcal{B}^{(r)}. \quad (3.20)$$

3.4 Mode decomposition through partitioning and integration

In the setting of Section 3.3, recall that $\mathcal{I}^{(q)} = \{1\}$ and $V_1^{(q)} = V$ so that the index j in $\Psi_{i,j}^{(k,q)}$ defined in (3.14) only has one value $j = 1$ and $1^{(k)} = \mathcal{I}^{(k)}$, and therefore

$$\Psi_{i,1}^{(k,q)}(v) := Q_i^{(k)} e_{i,1}^{(k,q)} Q_1^{(q,-1)} v, \quad v \in V, i \in \mathcal{I}^{(k)}.$$

Fix a $v \in V$ and for $k \in \{1, \dots, q\}$, let

$$E^{(k)} : \mathcal{I}^{(k)} \rightarrow \mathbb{R},$$

defined by

$$E^{(k)}(i) := \|\Psi_{i,1}^{(k,q)}(v)\|_{V_i^{(k)}}^2, \quad i \in \mathcal{I}^{(k)}, \quad (3.21)$$

be the alignment energy of the mode $i \in \mathcal{I}^{(k)}$. Under the nesting relations (3.19), the definition (3.10) of the norms and the semigroup properties of the subspace embeddings imply that

$$E^{(k+1)}(i) = \sum_{i' \in i^{(k)}} E^{(k)}(i'), \quad i \in \mathcal{I}^{(k+1)}, k \in \{1, \dots, q-1\}. \quad (3.22)$$

We will now consider applications where the space $(V, \|\cdot\|_V)$ is known, and the spaces $(V_i^{(1)}, \|\cdot\|_{V_i^{(1)}})$, including their index set $\mathcal{I}^{(1)}$, are known, but the spaces $(V_j^{(k)}, \|\cdot\|_{V_j^{(k)}})$ and their indices $\mathcal{I}^{(k)}$, are unknown for $1 < k < q$, as is any relation \rightsquigarrow connecting

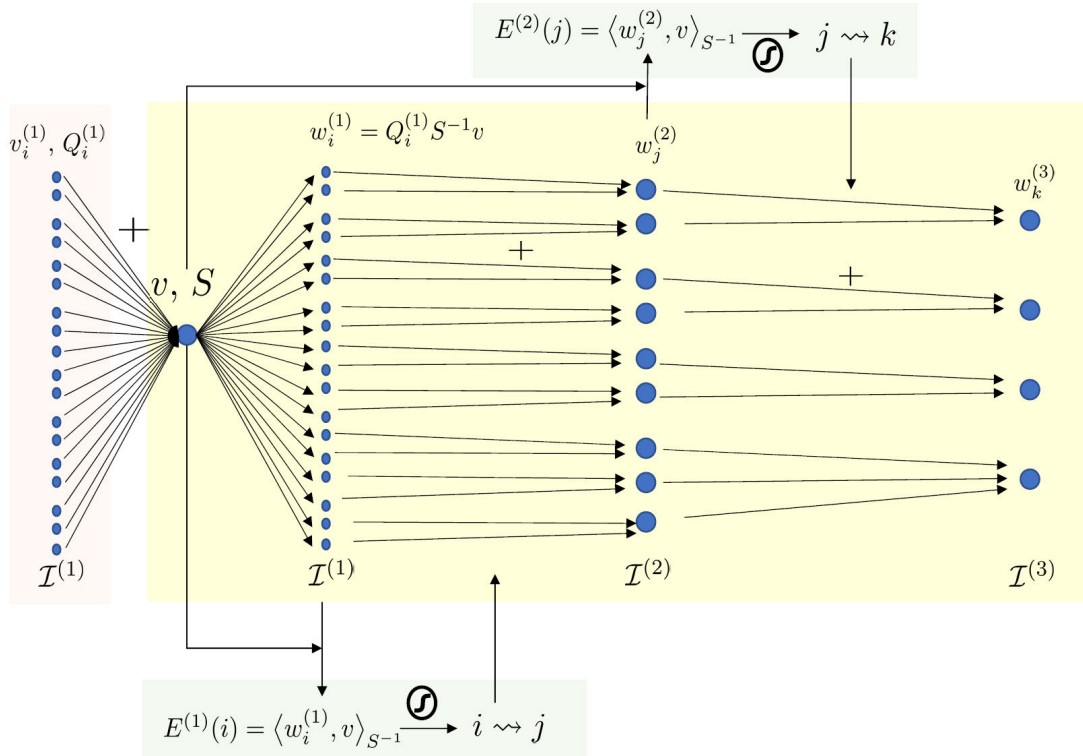


Figure 11: Derivation of the hierarchy from alignments.

them. Instead, they will be constructed by induction from model/data alignments as illustrated in Figures 7 and 11. In these applications

$$(V, \|\cdot\|_V) = (V_1^{(q)}, \|\cdot\|_{V_1^{(q)}}),$$

$V = \sum_{i \in \mathcal{I}^{(1)}} V_i^{(1)}$ and the operator $Q_1^{(q)} : V^* \rightarrow V$ associated with the norm $\|\cdot\|_{V_1^{(q)}}$ is the sum

$$Q_1^{(q)} = \sum_{i \in \mathcal{I}^{(1)}} e_{1,i}^{(q,1)} Q_i^{(1)} e_{i,1}^{(1,q)}. \quad (3.23)$$

In this construction we assume that the set of indices $\mathcal{I}^{(1)}$ are vertices of a graph $G^{(1)}$, whose edges provide neighbor relations among the indices. The following meta-algorithm, Algorithm 1, forms a general algorithmic framework for the adaptive determination of the intermediate spaces $(V_j^{(k)}, \|\cdot\|_{V_j^{(k)}})$, their indices $\mathcal{I}^{(k)}$, and a relation \rightsquigarrow , in such a way that Theorem 3.4 applies. Observe that this meta-algorithm is obtained by combining the elementary programming modules illustrated in Figures 8 and 9 and

Algorithm 1 Mode decomposition through partitioning and integration.

- 1: **for** $k = 1$ to $q - 2$ **do**
 - 2: Compute the function $E^{(k)} : \mathcal{I}^{(k)} \rightarrow \mathbb{R}_+$ defined by (3.21).
 - 3: Use the function $E^{(k)}$ to segment/partition the graph $G^{(k)}$ into subgraphs $(G_j^{(k+1)})_{j \in \mathcal{I}^{(k+1)}}$, thereby determining the indices $\mathcal{I}^{(k+1)}$. Define the ancestors $j^{(k)}$ of $j \in \mathcal{I}^{(k+1)}$ as the vertices $i \in \mathcal{I}^{(k)}$ of the sub-graph $G_j^{(k+1)}$.
 - 4: Identify the subspaces $V_j^{(k+1)}$ and the operators $Q_j^{(k+1)}$ through (3.5) and (3.19).
 - 5: **end for**
 - 6: Recover the modes $(\Psi_i^{(q-1,q)}(v))_{i \in \mathcal{I}^{(q-1)}}$ of v .
-

discussed in Section 3.2. In the following Section 3.5, it is demonstrated on a problem in time-frequency mode decomposition.

3.5 Application to time-frequency decomposition

We will now propose a solution to Problem 1 (note that for that problem the observed data is the whole function $v = u + v_\sigma$) based on the hierarchical segmentation approach described in Section 3.4. We will employ the GPR interpretation of Section 2.3 and assume that v is the realization of a Gaussian process ξ obtained by integrating Gabor wavelets [9] against white noise. To that end, for $\tau, \theta \in \mathbb{R}$ and $\omega, \alpha > 0$, let

$$\chi_{\tau,\omega,\theta}(t) := \left(\frac{2}{\pi^3}\right)^{\frac{1}{4}} \sqrt{\frac{\omega}{\alpha}} \cos(\omega(t - \tau) + \theta) e^{-\frac{\omega^2(t-\tau)^2}{\alpha^2}}, \quad t \in \mathbb{R}, \quad (3.24)$$

be the shifted/scaled Gabor wavelet, whose scaling is motivated by the normalization $\int_{-\pi}^{\pi} \int_{\mathbb{R}} \chi_{\tau,\omega,\theta}^2(t) dt d\theta = 1$. See Figure 12 for an illustration of the Gabor wavelets. Recall [9] that each χ is minimally localized in the time-frequency domain (it minimizes the product of standard deviations in the time and frequency domains) and the parameter α is proportional to the ratio between localization in frequency and localization in space.

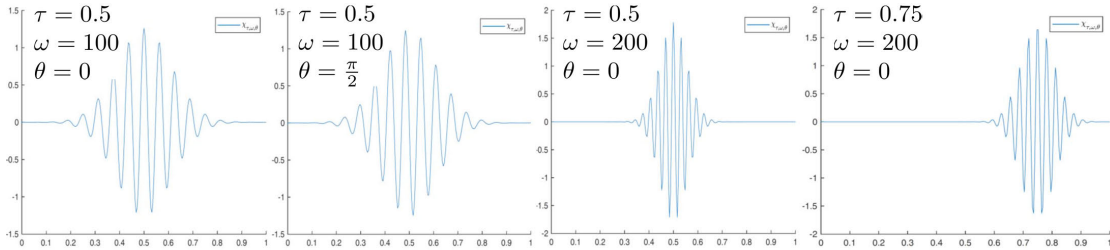


Figure 12: Gabor wavelets $\chi_{\tau,\omega,\theta}$ (3.24) for various parameter values.

Let $\zeta(\tau, \omega, \theta)$ be a white noise process on \mathbb{R}^3 (a centered GP with covariance function $\mathbb{E}[\zeta(\tau, \omega, \theta)\zeta(\tau', \omega', \theta')] = \delta(\tau - \tau')\delta(\omega - \omega')\delta(\theta - \theta')$) and let

$$\xi_u(t) := \int_{-\pi}^{\pi} \int_{\omega_{\min}}^{\omega_{\max}} \int_0^1 \zeta(\tau, \omega, \theta) \chi_{\tau, \omega, \theta}(t) d\tau d\omega d\theta, \quad t \in \mathbb{R}. \quad (3.25)$$

Letting, for each τ, ω and θ ,

$$K_{\tau, \omega, \theta}(s, t) := \chi_{\tau, \omega, \theta}(s) \chi_{\tau, \omega, \theta}(t), \quad s, t \in \mathbb{R}, \quad (3.26)$$

be the reproducing kernel associated with the wavelet $\chi_{\tau, \omega, \theta}$, it follows that ξ_u is a centered GP with covariance function

$$K_u(s, t) = \int_{-\pi}^{\pi} \int_{\omega_{\min}}^{\omega_{\max}} \int_0^1 K_{\tau, \omega, \theta}(s, t) d\tau d\omega d\theta, \quad s, t \in \mathbb{R}. \quad (3.27)$$

Given $\sigma > 0$, let $\xi_\sigma(t)$ be a white noise process on \mathbb{R} (independent from ζ) of variance σ^2 (a centered GP with covariance function $\mathbb{E}[\xi_\sigma(s)\xi_\sigma(t)] = \sigma^2\delta(s - t)$) and let ξ be the GP defined by

$$\xi := \xi_u + \xi_\sigma. \quad (3.28)$$

ξ is a centered GP with covariance function defined by the kernel

$$K := K_u + K_\sigma \quad (3.29)$$

with

$$K_\sigma(s, t) = \sigma^2\delta(s - t). \quad (3.30)$$

Hence, compared to the setting of Section 2, and apart from the mode corresponding to the noise ξ_σ , the finite number of modes indexed by \mathcal{I} has been turned into a continuum of modes indexed by

$$\mathcal{I} := \{(\tau, \omega, \theta) \in [0, 1] \times [\omega_{\min}, \omega_{\max}] \times (-\pi, \pi)\}$$

with corresponding one dimensional subspaces

$$V_{(\tau, \omega, \theta)}^{(1)} = \text{span}\{\chi_{\tau, \omega, \theta}\},$$

positive operators $Q_{\tau, \omega, \theta}$ defined by the kernels $K_{\tau, \omega, \theta}(s, t)$ and the integral

$$K_u(s, t) = \int_{-\pi}^{\pi} \int_{\omega_{\min}}^{\omega_{\max}} \int_0^1 K_{\tau, \omega, \theta}(s, t) d\tau d\omega d\theta, \quad s, t \in \mathbb{R},$$

of these kernels (3.27) to obtain a master kernel K_u instead of a sum

$$S = \sum_{i \in \mathcal{I}} e_i Q_i e_i^*$$

as in (2.12). Table 4 illustrates the time-frequency version of Table 2 we have just developed and the following remark explains the connection between kernels and operators in more detail.

Mode	GP	Kernel
$v_{\tau,\omega,\theta}(t) = a_{\tau,\omega,\theta}(t)\chi_{\tau,\omega,\theta}(t)$ $a_{\tau,\omega,\theta}$ unknown and L^2	$\xi_{\tau,\omega,\theta}(t) = \zeta(\tau,\omega,\theta)\chi_{\tau,\omega,\theta}(t)$ $\mathbb{E}[\zeta(\tau,\omega,\theta)\zeta(\tau',\omega',\theta')]$ $= \delta(\tau - \tau')\delta(\omega - \omega')\delta(\theta - \theta')$	$K_{\tau,\omega,\theta}(s,t) = \chi_{\tau,\omega,\theta}(s)\chi_{\tau,\omega,\theta}(t)$
$v_{\tau,\omega} = \int_{-\pi}^{\pi} v_{\tau,\omega,\theta} d\theta$	$\xi_{\tau,\omega}(t) = \int_{-\pi}^{\pi} \xi_{\tau,\omega,\theta}(t) d\theta$	$K_{\tau,\omega}(s,t) = \int_{-\pi}^{\pi} K_{\tau,\omega,\theta}(s,t) d\theta$
$v_u = \iiint v_{\tau,\omega,\theta} d\tau d\omega d\theta$	$\xi_u(t) = \iiint \xi_{\tau,\omega,\theta}(t) d\tau d\omega d\theta$	$K_u(s,t) = \iiint K_{\tau,\omega,\theta}(s,t) d\tau d\omega d\theta$
v_σ unknown white noise	$\mathbb{E}[\xi_\sigma(s)\xi_\sigma(t)] = \sigma^2\delta(s-t)$	$K_\sigma(s,t) = \sigma^2\delta(s-t)$
$v = v_u + v_\sigma$	$\xi = \xi_u + \xi_\sigma$	$K = K_u + K_\sigma$
$v_i = \int_{A(i)} v_{\tau,\omega} d\tau d\omega$	$\xi_i = \int_{A(i)} \xi_{\tau,\omega} d\tau d\omega$	$K_i = \int_{A(i)} K_{\tau,\omega} d\tau d\omega$

Table 4: The time-frequency version of Table 2

Remark 3.7 (Kernels, operators, and discretizations). *This kernel mode decomposition framework constructs reproducing kernels K through the integration of elementary reproducing kernels, but the recovery formula of Theorem 2.3 requires the application of operators, and their inverses, corresponding to these kernels. In general, there is no canonical connection between kernels and operators, but here we consider restricting to the unit interval $[0, 1] \subset \mathbb{R}$ in the time variable t . Then, each kernel K under consideration other than K_σ corresponds to the symmetric positive integral operator*

$$\bar{K} : L^2[0, 1] \rightarrow L^2[0, 1]$$

defined by

$$(\bar{K}f)(s) := \int_0^1 K(s, t)f(t)dt, \quad s \in [0, 1], f \in L^2[0, 1].$$

Moreover, these kernels all have sufficient regularity that \bar{K} is compact and therefore not invertible, see e.g. Steinwart and Christmann [33, Thm. 4.27]. On the other hand, the operator

$$\bar{K}_\sigma : L^2[0, 1] \rightarrow L^2[0, 1]$$

corresponding to the white noise kernel K_σ (3.30) is

$$\bar{K}_\sigma = \sigma^2 I$$

where

$$I : L^2[0, 1] \rightarrow L^2[0, 1]$$

is the identity map. Since $K = K_u + K_\sigma$ (3.29), the operator $\bar{K} = \bar{K}_u + \bar{K}_\sigma$ is a symmetric positive compact operator plus a positive multiple of the identity and therefore it is Fredholm and invertible. Consequently, we can apply Theorem 2.3 for the optimal recovery.

In addition, in numerical applications, τ and ω are discretized (using $N + 1$ discretization steps) and the integrals in (3.34) are replaced by sums over $\tau_k := k/N$ and $\omega_k := \omega_{\min} + \frac{k}{N}(\omega_{\max} - \omega_{\min})$ ($k \in \{0, 1, \dots, N\}$). Moreover, as in Example 2.6, the time interval $[0, 1]$ is discretized into M points and the corresponding operators on \mathbb{R}^M are $\sigma^2 I$, where $I : \mathbb{R}^M \rightarrow \mathbb{R}^M$ is the identity, plus the kernel matrix $(K_u(t_i, t_j))_{i,j=1}^M$ corresponding to the sample points $t_i, i = 1, \dots, M$. Nevertheless, for simplicity and conciseness, we will keep describing the proposed approach in the continuous setting. Moreover, we will overload notation and not use the \bar{K} notation, but instead use the same symbol for a kernel and its corresponding operator.

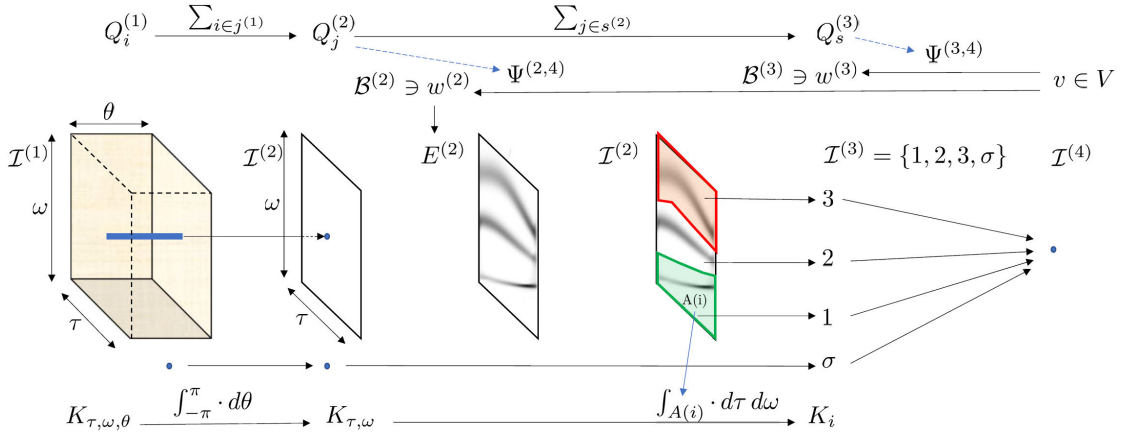


Figure 13: Mode decomposition through partitioning and integration. $q = 4$, $w^{(3)} := \Psi^{(3,4)}v$, $w^{(2)} := \Psi^{(2,4)}v$, and σ corresponds to the noise component.

We now describe the hierarchical approach of Section 3.4 to this time-frequency setting and illustrate it in Figure 13. To that end, we identify \mathcal{I} with $\mathcal{I}^{(1)}$ so that

$$\mathcal{I}^{(1)} = \{(\tau, \omega, \theta) \in [0, 1] \times [\omega_{\min}, \omega_{\max}] \times (-\pi, \pi)\} \cup \{\sigma\},$$

where the noise mode has been illustrated in Figure 13 by adding an isolated point with label σ to each set $\mathcal{I}^{(k)}$ with $k < q = 4$.

Although Line 3 of Algorithm 1 uses the energy $E^{(1)}$ at level $k = 1$ to partition the index set $\mathcal{I}^{(1)}$, the algorithm is flexible in how we use it or if we use it. In this particular application we first ignore the computation of $E^{(1)}$ and straightforward partition $\mathcal{I}^{(1)}$ into a family of subsets

$$\mathcal{I}_{\tau, \omega}^{(1)} := \{(\tau, \omega, \theta) : \theta \in (-\pi, \pi)\} \cup \{\sigma\}, \quad (\tau, \omega) \in [0, 1] \times [\omega_{\min}, \omega_{\max}],$$

indexed by τ and ω , so that the corresponding index set at level $k = 2$ is

$$\mathcal{I}^{(2)} = \{(\tau, \omega) \in [0, 1] \times [\omega_{\min}, \omega_{\max}]\} \cup \{\sigma\},$$

and the ancestors of (τ, ω, σ) are

$$(\tau, \omega, \sigma)^{(2)} = \{(\tau, \omega, \theta) : \theta \in (-\pi, \pi]\} \cup \{\sigma\}.$$

The subspace corresponding to the label (τ, ω) is then

$$V_{(\tau, \omega)}^{(2)} = \text{span}\{\chi_{\tau, \omega, \theta} \mid \theta \in (-\pi, \pi]\}$$

and, as in (3.19), its associated positive operator is characterized by the kernel

$$K_{\tau, \omega} := \int_{-\pi}^{\pi} K_{\tau, \omega, \theta} d\theta. \quad (3.31)$$

We can evaluate $K_{\tau, \omega}$ using (3.26) and (3.24) by defining

$$\begin{aligned} \chi_{\tau, \omega, c} &:= \left(\frac{2}{\pi}\right)^{\frac{1}{4}} \sqrt{\frac{\omega}{\alpha}} \cos(\omega(\cdot - \tau)) e^{-\frac{\omega^2(\cdot - \tau)^2}{\alpha^2}} \\ \chi_{\tau, \omega, s} &:= \left(\frac{2}{\pi}\right)^{\frac{1}{4}} \sqrt{\frac{\omega}{\alpha}} \sin(\omega(\cdot - \tau)) e^{-\frac{\omega^2(\cdot - \tau)^2}{\alpha^2}}, \end{aligned} \quad (3.32)$$

and using the trigonometric identity $\cos(a + \theta) = \cos a \cos \theta - \sin a \sin \theta$, to obtain

$$K_{\tau, \omega}(s, t) := \chi_{\tau, \omega, c}(s)\chi_{\tau, \omega, c}(t) + \chi_{\tau, \omega, s}(s)\chi_{\tau, \omega, s}(t). \quad (3.33)$$

Therefore $V_{(\tau, \omega)}^{(2)} = \text{span}\{\chi_{\tau, \omega, c}, \chi_{\tau, \omega, s}\}$ and (3.27) reduces to

$$K_u(s, t) = \int_{\omega_{\min}}^{\omega_{\max}} \int_0^1 K_{\tau, \omega}(s, t) d\tau d\omega. \quad (3.34)$$

Using $K := K_u + K_\sigma$ (3.29), let f be the solution of the linear system $\int_0^1 K(s, t)f(t) dt = v(s)$, i.e.

$$Kf = v, \quad (3.35)$$

and let $E(\tau, \omega)$ be the energy of the recovered mode indexed by (τ, ω) , i.e.

$$E(\tau, \omega) = \int_0^1 \int_0^1 f(s)K_{\tau, \omega}(s, t)f(t) ds dt, \quad (\tau, \omega) \in [0, 1] \times [\omega_{\min}, \omega_{\max}]. \quad (3.36)$$

Since $Kf = v$ implies that

$$v^T K^{-1}v = f^T Kf,$$

it follows that

$$v^T K^{-1}v = \int_{\omega_{\min}}^{\omega_{\max}} \int_0^1 E(\tau, \omega) d\tau d\omega + f^T K_\sigma f. \quad (3.37)$$

For the recovery of n modes using Algorithm 1, at the second level $k = 2$ we use $E(\tau, \omega)$ to partition the time-frequency domain of (τ, ω) into n disjoint subsets $A(1), A(2), \dots, A(n)$ as illustrated in Figure 13 for $n = 3$ (in particular, n is not assumed to be known beforehand and recovered from $E(\tau, \omega)$), and then define $\mathcal{I}^{(3)}$ as $\{1, 2, \dots, n, \sigma\}$, the subspace corresponding to the mode $i \neq \sigma$ as $V_i^{(3)} = \text{span}\{\chi_{\tau, \omega, c}, \chi_{\tau, \omega, s} \mid (\tau, \omega) \in A(i)\}$ and the kernel associated with the mode $i \neq \sigma$ as

$$K_i(s, t) = \int_{(\tau, \omega) \in A(i)} K_{\tau, \omega}(s, t) d\tau d\omega, \quad s, t \in \mathbb{R}, \quad (3.38)$$

as displayed in the bottom row in Table 4, so that

$$K_u = \sum_{i=1}^n K_i.$$

We then apply the optimal recovery formula of Theorem 2.3 to approximate the modes of v_1, \dots, v_n of u from the noisy observation of $v = u + v_\sigma$ (where v_σ is a realization of ξ_σ) with the elements w_1, \dots, w_n obtained via the integration

$$w_i = K_i K^{-1} v = K_i f,$$

that is,

$$w_i = K_i f. \quad (3.39)$$

Figure 14 illustrates a three mode $n = 3$ noisy signal and the recovery of its modes. Sub-figure (1) displays the total observed signal $v = u + v_\sigma$ and the three modes v_1, v_2, v_3 constituting $u = v_1 + v_2 + v_3$ are displayed in sub-figures (5), (6), and (7) along with their recoveries w_1, w_2 and w_3 . Sub-figure 8 of Figure 14 also shows approximations of the instantaneous frequencies obtained as

$$\omega_{i,E}(t) := \operatorname{argmax}_{\omega: (t, \omega) \in A(i)} E(t, \omega). \quad (3.40)$$

4 Additional programming modules and squeezing

In the approach described in Section 3.4, $\mathcal{I}^{(k)}$ was partitioned into subsets $(j^{(k)})_{j \in \mathcal{I}^{(k+1)}}$ and the $Q_i^{(k)}$ were integrated (that is, summed over or average-pooled) using (3.5) and (3.19) in Line 4 of Algorithm 1, over each subset to obtain the $Q_j^{(k+1)}$. This partitioning approach can naturally be generalized to a *domain decomposition* approach by letting the subsets be non-disjoint and such that $\cup_{j \in \mathcal{I}^{(k+1)}} j^{(k)}$ forms a strict subset² of $\mathcal{I}^{(k)}$ (i.e. some $i \in \mathcal{I}^{(k)}$ may not have descendants). We will now generalize the relation \rightsquigarrow so as to (1) not satisfy Condition 3.3 (2) be non directed, that is, not satisfy Definition 3.2

²Although the results of Theorem 3.4 do not hold true under this general domain-decomposition, those of Theorem 2.3 remain true between levels k and q (at each level k the $v_i^{(k)}$ are optimal recovered modes given the $Q_i^{(k)}$ and the observation v).

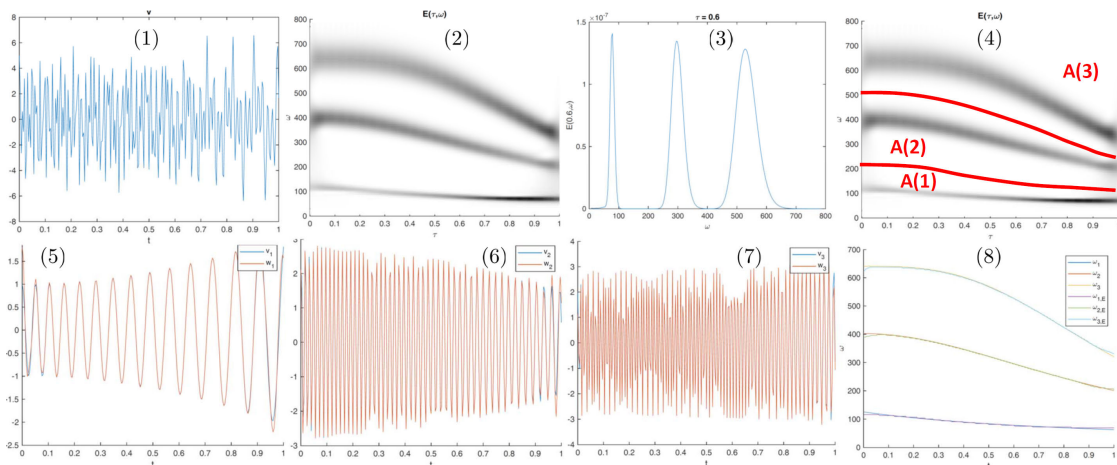


Figure 14: (1) The signal $v = u + v_\sigma$ where $u = v_1 + v_2 + v_3$, $v_\sigma \sim \mathcal{N}(0, \sigma^2 \delta(t - s))$ and $\sigma = 0.01$ (2) $(\tau, \omega) \rightarrow E(\tau, \omega)$ defined by (3.36) (one can identify three stripes) (3) $\omega \rightarrow E(0.6, \omega)$ (4) Partitioning $[0, 1] \times [\omega_{\min}, \omega_{\max}] = \cup_{i=1}^3 A(i)$ of the time frequency domain into three disjoint subsets identified from E (5) v_1 and its approximation w_1 (6) v_2 and its approximation w_2 (7) v_3 and its approximation w_3 (8) $\omega_{1,E}, \omega_{2,E}, \omega_{3,E}$.

(some $j \in \mathcal{I}^{(k+1)}$ may have descendants in $\mathcal{I}^{(k)}$) (3) to not define a map (a label i may have multiple descendants) and (4) enable loops.

With this generalization the proposed framework is closer (in spirit) to an object oriented programming language than to a meta-algorithm. We will therefore describe it as such via the introduction of additional elementary programming modules and illustrate the proposed language by programming increasingly efficient networks for mode decomposition.

4.1 Elementary programming modules

We will now introduce new elementary programming modules in addition to the five illustrated in Figure 8 and discussed in Section 3.2. These new modules, beginning with module (6), are illustrated in Figure 15. Here they will be discussed abstractly but forward reference to specific examples.. The first module (module (6)) of Figure 15 replaces the average-pooling operation to the define the energy E by a max-pool operation. More precisely module (6) combines a $i \rightsquigarrow j$ relation with an energy E to produce a *max-pool energy* via

$$\mathcal{S}(j) = \max_{i \rightsquigarrow j} E(i), \quad (4.1)$$

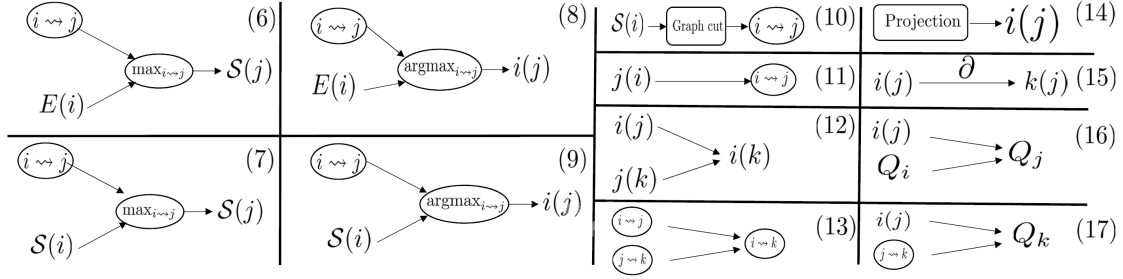


Figure 15: Elementary programming modules.

where $i \rightsquigarrow j$ here is over i from the previous level to that of j . In what follows we will adhere to this semantic convention. As shown in module (7), this combination can also be performed starting with a *max-pool energy*, i.e. module (7) combines a $i \rightsquigarrow j$ relation with a max-pool energy \mathcal{S} to produce a *max-pool energy* via

$$\mathcal{S}(j) = \max_{i \rightsquigarrow j} \mathcal{S}(i). \quad (4.2)$$

Maximizers can naturally be derived from this max-pooling operation and modules (8) and (9) define $i(j)$ as the maximizer (or the set of maximizers if non-unique) of the energy or the max-pool energy. More precisely module (8) combines an $i \rightsquigarrow j$ relation with an energy function $E(i)$ to produce

$$i(j) = \operatorname{argmax}_{i \rightsquigarrow j} E(i), \quad (4.3)$$

and module (9) combines an $i \rightsquigarrow j$ relation with a max-pool energy function $\mathcal{S}(i)$ to produce

$$i(j) = \operatorname{argmax}_{i \rightsquigarrow j} \mathcal{S}(i). \quad (4.4)$$

Similarly to module (3) of Figure 8, module (10) of Figure 15 combines the max-pool energy \mathcal{S} with a graph operation to produce the ancestor-descendant relation $i \rightsquigarrow j$. We will show that module (10) leads to a more robust domain discretization than module (3) due to its insensitivity to domain discretization. Module (11) uses the functional dependence $j(i)$ to define the relation $i \rightsquigarrow j$. Module (12) expresses the transitivity of function dependence, i.e. it combines $j(i)$ and $k(j)$ to produce $k(i)$. Similarly, module (13) expresses the transitivity of the \rightsquigarrow relation, i.e. $i \rightsquigarrow j$ and $j \rightsquigarrow k$ can be combined to produce $i \rightsquigarrow k$. Module (14) (analogously to module (4)) uses an injection step to define a functional dependence $i(j)$ (e.g. for the time-frequency application in Figure 19, if \mathcal{J} is the set of (τ, ω') and \mathcal{I} is that of (τ, ω) the injection $\iota : \mathcal{I} \cap \mathcal{J} \rightarrow \mathcal{I}$ defines a functional dependence $i(j)$). Module (15) uses a functional dependence $i(j)$ to produce another functional dependence $k(j)$ (e.g. for the time-frequency-phase application in Figures 21 and 22, we can define the functional dependence $(\tau, \omega')(\tau, \omega)$ from the functional dependence $(\tau, \omega, \theta)(\tau, \omega)$ via $\omega'(\tau, \omega) = \partial_\tau \theta(\tau, \omega)$). Module (16) utilizes the functional

dependence $i(j)$ to produce a pullback covariance operator $Q_j := Q_{i(j)}$ ($:= \sum_{i \in i(j)} Q_i$ if $i(j)$ is a set-valued rather than a single-valued mapping). Module (17) combines a functional dependence $i(j)$ with a relation $j \rightsquigarrow k$ to produce a covariance operator Q_k (e.g. for the time-frequency-phase application of Figures 21 and 22, for $i = (\tau, \omega, \theta) \in \mathcal{I}^{(1)}$ and $j = (\tau, k) \in \mathcal{I}^{(4)}$ where the index k is the mode index, the functional dependence $i(j)$ defines through (4.16) estimated phases $\theta_{k,e}(\tau)$ which can then be substituted for $\theta(\cdot)$ in the kernel $K(s, t) = e^{-|s-t|^2/\gamma^2} (\cos(\theta(s)) \cos(\theta(t)) + \sin(\theta(s)) \sin(\theta(t)))$, producing for each mode index k a kernel with corresponding operator Q_k).

4.2 Programming the network

Programming of the network is achieved by assembling the modules of Figures 8 and 15 in a manner that (1) v is one of the inputs of the network and (if the network is used for mode decomposition/pattern recognition) (2) the modes v_m are one of the outputs of the network. As with any interpretable programming language avoiding inefficient coding and bugs remains important. We will now use this language to program KMDNets.

4.3 Squeezing

We will now present an interpretation and a variant (illustrated in Figure 17) of the synchrosqueezing transform due to Daubechies, Lu and Wu [3] in the setting of KMDNets, and thereby initiate its GP regression version. We will demonstrate that this version generalizes to the case where the basic waveform is non-periodic and/or unknown. We use the setting and notations of Section 3.5.

Let f be the solution of $Kf = v$ (3.35) and let

$$E(\tau, \omega, \theta) := \int_0^1 \int_0^1 f(s) K_{\tau, \omega, \theta}(s, t) f(t) ds dt \quad (4.5)$$

be the energy of the mode indexed by (τ, ω, θ) . For $(\tau, \omega) \in [0, 1] \times [\omega_{\min}, \omega_{\max}]$, write

$$\theta_e(\tau, \omega) := \operatorname{argmax}_{\theta \in (-\pi, \pi]} E(\tau, \omega, \theta). \quad (4.6)$$

Since the definitions (3.24) of $\chi_{\tau, \omega, \theta}$ and $\chi_{\tau, \omega, c}$ and $\chi_{\tau, \omega, s}$ in (3.32), together with the identity $\cos(a + \theta) = \cos a \cos \theta - \sin a \sin \theta$ imply that

$$\chi_{\tau, \omega, \theta}(t) = \frac{1}{\sqrt{\pi}} (\chi_{\tau, \omega, c}(t) \cos(\theta) - \chi_{\tau, \omega, s}(t) \sin(\theta)), \quad t \in \mathbb{R},$$

it follows that, if we define

$$\begin{aligned} W_c(\tau, \omega) &:= \int_0^1 \chi_{\tau, \omega, c}(t) f(t) dt \\ W_s(\tau, \omega) &:= \int_0^1 \chi_{\tau, \omega, s}(t) f(t) dt, \end{aligned} \quad (4.7)$$

we obtain

$$\int_0^1 \chi_{\tau,\omega,\theta}(t) f(t) dt = \frac{1}{\sqrt{\pi}} (\cos(\theta) W_c(\tau, \omega) - \sin(\theta) W_s(\tau, \omega)). \quad (4.8)$$

Consequently, we deduce from (4.5) and (3.26) that

$$E(\tau, \omega, \theta) = \frac{1}{\pi} (\cos(\theta) W_c(\tau, \omega) - \sin(\theta) W_s(\tau, \omega))^2. \quad (4.9)$$

It follows that, when either $W_c(\tau, \omega) \neq 0$ or $W_s(\tau, \omega) \neq 0$, that

$$\theta_e(\tau, \omega) = \text{phase}(W_c(\tau, \omega) - iW_s(\tau, \omega)), \quad (4.10)$$

where, for a complex number z , $\text{phase}(z) := \theta \in (-\pi, \pi] : z = r e^{i\theta}, r > 0$. Moreover, it follows from (4.9) that with $E(\tau, \omega)$ defined as in (3.36), that

$$E(\tau, \omega) = W_c^2(\tau, \omega) + W_s^2(\tau, \omega). \quad (4.11)$$

Now consider the mode decomposition problem with observation $v = \sum v_i$, and let $t \rightarrow \theta_i(t)$ be the phase of the mode

$$v_i(t) = a_i(t) \cos(\theta_i(t)) + b_i(t) \sin(\theta_i(t))$$

where a_i and b_i are slowly varying compared to θ_i . Since near the time τ , $v_i(t) \approx a_i(\tau) \cos((t - \tau)\dot{\theta}_i(\tau) + \theta_i(\tau)) + b_i(\tau) \sin((t - \tau)\dot{\theta}_i(\tau) + \theta_i(\tau))$. It follows from the representation (3.32) of $\chi_{\tau,\omega,c}$ and $\chi_{\tau,\omega,s}$ that for $\omega \approx \dot{\theta}_i(\tau)$, $\theta_e(\tau, \omega)$ is an approximation of $\theta_i(\tau)$ and

$$\omega_e(\tau, \omega) = \frac{\partial \theta_e}{\partial \tau}(\tau, \omega), \quad (4.12)$$

is an approximation of the instantaneous frequency $\dot{\theta}_i(\tau)$.

Remark 4.1. In the discrete setting, to minimize errors, (4.12) is approximated by the solution of $e^{i\omega_e(\tau_k, \omega)(\tau_{k+1} - \tau_k)} e^{i \text{phase}(W_c(\tau_k, \omega) - iW_s(\tau_k, \omega))} = e^{i \text{phase}(W_c(\tau_{k+1}, \omega) - iW_s(\tau_{k+1}, \omega))}$, i.e. (writing `atan2` for Matlab's four-quadrant inverse tangent)

$$\omega_e(\tau_k, \omega) = \frac{1}{\tau_{k+1} - \tau_k} \text{atan2} \left(\frac{W_c(\tau_{k+1}, \omega) W_s(\tau_k, \omega) - W_s(\tau_{k+1}, \omega) W_c(\tau_k, \omega)}{W_c(\tau_{k+1}, \omega) W_c(\tau_k, \omega) + W_s(\tau_{k+1}, \omega) W_s(\tau_k, \omega)} \right) \quad (4.13)$$

In preparation for illustrating the application of the programming of KMDNets, as a synchrosqueezing algorithm, to the decomposition problem when v and its modes are as in Figure 14, Figure 16 illustrates the basic quantities we have just been developing. In particular,

- The functions W_c and W_s are shown in sub-figures (1) and (2) of Figure 16.
- The function $\tau \rightarrow (W_c(\tau, 300), -W_s(\tau, 300))$ is shown in sub-figure (3) of Figure 16. The functions $\theta_e(\tau, 300)$, $E(\tau, 300)$ and $\omega_e(\tau, 300)$ are the phase, square modulus and angular velocity of this function.

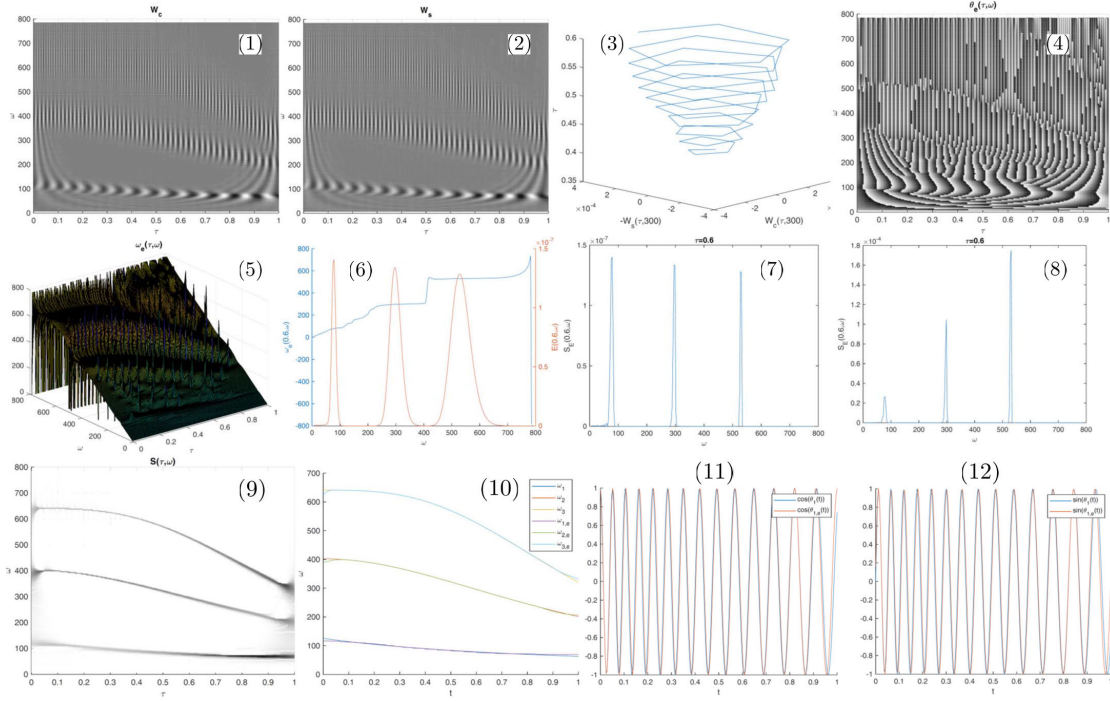


Figure 16: (1) $W_c(\tau, \omega)$ (2) $W_s(\tau, \omega)$ (3) $\tau \rightarrow (W_c(\tau, 300), W_s(\tau, 300), \tau)$ (4) $(\tau, \omega) \rightarrow \theta_e(\tau, \omega)$ (5) $(\tau, \omega) \rightarrow \omega_e(\tau, \omega)$ (6) $\omega \rightarrow \omega_e(0.6, \omega)$ and $\omega \rightarrow E(0.6, \omega)$ (7) $\omega \rightarrow \mathcal{S}(0.6, \omega)$ (8) $\omega \rightarrow \mathcal{S}_E(0.6, \omega)$ (9) $(\tau, \omega) \rightarrow \mathcal{S}(\tau, \omega)$ (10) $t \rightarrow \omega_i(t)$ and $t \rightarrow \omega_{i,e}(t)$ for $i \in \{1, 2, 3\}$ (11) $t \rightarrow \cos(\theta_1(t))$ and $t \rightarrow \cos(\theta_{1,e}(t))$ (12) $t \rightarrow \sin(\theta_1(t))$ and $t \rightarrow \sin(\theta_{1,e}(t))$.

- The functions $(\tau, \omega) \rightarrow \theta_e(\tau, \omega)$, $\tau \rightarrow \theta_e(\tau, \omega_{i,E}(\tau))$ (with $\omega_{i,E}$ defined in (3.40)) and $t \rightarrow \theta_i(t)$ are shown in sub-figures (4), (11) and (12) of Figure 16. Observe that $\tau \rightarrow \theta_e(\tau, \omega_{i,E}(\tau))$ is an approximation of $\tau \rightarrow \theta_i(\tau)$.
- The functions $(\tau, \omega) \rightarrow \omega_e(\tau, \omega)$, $\omega \rightarrow \omega_e(0.6, \omega)$ and $\tau \rightarrow \omega_e(\tau, \omega_{i,E}(\tau))$ are shown in sub-figures (5), (6) and (10) of Figure 16. Observe that $\tau \rightarrow \omega_e(\tau, \omega_{i,E}(\tau))$ is an approximation of the instantaneous frequency $\tau \rightarrow \omega_i(\tau) = \dot{\theta}_i(\tau)$ of the mode v_i .

To describe the remaining components of Figure 16 and simultaneously complete the application of the programming of KMDNets as a synchrosqueezing algorithm and introduce a *max-pool* version of synchrosqueezing, we now introduce the synchrosqueezed energy $\mathcal{S}_E(\tau, \omega)$ and the max-pool energy $\mathcal{S}(\tau, \omega)$: The synchrosqueezed energy $\mathcal{S}_E(\tau, \omega)$ is defined by

$$\int_{\omega_{\min}}^{\omega_{\max}} \varphi(\omega) \mathcal{S}_E(\tau, \omega) d\omega = \int_{\omega_{\min}}^{\omega_{\max}} \varphi(\omega_e(\tau, \omega')) E(\tau, \omega') d\omega'$$

for all regular test function φ , i.e.

$$\mathcal{S}_E(\tau, \omega) = \lim_{\delta \rightarrow 0} \frac{1}{\delta} \int_{\omega': \omega \leq \omega_e(\tau, \omega') \leq \omega + \delta} E(\tau, \omega') d\omega',$$

where numerically we use the approximation

$$\mathcal{S}_E(\tau, \omega) = \frac{1}{\delta} \int_{\omega': \omega \leq \omega_e(\tau, \omega') \leq \omega + \delta} E(\tau, \omega') d\omega' \quad (4.14)$$

for δ small. The function $\mathcal{S}_E(\tau, \omega)$ is closely related to the synchrosqueezed transform introduced in [3] in that the value of $\mathcal{S}_E(\tau, \omega)$ is obtained by transporting the energy $E(\tau, \omega)$ via the map $(\tau, \omega) \rightarrow (\tau, \omega_e(\tau, \omega))$.

Returning to the application, the transport of the energy $E(\tau, \omega)$ via the map $(\tau, \omega) \rightarrow (\tau, \omega_e(\tau, \omega))$ is illustrated for $\tau = 0.6$ by comparing the plots of the functions $\omega \rightarrow \omega_e(0.6, \omega)$ and $\omega \rightarrow E(0.6, \omega)$ in sub-figure (6) with the function $\omega \rightarrow \mathcal{S}_E(0.6, \omega)$ shown in sub-figure (8) of Figure 16. As in [3] the value of $\mathcal{S}_E(\tau, \omega)$ (and thereby the height of the peaks in sub-figure (8)) depends on the discretization and the measure $d\omega'$ used in the integration (4.14). For example, using a logarithmic discretization or replacing the Lebesgue measure $d\omega'$ by $\omega' d\omega'$ in (4.14) will impact the height of those peaks. To avoid this dependence on the choice of measure, we define the max-pool energy

$$\mathcal{S}(\tau, \omega) = \max_{\omega': \omega_e(\tau, \omega') = \omega} E(\tau, \omega'), \quad (4.15)$$

illustrated in sub-figure (9) of Figure 16. Comparing sub-figures (6), (7) and (8) of Figure 16, observe that, although both synchrosqueezing and max-pooling decrease the width of the peaks of the energy plot $\omega \rightarrow E(0.6, \omega)$, only max-squeezing preserves their heights (as noted in [3, Sec. 2] a discretization dependent weighting of $d\omega'$ would have to be introduced to avoid this dependence).

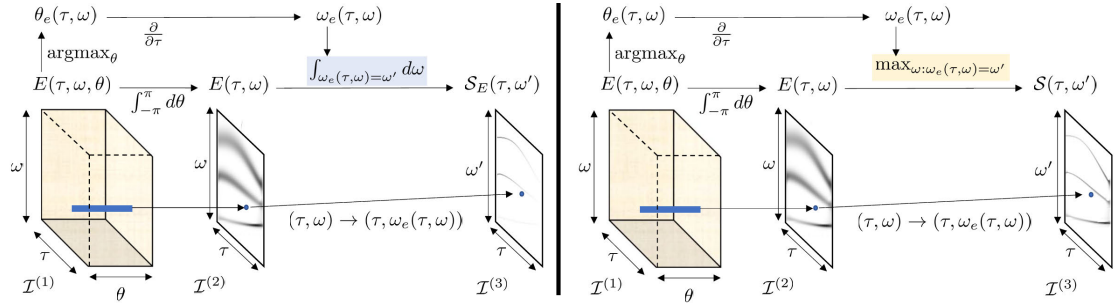


Figure 17: Synchro-squeezed (left) and max-pool (right) energies.

Figure 17 provides an interpretation of the synchrosqueezed and max-pool energies $\mathcal{S}_E(\tau, \omega)$ and $\mathcal{S}(\tau, \omega)$ in the setting of KMDNet programming. The left (synchrosqueezed)

and right (max-pool) sub-figures are identical except for the highlighted portions near their top center. In that interpretation $\mathcal{I}^{(1)}$ and $\mathcal{I}^{(2)}$ are, as in Section 3.5 and modulo the noise mode σ , respectively, the set of time-frequency-phase labels $(\tau, \omega, \theta) \in [0, 1] \times [\omega_{\min}, \omega_{\max}] \times (-\pi, \pi]$ and the set of time-frequency labels $(\tau, \omega) \in [0, 1] \times [\omega_{\min}, \omega_{\max}]$. Modulo the noise label σ , $\mathcal{I}^{(3)}$ is the range of $(\tau, \omega) \rightarrow (\tau, \omega_e(\tau, \omega))$ and the ancestors of $(\tau, \omega') \in \mathcal{I}^{(3)}$ are the (τ, ω) such that $\omega' = \omega_e(\tau, \omega)$. Then, in that interpretation, the synchrosqueezed energy is simply the level 3 energy $E^{(3)}$, whereas $\mathcal{S}(\tau, \omega)$ is the level 3 max-pool energy $\mathcal{S}^{(3)}$. Note that the proposed approach naturally generalizes to the case where the periodic waveform y is known and non-trigonometric by simply replacing the cosine function in (3.24) by y .

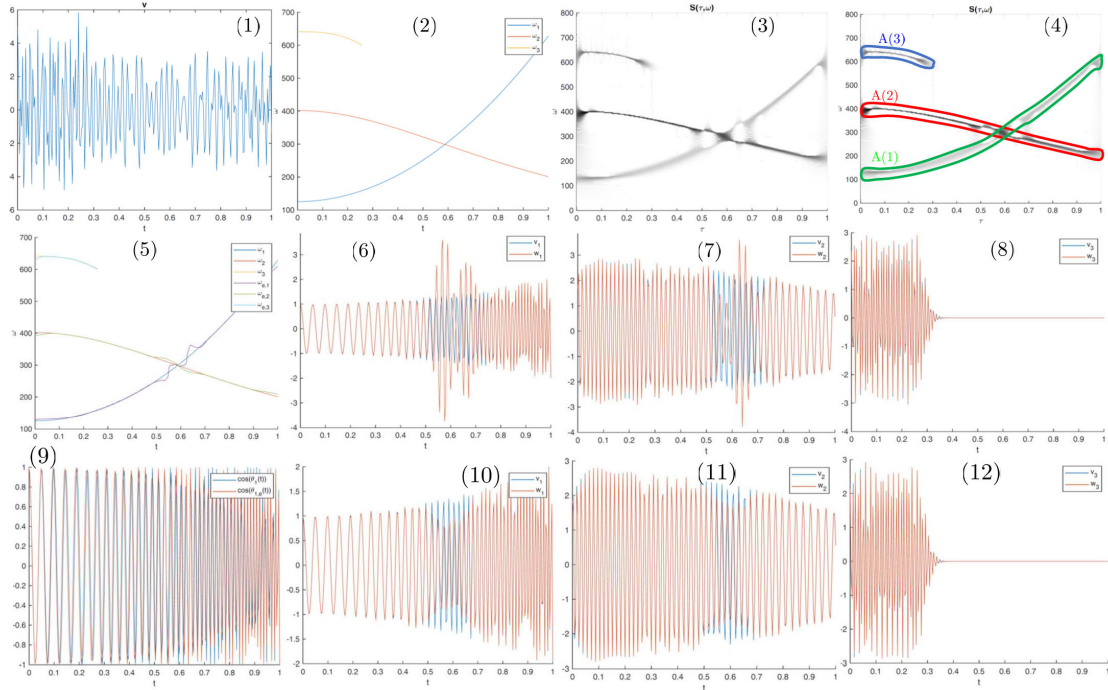


Figure 18: (1) The signal $v = v_1 + v_2 + v_3 + v_\sigma$ where $v_\sigma \sim \mathcal{N}(0, \sigma^2 \delta(s-t))$ and $\sigma = 0.01$ (2) instantaneous frequencies $t \rightarrow \omega_i(t)$ of the modes $i = 1, 2, 3$ (3) $(\tau, \omega) \rightarrow \mathcal{S}(\tau, \omega)$ (4) Sub-domains $A(1), A(2)$ and $A(3)$ of the time-frequency domain (5) approximated instantaneous frequencies $t \rightarrow \omega_{i,e}(t)$ of the modes $i = 1, 2, 3$ (6, 7, 8) v_1, v_2, v_3 and their approximations w_1, w_2, w_3 obtained from the network shown in Figure 19 (9) phase θ_1 and its approximation $\theta_{1,e}$ (10, 11, 12) v_1, v_2, v_3 and their approximations w_1, w_2, w_3 obtained from the network shown in Figure 21.

4.4 Crossing instantaneous frequencies

Let us now demonstrate the effectiveness of the max-pooling technique in its ability to perform mode recovery when the instantaneous frequencies of the modes cross. Consider the noisy signal v illustrated in sub-figure (1) of Figure 18. This signal is composed of 4 modes, $v = v_1 + v_2 + v_3 + v_\sigma$, where $v_\sigma \sim \mathcal{N}(0, \sigma^2 \delta(s - t))$ is a white noise realization with $\sigma = 0.01$. The modes v_1, v_2, v_3 are shown in sub-figures (6), (7), (8) and their instantaneous frequencies $\omega_1, \omega_2, \omega_3$ are shown in sub-figure (2). Note that ω_1 and ω_2 cross each other around $t \approx 0.6$ and v_3 vanishes around $t \approx 0.3$. We now program two KMDNets and describe their accuracy in recovering those modes.

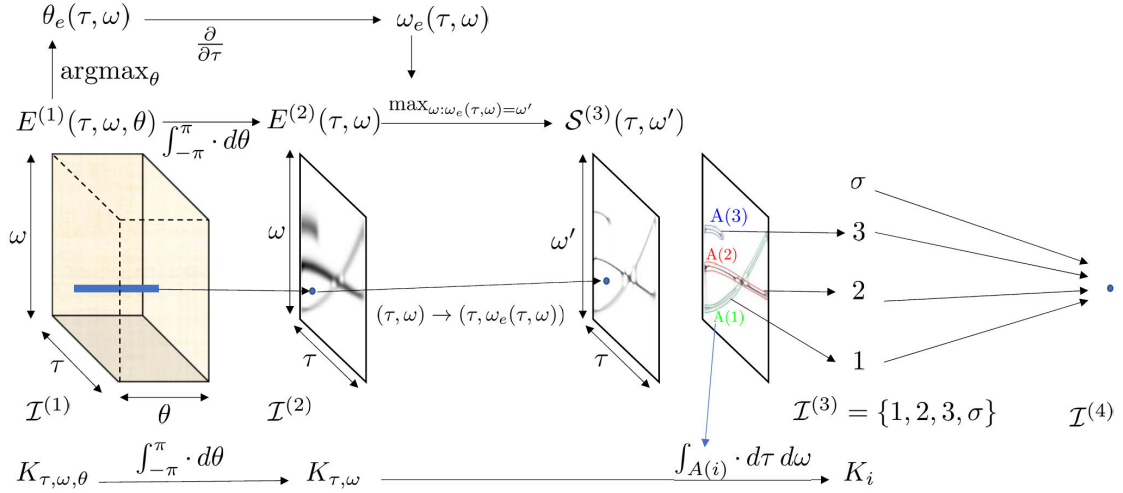


Figure 19: Recovery from domain decomposition. The left-hand side of the figure is that of the right-hand side (corresponding to max-pooling) of Figure 17. The remaining part is obtained by identifying three subsets $A(1), A(2), A(3)$ of the time-frequency domain (τ, ω) and integrating the kernel $K_{\tau, \omega}$ (defined as in (3.31)) over those subsets (as in (3.38)).

The first network, illustrated in Figures 19 and 20 recovers approximations to v_1, v_2, v_3 by identifying three subsets $A(1), A(2), A(3)$ of the time-frequency domain (τ, ω) and integrating the kernel $K_{\tau, \omega}$ (defined as in (3.31)) over those subsets (as in (3.38)). For this example, the subsets $A(1), A(2), A(3)$ are shown in sub-figure (4) of Figure 18 and identified as narrow sausages defined by the peaks of the max-pool energy $\mathcal{S}^{(3)}(\tau, \omega')$ (computed as in (4.15)) shown in sub-figure (3). The corresponding approximations w_1, w_2, w_3 (obtained as in (3.39)) of the modes v_1, v_2, v_3 are shown in sub-figures (6), (7) and (8) of Figure 18. Note the increased approximation error around $t \approx 0.6$ corresponding to the crossing point between ω_1 and ω_2 and $A(1)$ and $A(2)$. The estimated instantaneous frequencies $\omega_{i,e}(\tau) = \omega_e(\tau, \arg\max_{\omega: (\tau, \omega) \in A(i)} \mathcal{S}^{(3)}(\tau, \omega))$ illustrated in sub-

figure (5) of Figure 18 also show an increased estimation error around that crossing point.

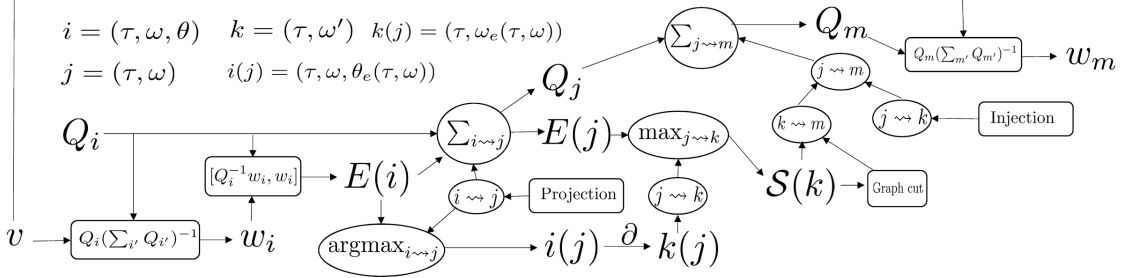


Figure 20: The KMDNet program corresponding to Figure 19. Upper left provides the symbolic connections between the indices i, j, k and the time-frequency parameters along with the functional dependencies $i(j)$ and $k(j)$. Beginning with the input v in the lower left, the operators Q_i corresponding to the baby kernels $K_{\tau, \omega, \theta}$ are used to produce optimal recovery estimates w_i and the corresponding alignment energies $E(i)$. The projection function $j(i)$ taking (τ, ω, θ) to (τ, ω) is the relation $i \rightsquigarrow j$ which determines the integration operation $\int d\theta$ indicated as $\sum_{i \rightsquigarrow j}$ which then determines summed energies $E(j) := \sum_{i \rightsquigarrow j} E(i)$ and covariances $Q_j := \sum_{i \rightsquigarrow j} Q_i$. Moreover, the projection $i \rightsquigarrow j$ also determines a max operation $\arg \max_{\theta}$ which we denote by $\arg \max_{i \rightsquigarrow j}$ and the resulting function $\theta_e(\tau, \omega) := \arg \max_{\theta} E_{\tau, \omega, \theta}$, which determines the functional dependency $i(j) = (\tau, \omega, \theta_e(\tau, \omega))$. This function is then differentiated to obtain the functional relation $k(j) = (\tau, \omega_e(\tau, \omega))$ where $\omega_e(\tau, \omega) := \frac{\partial}{\partial \tau} \theta_e(\tau, \omega)$. This determines the relation $j \rightsquigarrow k$ which determines the maximization operation $\max_{j \rightsquigarrow k}$ that, when applied to the alignment energies $E(j)$, produces the max-pooled energies $S(k)$. These energies are then used to determine a graph cut establishing a relation $k \rightsquigarrow m$ where m is a mode index. Combining this relation with the injection $j \rightsquigarrow k$ determines the relation $j \rightsquigarrow m$, that then determines the summation $\sum_{j \rightsquigarrow m}$ over the preimages of the relation, thus determining operators Q_m indexed by the mode m by $Q_m := \sum_{j \rightsquigarrow m} Q_j$. Optimal recovery is then applied to obtain the estimates $w_m := Q_m(\sum_{m'} Q_{m'})^{-1}$.

The second network, illustrated in Figures 21 and 22, proposes a more robust ap-

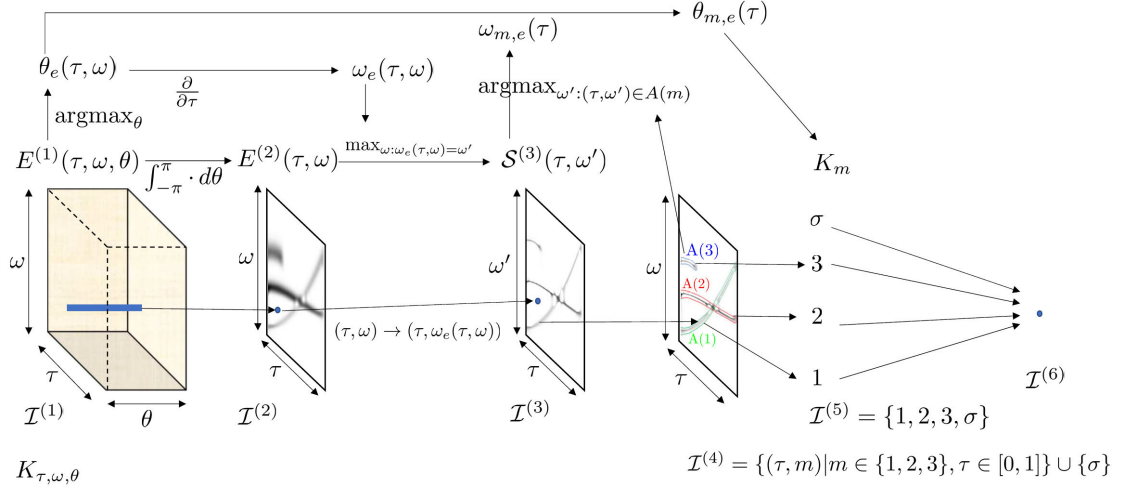


Figure 21: Recovery from instantaneous phases approximations. The left-hand side of the figure is that of the right-hand side (corresponding to max-pooling) of Figure 17 and therefore also that of Figure 19, and proceeding to the right as in Figure 19, the three subsets $A(1), A(2), A(3)$ of the time-frequency domain (τ, ω) and integrating the kernel $K_{\tau, \omega}$ (defined as in (3.31)) over those subsets (as in (3.38)). However, to define the kernels K_m for the final optimal recovery, we define $\omega_{m,e}(\tau) := \arg \max_{\omega': (\tau, \omega') \in A(i)} \mathcal{S}^3(\tau, \omega')$ to produce the θ function for each mode m through $\theta_{m,e}(\tau) = \theta_e(\tau, \omega_{m,e}(\tau))$. These functions are inserted into (4.17) to produce K_m and their associated operators Q_m which are then used in the finally recovery $w_m = Q_m(\sum_{m'} Q_{m'})^{-1}v$.

proach based on the estimates $\theta_{i,e}$ of instantaneous phases θ_i obtained as

$$\theta_{i,e}(\tau) = \theta_e(\tau, \arg \max_{\omega: (\tau, \omega) \in A(i)} \mathcal{S}^3(\tau, \omega)), \quad (4.16)$$

where the $A(i)$ are obtained as in the first network, illustrated in Figure 19, and $\theta_e(\tau, \omega)$, used in the definition (4.16) of $\theta_{e,i}(\tau)$, is identified as in (4.10). To recover the modes v_i , the proposed network proceeds as in Example 2.6 by introducing the kernels

$$K_i(s, t) = e^{-\frac{(t-s)^2}{\gamma^2}} (\cos(\theta_{i,e}(t)) \cos(\theta_{i,e}(s)) + \sin(\theta_{i,e}(t)) \sin(\theta_{i,e}(s))), \quad (4.17)$$

with $\gamma = 0.2$. Defining K_σ as in (3.30), the approximations w_1, w_2, w_3 of the modes v_1, v_2, v_3 , shown in sub-figures (10), (11) and (12) of Figure 18, are obtained as in (3.39) with f defined as the solution of $(K_1 + K_2 + K_3 + K_\sigma)f = v$. Note that the network illustrated in Figure 21 can be interpreted as the concatenation of 2 networks. One aimed at estimating the instantaneous phases and the other aimed at recovering the modes based on those phases. This principle of network concatenation is evidently generic.

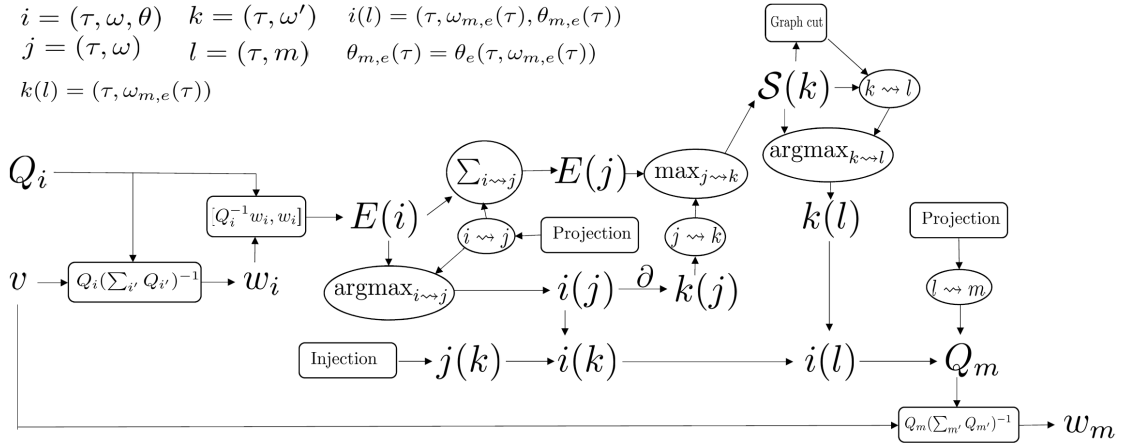


Figure 22: The KMDNet program corresponding to Figure 21. Upper left provides the symbolic connections between the indices i, j, k, l and the time-frequency parameters along with the functional dependencies $i(l)$ and $k(l)$ and the definition of $\theta_{m,e}$. Beginning with the input v in the lower left, ignoring the bottom two rows for the moment, we begin very much as in Figure 20 moving to the right until the determination of the energies $\mathcal{S}(k)$, the determination of a graph cut and its resulting $k \rightsquigarrow l$, and the resulting arg max relation $k(l) := \arg \max_{k \rightsquigarrow l} \mathcal{S}(k)$ which amounts to $k(l) = (\tau, \omega_{m,e}(\tau))$. Returning to the second row from the bottom, we compose the functional relations of the injection $j(k)$ and the arg max function $i(j)$ determined by the relation $i \rightsquigarrow j$ and the energy $E(i)$, to obtain $i(k)$ and then compose this with the argmax function $k(l)$ to produce the functional dependence $i(l)$ defined by $i(l) = (\tau, \omega_{m,e}(\tau), \theta_{m,e}(\tau))$. Using the projection $l \rightsquigarrow m$, this determines the function $\theta_{m,e}(\cdot)$ corresponding to the mode label m . These functions are inserted into (4.17) to produce K_m and their associated operators Q_m which are then used in the finally recovery $w_m = Q_m(\sum_{m'} Q_{m'})^{-1}v$.

5 Alignments calculated in L^2

The calculation of the energies for our prototypical application was done with respect to the inner product defined by the inverse of the operator associated with K defined in (3.29), i.e. the energy of the mode (τ, ω, θ) was defined as $E(\tau, \omega, \theta) = v^T K^{-1} K_{\tau, \omega, \theta} K^{-1} v$ with $K_{\tau, \omega, \theta}$ defined in (3.26). The computational complexity of the method can be accelerated by (1) using the L^2 inner product instead of the one defined by K^{-1} (i.e. defining the energy of the mode (τ, ω, θ) by $E_2(\tau, \omega, \theta) = v^T K_{\tau, \omega, \theta} v$ (2) localizing this calculation in a time-window centered around τ and of width proportional to $1/\omega$.

Our experiments shows that simplification lowers the computational complexity of the proposed approach without impacting its accuracy. Three points justify this observation: (1) Replacing E by E_2 is equivalent to calculating mean-squared alignments with respect to the L^2 -scalar product instead of the one induced by the inverse of the operator

defined by K (2) In the limit where $\sigma \rightarrow \infty$ we have $E \approx \sigma^{-4}E_2$, therefore E and E_2 are proportional to each other in the high noise regime (3) If $\omega_{\min} = 0$ and $\omega_{\max} = \infty$ then K_u defined by (3.27) is the identity operator on L^2 . We will now rigorously show that point (3) holds true when the periodic waveform is trigonometric and show in Section 6 that this results holds true independently of the periodic waveform being used.

Let us recall the Schwartz class of test functions

$$\mathcal{S} := \{f \in C^\infty(\mathbb{R}) : \sup_{x \in \mathbb{R}} |x^{m_1} D^{m_2} f(x)| < \infty, m_1, m_2 \in \mathbf{N}\}$$

and the confluent hypergeometric function ${}_1F_1$, defined by

$${}_1F_1(\alpha, \gamma; z) = 1 + \frac{\alpha}{\gamma} \frac{z}{1!} + \frac{\alpha(\alpha+1)}{\gamma(\gamma+1)} \frac{z^2}{2!} + \frac{\alpha(\alpha+1)(\alpha+2)}{\gamma(\gamma+1)(\gamma+2)} \frac{z^3}{3!} + \dots,$$

see e.g. see Gradshteyn and Ryzhik [10, Sec. 9.21].

Theorem 5.1. *Consider extending the definition (3.27) of the kernel K_u so that the range of ω is extended from $[0, 1]$ to \mathbb{R}_+ and that of τ is extended from $[0, 1]$ to \mathbb{R} , so that*

$$K_\beta(s, t) = \int_{-\pi}^{\pi} \int_{\mathbb{R}_+} \int_{\mathbb{R}} K_{\tau, \omega, \theta}(s, t) d\tau d\omega d\theta, \quad s, t \in \mathbb{R},$$

where, as before,

$$K_{\tau, \omega, \theta}(s, t) := \chi_{\tau, \omega, \theta}(s) \chi_{\tau, \omega, \theta}(t), \quad s, t \in \mathbb{R},$$

but where we have introduced a perturbation parameter $0 \leq \beta \leq 1$ defining the Gabor wavelets

$$\chi_{\tau, \omega, \theta}(t) := \left(\frac{2}{\alpha^2 \pi^3} \right)^{\frac{1}{4}} \omega^{\frac{1-\beta}{2}} \cos(\omega(t-\tau) + \theta) e^{-\frac{\omega^2(t-\tau)^2}{\alpha^2}}, \quad t \in \mathbb{R}, \quad (5.1)$$

defining the baby kernels. Defining the scaling constant

$$H(\beta) := 2^{\beta-1} \sqrt{\pi} (\sqrt{2}\alpha)^{1-\beta} \Gamma\left(\frac{\beta}{2}\right) e^{-\frac{\alpha^2}{2}} {}_1F_1\left(\frac{\beta}{2}, \frac{1}{2}; \frac{\alpha^2}{2}\right),$$

let \mathcal{K}_β denote the integral operator

$$(\mathcal{K}_\beta f)(s) := \frac{1}{H(\beta)} \int_{\mathbb{R}} K_\beta(s, t) f(t) dt$$

associated to the kernel K_β scaled by $H(\beta)$. Then we have the semigroup property

$$\mathcal{K}_{\beta_1} \mathcal{K}_{\beta_2} f = \mathcal{K}_{\beta_1 + \beta_2} f, \quad f \in \mathcal{S}, \quad \beta_1, \beta_2 > 0, \beta_1 + \beta_2 < 1,$$

and

$$\lim_{\beta \rightarrow 0} (\mathcal{K}_\beta f)(x) = f(x), \quad x \in \mathbb{R}, \quad f \in \mathcal{S}$$

where the limit is taken from above.

6 Universality of the aggregated kernel

Let

$$y(t) := \sum_{-N}^N c_n e^{int}$$

be the Fourier expansion of a general 2π periodic complex-valued waveform and use it to define wavelets

$$\chi_{\tau,\omega,\theta}(t) := \omega^{\frac{1-\beta}{2}} y(\omega(t-\tau) + \theta) e^{-\frac{\omega^2}{\alpha^2}|t-\tau|^2}$$

as in the β -parameterized wavelet versions of (3.24) in Theorem 5.1, using the waveform y instead of the cosine. The following lemma evaluates the mama kernel

$$K_\beta(s, t) := \Re \int_{-\pi}^{\pi} \int_{\mathbb{R}_+} \int_{\mathbb{R}} \chi_{\tau,\omega,\theta}(s) \chi_{\tau,\omega,\theta}^*(t) d\tau d\omega d\theta. \quad (6.1)$$

Lemma 6.1. *Define the norm*

$$\|y\|^2 := \sum_{n=-N}^N e^{-\frac{|n|\alpha^2}{2}} |c_n|^2 \quad (6.2)$$

of the base waveform y . We have

$$K_\beta(s, t) = 2\pi |s-t|^{\beta-1} \sum_{n=-N}^N a_n(s, t) |c_n|^2$$

where

$$a_n(s, t) = \frac{\alpha\sqrt{\pi}}{2\sqrt{2}} (\sqrt{2}\alpha)^{1-\beta} \Gamma\left(\frac{1-\beta}{2}\right) e^{-\frac{|n|\alpha^2}{2}} {}_1F_1\left(\frac{\beta}{2}; \frac{1}{2}; \frac{|n|\alpha^2}{2}\right).$$

In particular, at $\beta = 0$ we have

$$K_0(s, t) = \alpha^2 \pi^2 |s-t|^{-1} \|y\|^2.$$

6.1 Characterizing the norm $\sum_{n=-N}^N e^{-\frac{|n|\alpha^2}{2}} |c_n|^2$

The norm (6.2) of the function $y(t) := \sum_{-N}^N c_n e^{int}$ is expressed in terms of its Fourier coefficients c_n . The following lemma evaluates it directly in terms of the function y .

Lemma 6.2. *The norm (6.2) of the function $y(t) := \sum_{-N}^N c_n e^{int}$ satisfies*

$$\|y\|^2 = \int_{-\pi}^{\pi} \int_{-\pi}^{\pi} G(t, t') y(t) y^*(t') dt dt'$$

where

$$G(t, t') = 2\pi \frac{\sinh\left(\frac{\alpha^2}{2}\right)}{\cosh\left(\frac{\alpha^2}{2}\right) - \cos(t-t')}, \quad t, t' \in [-\pi, \pi].$$

Remark 6.3. The norm (6.2) is clearly insensitive to the size of the high frequency (large n) components $c_n e^{int}$ of y . On the other hand, the alternative representation of this norm in Lemma 6.2 combined with the fact that the kernel G satisfies

$$\frac{\sinh(\frac{\alpha^2}{2})}{\cosh(\frac{\alpha^2}{2}) + 1} \leq G(t, t') \leq 2\pi \frac{\sinh(\frac{\alpha^2}{2})}{\cosh(\frac{\alpha^2}{2}) - 1}, \quad t, t' \in [-\pi, \pi],$$

which, for $\alpha \geq 10$, implies

$$1 - 10^{-21} \leq G(t, t') \leq 1 + 10^{-21}, \quad t, t' \in [-\pi, \pi],$$

implies that

$$\left| \|y\|^2 - \left| \int_{-\pi}^{\pi} y(t) dt \right|^2 \right| \leq 10^{-21} \left| \int_{-\pi}^{\pi} |y(t)| dt \right|^2$$

that is, $\|y\|^2$ is exponentially close to the square of its integral.

7 Non-trigonometric waveform and iterated KMD

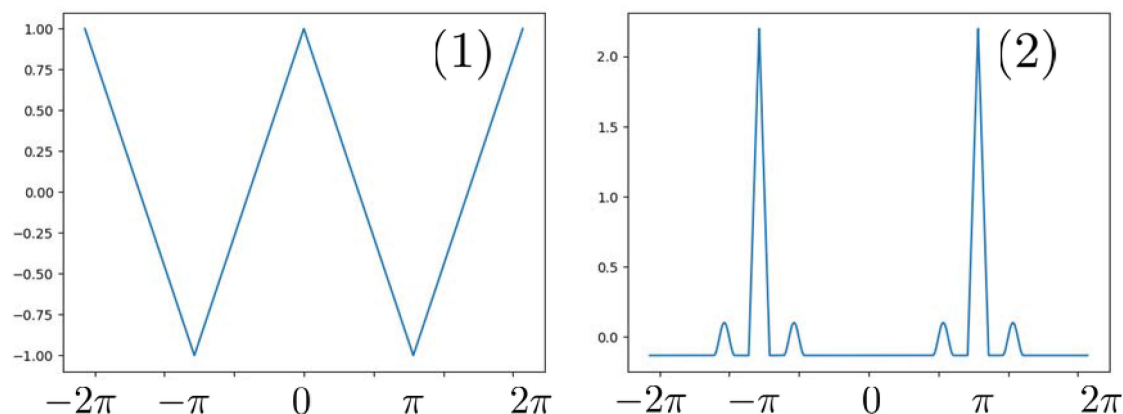


Figure 23: (1) Triangle base waveform (2) EKG base waveform.

We will now consider the mode recovery Problem 1 generalized to the case where the periodic waveform of each mode is the same known, possibly non-trigonometric, square-integrable 2π -periodic function $t \rightarrow y(t)$, which we will refer to as the *base waveform*. The objective of this problem can be loosely expressed as solving the following generalization of Problem 1 towards the resolution of the more general Problem 2. We now switch the time domain from $[0, 1]$ to $[-1, 1]$.

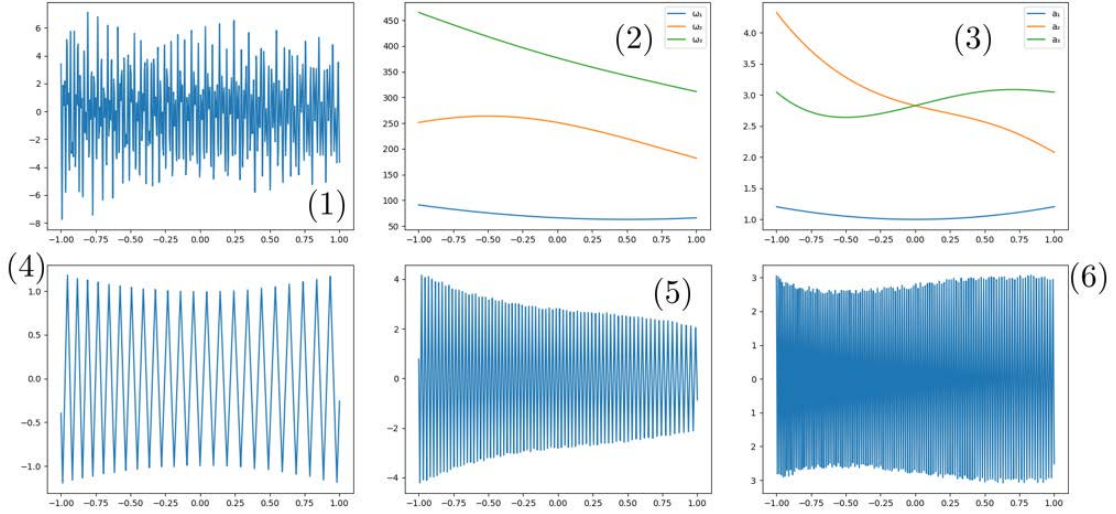


Figure 24: (1) Signal v (2) Instantaneous frequencies $\omega_i := \dot{\theta}_i$ (3) Amplitudes a_i (4, 5, 6) Modes v_1, v_2, v_3 .

Problem 4. For $m \in \mathbb{N}^*$, let a_1, \dots, a_m be piecewise smooth functions on $[-1, 1]$, let $\theta_1, \dots, \theta_m$ be strictly positive and increasing functions on $[-1, 1]$, and let y be a square-integrable 2π -periodic function. Assume that m and the a_i, θ_i are unknown and the base waveform y is known. Given the observation $v(t) = \sum_{i=1}^m a_i(t)y(\theta_i(t))$ (for $t \in [-1, 1]$) recover the modes $v_i := a_i(t)y(\theta_i(t))$.

Example 7.1. Figure 23 shows two 2π -periodic base waveforms (triangle and EKG) which we will use in our numerical experiments/illustrations. The EKG (-like) waveform is $(y_{EKG}(t) - (2\pi)^{-1} \int_0^{2\pi} y_{EKG}(s) ds) / \|y_{EKG}\|_{L^2([0, 2\pi])}$ with $y_{EKG}(t)$ defined on $[0, 2\pi)$ as (1) $0.3 - |t - \pi|$ for $|t - \pi| < 0.3$ (2) $0.03 \cos^2(\frac{\pi}{0.6}(t - \pi + 1))$ for $|t - \pi + 1| < 0.3$ (3) $0.03 \cos^2(\frac{\pi}{0.6}(t - \pi - 1))$ for $|t - \pi - 1| < 0.3$ and (4) 0 otherwise.

Our approach, summarized in Algorithm 2 and explained in the following sections, will be to (1) use the max-pool energy \mathcal{S} (4.15) to obtain, using (4.16), an estimate of the phase $\theta_{\text{low}}(t)$ associated with the lowest instantaneous frequency $\omega_{\text{low}} = \dot{\theta}_{\text{low}}$ (as described in Section 7.2) (2) iterate a *micro-local* KMD (presented in Section 7.1) of the signal v to obtain a highly accurate estimate of the phase/amplitude θ_i, a_i of the corresponding mode v_i (this iteration can achieve near machine-precision accuracies when the instantaneous frequencies are separated) (3) Peel off the mode v_i from v (4) iterate to obtain all the modes (5) perform a last micro-local KMD of the signal for higher accuracy. To illustrate this approach, in the next two sections we will apply it to the signals v displayed in Figures 24 and 25, where the modes of Figure 24 are triangular and those of Figure 25 are EKG.

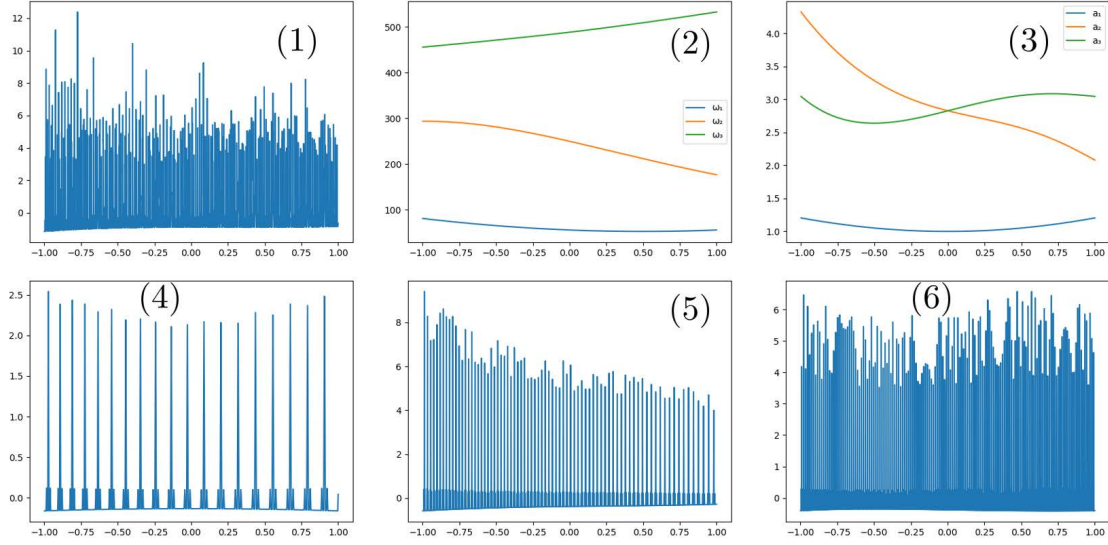


Figure 25: (1) Signal v (2) Instantaneous frequencies $\omega_i := \dot{\theta}_i$ (3) Amplitudes a_i (4, 5, 6) Modes v_1, v_2, v_3 .

7.1 Micro-local KMD

We will now describe the micro-local KMD which takes a time τ , a model (estimate) phase function $t \rightarrow \theta_e(t)$ and a signal $v(t) := a(t) \cos(\theta(t))$ as inputs and produces, as outputs, (1) an estimate $a(\tau, \theta_e, v)$ of the amplitude $a(\tau)$ of the mode v and (2) a correction $\delta\theta(\tau, \theta_e, v)$ determining an estimate $\theta(\tau) \sim \theta_e(\tau) + \delta\theta(\tau, \theta_e, v)$ of the mode phase function θ .

Indeed, given $\alpha > 0$, $\tau \in [-1, 1]$, a differentiable function $t \rightarrow \theta_e(t)$ on $[-1, 1]$, and $n \in \{0, 1, 2\}$, let $\chi_{n,c}^{\tau, \theta_e}$ and $\chi_{n,s}^{\tau, \theta_e}$ be the wavelets defined by

$$\begin{aligned} \chi_{n,c}^{\tau, \theta_e}(t) &:= \cos(\theta_e(t))(t - \tau)^n e^{-\left(\frac{\dot{\theta}_e(\tau)(t-\tau)}{\alpha}\right)^2} \\ \chi_{n,s}^{\tau, \theta_e}(t) &:= \sin(\theta_e(t))(t - \tau)^n e^{-\left(\frac{\dot{\theta}_e(\tau)(t-\tau)}{\alpha}\right)^2}, \end{aligned} \quad (7.1)$$

where the derivative $\dot{\theta}_e(\tau)$ of θ_e at time τ is the instantaneous frequency, and let ξ_{τ, θ_e} be the Gaussian process defined by

$$\xi_{\tau, \theta_e}(t) := \sum_{n=0}^2 (X_{n,c} \chi_{n,c}^{\tau, \theta_e}(t) + X_{n,s} \chi_{n,s}^{\tau, \theta_e}(t)), \quad (7.2)$$

where $X_{n,c}, X_{n,s}$ are independent $\mathcal{N}(0, 1)$ random variables. Let v_{τ, θ_e} be the Gaussian windowed signal defined by

$$v_{\tau, \theta_e}(t) = e^{-\left(\frac{\dot{\theta}_e(\tau)(t-\tau)}{\alpha}\right)^2} v(t), \quad t \in [-1, 1], \quad (7.3)$$

and, for $(n, j) \in \{0, 1, 2\} \times \{c, s\}$ ³,

$$Z_{n,j}(\tau, \theta_e, v) := \lim_{\sigma \downarrow 0} \mathbb{E}[X_{n,j} | \xi_{\tau, \theta_e} + \xi_\sigma = v_{\tau, \theta_e}], \quad (7.4)$$

where ξ_σ is white noise, independent of ξ_{τ, θ_e} , with variance σ^2 . To compute $Z_{n,j}$, observe that since both ξ_{τ, θ_e} and ξ_σ are Gaussian fields, it follows from (2.22) that

$$\mathbb{E}[\xi_{\tau, \theta_e} | \xi_{\tau, \theta_e} + \xi_\sigma] = A_\sigma(\xi_{\tau, \theta_e} + \xi_\sigma)$$

for the linear mapping

$$A_\sigma = Q_{\tau, \theta_e} (Q_{\tau, \theta_e} + \sigma^2 I)^{-1},$$

where $Q_{\tau, \theta_e} : L^2 \rightarrow L^2$ is the covariance operator of the Gaussian field ξ_{τ, θ_e} and $\sigma^2 I$ is the covariance operator of ξ_σ . Using the characterization of the limit of Tikhonov regularization as the Moore-Penrose inverse, see e.g. Barata and Hussein [2, Thm. 4.3], along with the orthogonal projections connected with the Moore-Penrose inverse, we conclude that $\lim_{\sigma \rightarrow 0} A_\sigma = P_\chi$ and therefore

$$\lim_{\sigma \rightarrow 0} \mathbb{E}[\xi_{\tau, \theta_e} | \xi_{\tau, \theta_e} + \xi_\sigma] = P_\chi(\xi_{\tau, \theta_e} + \xi_\sigma), \quad (7.5)$$

where P_χ is the L^2 orthogonal projection onto the span $\chi := \text{span}\{\chi_{n,c}, \chi_{n,s}, n = 0, 1, 2\}$.

Since the definition (7.2) can be written $\xi_{\tau, \theta_e} = \sum_{n,j} X_{n,j} \chi_{n,j}^{\tau, \theta_e}$, summing (7.4) and using (7.5), we obtain

$$\sum_{n,j} Z_{n,j}(\tau, \theta_e, v) \chi_{n,j}^{\tau, \theta_e}(t) = P_\chi v_{\tau, \theta_e}(t), \quad t \in [-1, 1]. \quad (7.6)$$

Consider the vector function $Z(\tau, \theta_e, v) \in \mathbb{R}^6$ with components $Z_{n,j}(\tau, \theta_e, v)$, the 6 dimensional Gaussian random vector X with components $X_{n,j}$, $(n, j) \in \{0, 1, 2\} \times \{c, s\}$, and the 6×6 matrix A^{τ, θ_e} defined by $A_{(n,j), (n',j')}^{\tau, \theta_e} := \langle \chi_{n,j}^{\tau, \theta_e}, \chi_{n',j'}^{\tau, \theta_e} \rangle_{L^2}$. Straightforward linear algebra along with (7.6) establish that the vector $Z(\tau, \theta_e, v)$ can be computed as the solution of the linear system

$$A^{\tau, \theta_e} Z(\tau, \theta_e, v) = b^{\tau, \theta_e}(v), \quad (7.7)$$

where $b^{\tau, \theta_e}(v)$ is the \mathbb{R}^6 vector with components $b_{n,j}^{\tau, \theta_e}(v) := \langle \chi_{n,j}^{\tau, \theta_e}, v_{\tau, \theta_e} \rangle_{L^2}$. See sub-figures (1) and (2) of both the top and bottom of Figure 26 for illustrations of the windowed signal $v_{\tau, \theta_e}(t)$ and of its projection $\lim_{\sigma \downarrow 0} \mathbb{E}[\xi_{\tau, \theta_e} | \xi_{\tau, \theta_e} + \xi_\sigma = v_{\tau, \theta_e}]$ in (7.5) corresponding to the signals v displayed in Figures 24 and 25.

Now suppose that

$$v(t) = a(t) \cos(\theta(t)),$$

³Experimental evidence indicates that the extra fitting power obtained using $n \in \{0, 1, 2\}$ versus $n = 0$ or $n \in \{0, 1\}$ provides better results. The quantitative analysis of these options we do not consider here.

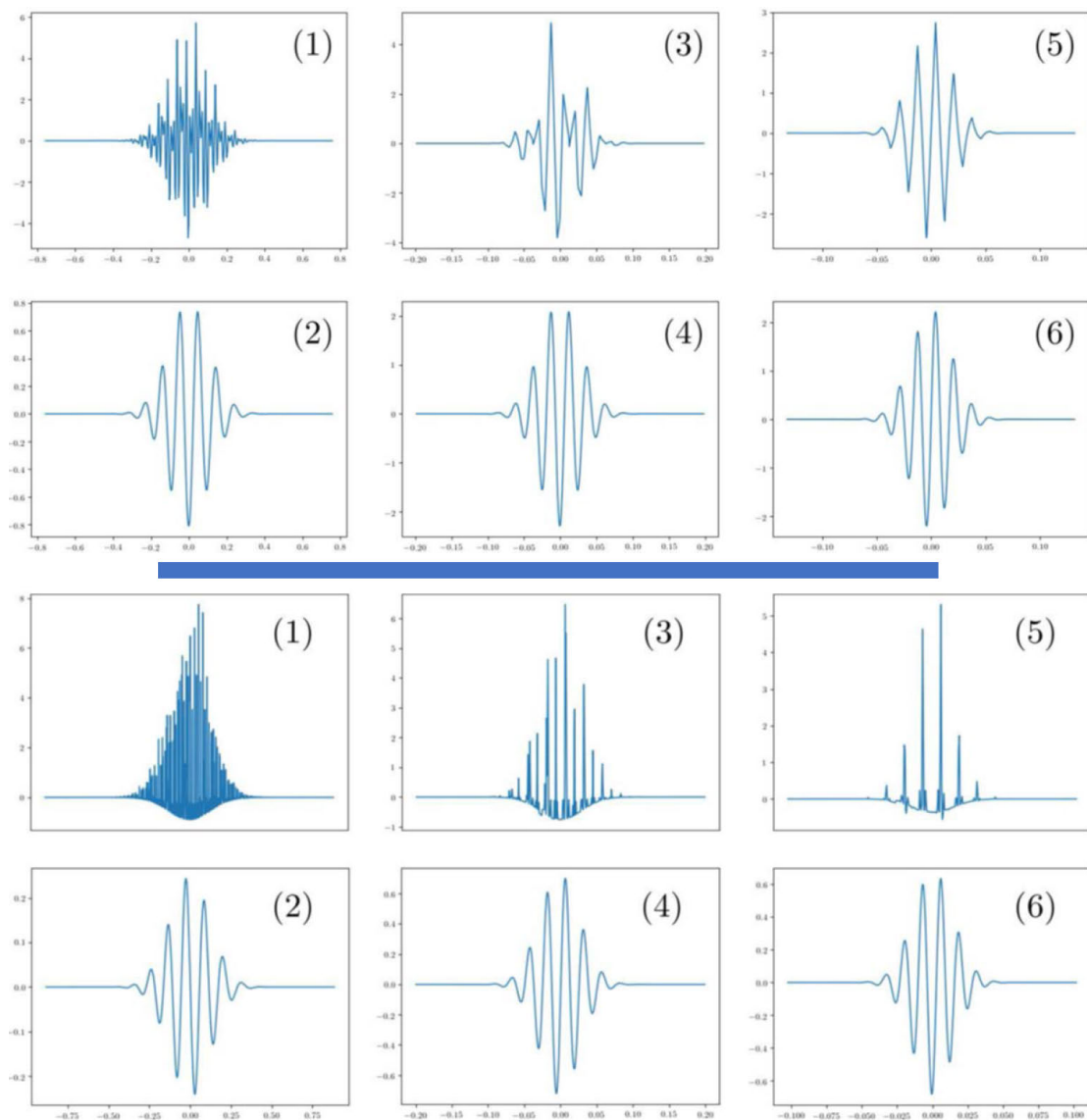


Figure 26: Top: v is as in Figure 24 (the periodic waveform is triangular). Bottom: v is as in Figure 25 (the periodic waveform is EKG). Both top and bottom: (1) The windowed signal $v_{\tau, \theta_{1,e}}(t)$ (2) $\lim_{\sigma \downarrow 0} \mathbb{E}[\xi_{\tau, \theta_{1,e}} | \xi_{\tau, \theta_{1,e}} + \xi_{\sigma} = v_{\tau, \theta_{1,e}}]$ (3) $(v - v_{1,e})_{\tau, \theta_{2,e}}(t)$ (4) $\lim_{\sigma \downarrow 0} \mathbb{E}[\xi_{\tau, \theta_{2,e}} | \xi_{\tau, \theta_{2,e}} + \xi_{\sigma} = (v - v_{1,e})_{\tau, \theta_{2,e}}]$ (5) $(v - v_{1,e} - v_{2,e})_{\tau, \theta_{3,e}}(t)$ (6) $\lim_{\sigma \downarrow 0} \mathbb{E}[\xi_{\tau, \theta_{2,e}} | \xi_{\tau, \theta_{3,e}} + \xi_{\sigma} = (v - v_{1,e} - v_{2,e})_{\tau, \theta_{3,e}}]$.

where the model θ_e is some approximation of the unknown θ and a oscillates slower than

θ , so that

$$v_{\tau, \theta_e}(t) = e^{-\left(\frac{\theta_e(\tau)(t-\tau)}{\alpha}\right)^2} a(t) \cos(\theta(t)), \quad (7.8)$$

and consider the modified function

$$\bar{v}_{\tau, \theta_e}(t) = e^{-\left(\frac{\theta_e(\tau)(t-\tau)}{\alpha}\right)^2} \left(a(\tau) + \dot{a}(\tau)(t-\tau) + \frac{1}{2} \ddot{a}(\tau)(t-\tau)^2 \right) \cos(\theta(t)) \quad (7.9)$$

obtained by replacing the function a with the first three terms of its Taylor series about τ . In what follows, we will use the expression \sim to articulate an informal approximation analysis. All these ‘‘approximations’’ will be quantified when we proceed to a quantitative performance analysis of our methods. It is clear that $\bar{v}_{\tau, \theta_e} \in \chi$ and, since α is small and θ_e is positive and bounded away from 0, that $\langle \chi_{n,j}, v_{\tau, \theta_e} - \bar{v}_{\tau, \theta_e} \rangle_{L^2} \sim 0$, and therefore $P_\chi v_{\tau, \theta_e} \sim \bar{v}_{\tau, \theta_e}$, which implies that $(P_\chi v_{\tau, \theta_e})(t) \sim \bar{v}_{\tau, \theta_e}(t)$, $t \in [-1, 1]$, and therefore (7.6) implies that

$$\sum_{n', j'} Z_{n', j'}(\tau, \theta_e, v) \chi_{n', j'}^{\tau, \theta_e}(t) \sim e^{-\left(\frac{\theta_e(\tau)(t-\tau)}{\alpha}\right)^2} \left(a(\tau) + \dot{a}(\tau)(t-\tau) + \frac{1}{2} \ddot{a}(\tau)(t-\tau)^2 \right) \cos(\theta(t)) \quad (7.10)$$

for all $t \in [-1, 1]$. Let $B_\epsilon(\tau)$ be the open ball about τ of radius ϵ and select ϵ small enough so that (7.10) implies that

$$\sum_{n', j'} Z_{n', j'}(\tau, \theta_e, v) \chi_{n', j'}^{\tau, \theta_e}(t) \sim e^{-\left(\frac{\theta_e(\tau)(t-\tau)}{\alpha}\right)^2} a(\tau) \cos(\theta(t)), \quad t \in B_\epsilon(\tau). \quad (7.11)$$

Furthermore, observing that the definition (7.1) of $\chi_{n,c}^{\tau, \theta_e}$ and $\chi_{n,s}^{\tau, \theta_e}$ implies that we can further reduce the size of ϵ so that, for $n > 0$, $\chi_{n,c}^{\tau, \theta_e}$ and $\chi_{n,s}^{\tau, \theta_e}$ are small for $t \in B_\epsilon(\tau)$, so that consequently

$$\sum_{j'} Z_{0, j'}(\tau, \theta_e, v) \chi_{0, j'}^{\tau, \theta_e}(t) \sim e^{-\left(\frac{\theta_e(\tau)(t-\tau)}{\alpha}\right)^2} a(\tau) \cos(\theta(t)), \quad t \in B_\epsilon(\tau), \quad (7.12)$$

which implies that

$$Z_{0,c}(\tau, \theta_e, v) \cos(\theta_e(t)) + Z_{0,s}(\tau, \theta_e, v) \sin(\theta_e(t)) \sim a(\tau) \cos(\theta(t)), \quad t \in B_\epsilon(\tau), \quad (7.13)$$

for ϵ small enough. Setting $\theta_\delta := \theta - \theta_e$ as the approximation error, using the cosine sum formula $\cos \theta = \cos(\theta_\delta + \theta_e) = \cos \theta_\delta \cos \theta_e - \sin \theta_\delta \sin \theta_e$, we obtain

$$Z_{0,c}(\tau, \theta_e, v) \cos(\theta_e(t)) + Z_{0,s}(\tau, \theta_e, v) \sin(\theta_e(t)) = a(\tau) (\cos(\theta_\delta(t)) \cos(\theta_e(t)) - \sin(\theta_\delta(t)) \sin(\theta_e(t))).$$

Moreover, the smoothness of θ_δ implies, further reducing the size of ϵ , that $\theta_\delta(t) \sim \theta_\delta(\tau)$, $t \in B_\epsilon(\tau)$, so that, for all $t \in B_\epsilon(\tau)$, we have

$$Z_{0,c}(\tau, \theta_e, v) \cos(\theta_e(t)) + Z_{0,s}(\tau, \theta_e, v) \sin(\theta_e(t)) \sim a(\tau) (\cos(\theta_\delta(\tau)) \cos(\theta_e(t)) - \sin(\theta_\delta(\tau)) \sin(\theta_e(t))),$$

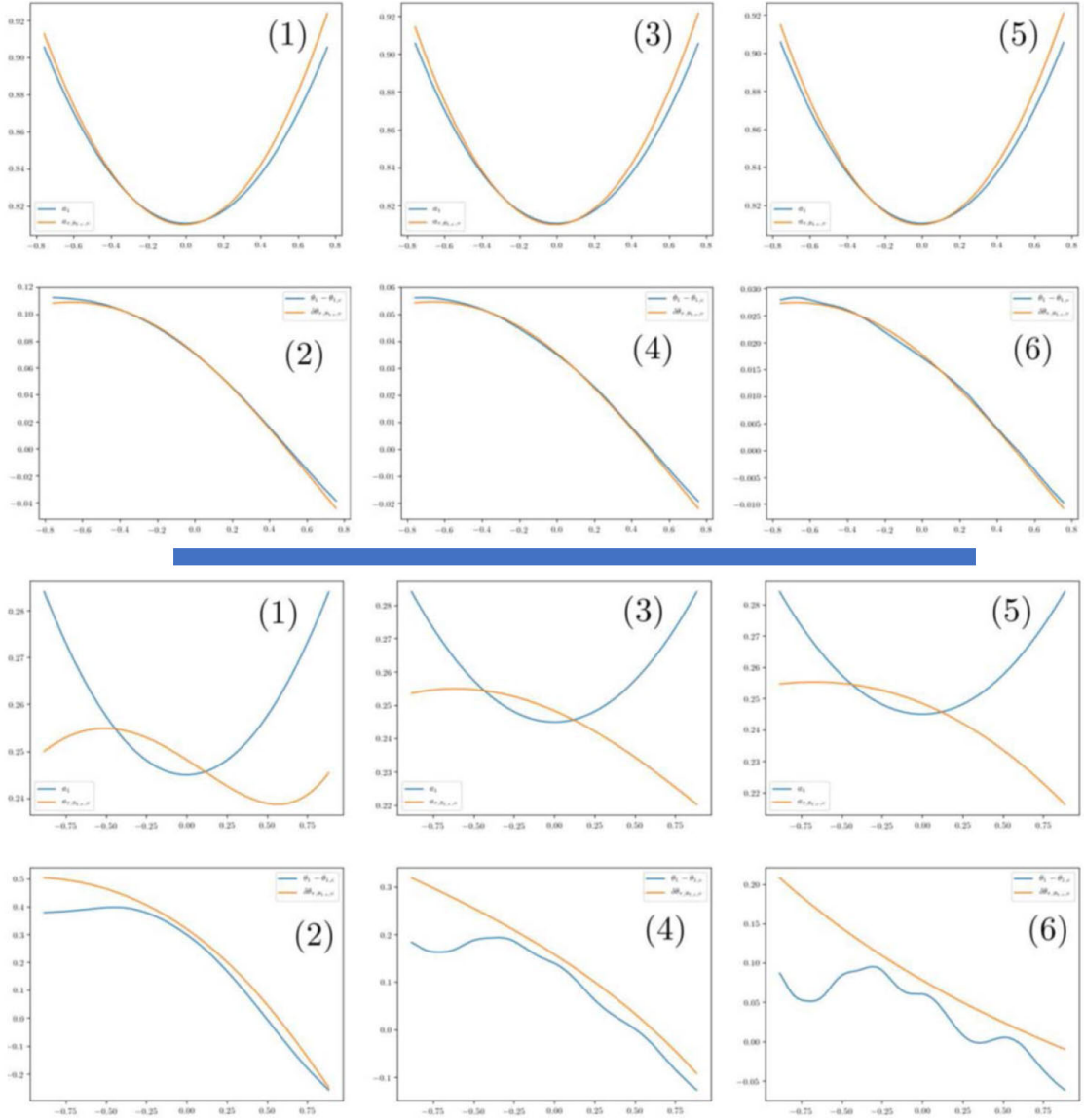


Figure 27: Top: v is as in Figure 24 (the periodic waveform is triangular). Bottom: v is as in Figure 25 (the periodic waveform is EKG). Both top and bottom: $\tau = 0$. (1) the amplitude of the first mode $a_1(t)$ and its local Gaussian regression estimation $a(\tau, \theta_{1,e}, v)(t)$ (2) the error in estimated phase of the first mode $\theta_1(t) - \theta_{1,e}(t)$ and its local Gaussian regression $\delta\theta(\tau, \theta_{1,e}, v)(t)$ (3, 4) are as (1,2) with v and $\theta_{1,e}$ replaced by $v - v_{1,e}$ and $\theta_{2,e}$ (5,6) are as (1,2) with v and $\theta_{1,e}$ replaced by $v - v_{1,e} - v_{2,e}$ and $\theta_{3,e}$.

which, since $\dot{\theta}_e(t)$ positive and bounded away from 0, implies that

$$\begin{aligned} Z_{0,c}(\tau, \theta_e, v) &\sim a(\tau) \cos(\theta_\delta(\tau)) \\ Z_{0,s}(\tau, \theta_e, v) &\sim -a(\tau) \sin(\theta_\delta(\tau)). \end{aligned}$$

Consequently, writing

$$\begin{aligned} a(\tau, \theta_e, v) &:= \sqrt{Z_{0,c}^2(\tau, \theta_e, v) + Z_{0,s}^2(\tau, \theta_e, v)} \\ \delta\theta(\tau, \theta_e, v) &:= \text{atan2}(-Z_{0,s}(\tau, \theta_e, v), Z_{0,c}(\tau, \theta_e, v)), \end{aligned}$$

we obtain that $a(\tau, \theta_e, v) \sim a(\tau)$ and $\delta\theta(\tau, \theta_e, v) \sim \theta_\delta(\tau)$. We will therefore use $a(\tau, \theta_e, v)$ to estimate the amplitude $a(\tau)$ of the mode v using the model estimate θ_e and $\delta\theta(\tau, \theta_e, v)$ to estimate the mode phase θ through $\theta(\tau) = \theta_e(\tau) + \theta_\delta(\tau) \sim \theta_e(\tau) + \delta\theta(\tau, \theta_e, v)$. Iterating this refinement process will allow us to achieve near machine-precision accuracies in our phase/amplitude estimates. See sub-figures (1) and (2) of the top and bottom of Figure 27 for illustrations of $a(t)$, $a_{\tau, \theta_e, v}(t)$, $\theta(t) - \theta_e(t)$ and $\delta\theta(\tau, \theta_e, v)(t)$ corresponding to the first mode v_1 of the signals v displayed in sub-figure (4) of Figures 24 and 25.

7.2 The lowest instantaneous frequency

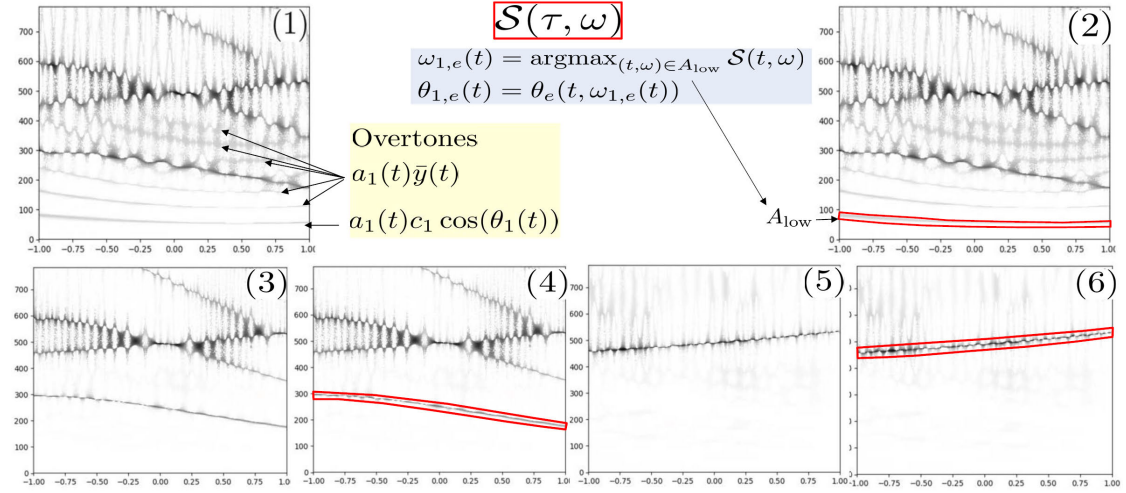


Figure 28: Max-squeezing with the EKG base waveform and derivation of the instantaneous phase estimates $\theta_{i,e}$. (1,2) $(\tau, \omega) \rightarrow \mathcal{S}(\tau, \omega, v)$ and identification of A_{low} (3, 4) $(\tau, \omega) \rightarrow \mathcal{S}(\tau, \omega, v - v_{1,e})$ and identification of its A_{low} (5,6) $(\tau, \omega) \rightarrow \mathcal{S}(\tau, \omega, v - v_{1,e} - v_{2,e})$ and identification of its A_{low} .

We will use the network illustrated in Figure 18 to design a module taking a signal v as input and producing, as output, the instantaneous phase $\theta_{\text{low}}(v)$ of the mode of v having

the lowest instantaneous frequency. The main steps of the computation performed by this module are as follows. Let $\mathcal{S}(\tau, \omega, v)$ be the max-pool energy defined as in (4.15), where now it is useful to indicate its dependence on v .

Let A_{low} be a subset of the time-frequency domain (τ, ω) identified (as in sub-figure (2) of Figure 28) as a narrow sausage around the lowest instantaneous frequency defined by the local maxima of the $\mathcal{S}(\tau, \omega, v)$ (we restrict our presentation to the situation where the instantaneous frequencies θ_i do not cross each other). If no modes can be detected (above a given threshold) in $\mathcal{S}(\tau, \omega, v)$ then we set $\theta_{\text{low}}(v) = \emptyset$ otherwise we proceed as follows.

Let $\omega_{\text{low}}(\tau) = \omega_e(\tau, \text{argmax}_{\omega: (\tau, \omega) \in A_{\text{low}}} \mathcal{S}(\tau, \omega))$ be the estimated instantaneous frequency of the mode having the lowest instantaneous frequency and, with θ_e defined as in (4.6), let

$$\theta_{\text{low}}(t) := \theta_e(t, \omega_{\text{low}}(t)), \quad (7.14)$$

be the corresponding estimated instantaneous phase (obtained as in (4.16)).

7.3 The iterated micro-local KMD algorithm.

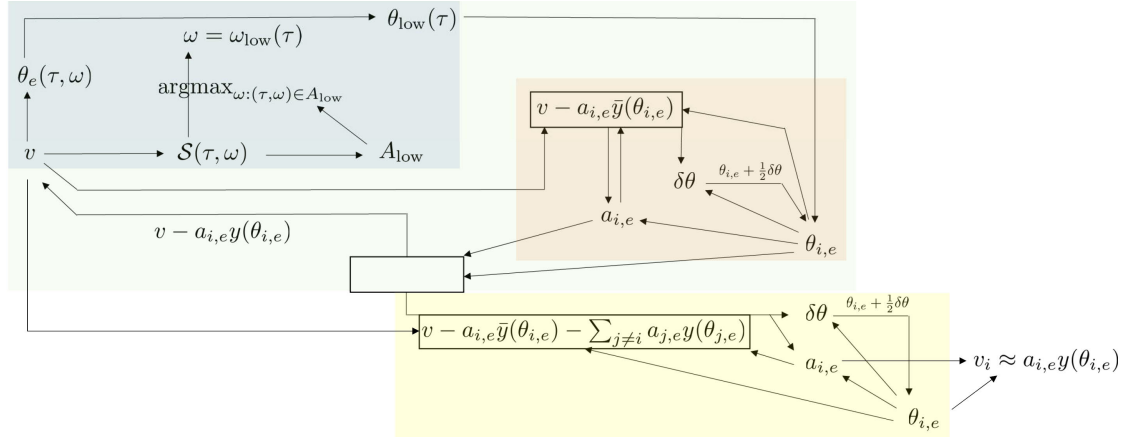


Figure 29: Modular representation of Algorithm 2, described in this section. The blue module represents the estimation of the lowest frequency as illustrated in Figure 28. The brown module represents the iterative estimation of the mode with lowest instantaneous frequency of steps 10 through 13. The yellow module represents the iterative refinement of all the modes in steps 20 through 29. The brown and yellow modules used to refine phase/amplitude estimates use the same code.

The method of estimating the mode with the lowest instantaneous frequency, described in Section 7.2, provides a foundation for the iterated micro-local KMD algo-

Algorithm 2 Iterated micro-local KMD.

```
1:  $i \leftarrow 1$ 
2:  $v^{(1)} \leftarrow v$ 
3: while true do
4:   if  $\theta_{\text{low}}(v^{(i)}) = \emptyset$  then
5:     break loop
6:   else
7:      $\theta_{i,e} \leftarrow \theta_{\text{low}}(v^{(i)})$ 
8:   end if
9:    $a_{i,e}(t) \leftarrow 0$ 
10:  while  $\sup_t |\delta\theta_{i,e}(t)| > \epsilon_1$  do
11:     $v_{\text{res}}^{(i)} \leftarrow v^{(i)} - a_{i,e}\bar{y}(\theta_{i,e})$ 
12:     $a_{i,e}(\tau) \leftarrow a(\tau, \theta_{i,e}, v_{\text{res}}^{(i)})$ 
13:     $\theta_{i,e}(\tau) \leftarrow \theta_{i,e}(\tau) + \frac{1}{2}\delta\theta(\tau, \theta_{i,e}, v_{\text{res}}^{(i)})$ 
14:  end while
15:   $v^{(i+1)} \leftarrow v^{(i)} - a_{i,e}y(\theta_{i,e})$ 
16:   $i \leftarrow i + 1$ 
17: end while
18:  $m \leftarrow i - 1$ 
19:  $i \leftarrow 1$ 
20: while  $\sup_{i,t} |\delta\theta_{i,e}(t)| > \epsilon_2$  do
21:   $v_{i,\text{res}} \leftarrow v - a_{i,e}\bar{y}(\theta_{i,e}) - \sum_{j \neq i} a_{j,e}y(\theta_{j,e})$ 
22:   $a_{i,e}(\tau) \leftarrow a(\tau, \theta_{i,e}, v_{i,\text{res}})$ 
23:   $\theta_{i,e}(\tau) \leftarrow \theta_{i,e}(\tau) + \frac{1}{2}\delta\theta(\tau, \theta_{i,e}, v_{i,\text{res}})$ 
24:  if  $i < m$  then
25:     $i \leftarrow i + 1$ 
26:  else
27:     $i \leftarrow m$ 
28:  end if
29: end while
30: Return the modes  $v_{i,e} \leftarrow a_{i,e}(t)y(\theta_{i,e}(t))$  for  $i = 1, \dots, m$ 
```

rithm, Algorithm 2. We now describe Algorithm 2 using Figures 26, 27, 28, presenting its modular representation in Figure 29. To that end, let

$$y(t) = c_1 \cos(t) + \sum_{n=2}^{\infty} c_n \cos(nt + d_n) \quad (7.15)$$

be the Fourier representation of the base waveform y (which, without loss of generality, has been shifted so that the first sine coefficient is zero) and write

$$\bar{y}(t) := y(t) - c_1 \cos(t) \quad (7.16)$$

for its overtones.

Let us describe how steps 1 to 17 provide refined estimates for the amplitude and the phase of each mode $v_i, i \in \{1, \dots, m\}$ of the signal v . Although the overtones of y prevent us from simultaneously approximating all the instantaneous frequencies θ_i from the max-pool energy of the signal v , since the lowest mode $v_{\text{low}} = a_{\text{low}}y(\theta_{\text{low}})$ can be decomposed into the sum $v_{\text{low}} = a_{\text{low}}c_1 \cos(\theta_{\text{low}}) + a_{\text{low}}\bar{y}(\theta_{\text{low}})$ of a signal $a_{\text{low}}c_1 \cos(\theta_{\text{low}})$ with a cosine waveform plus the signal $a_{\text{low}}\bar{y}(\theta_{\text{low}})$ containing its higher frequency overtones, the method of Section 7.2 can be applied to obtain an estimate $a_{\text{low},e}c_1 \cos(\theta_{\text{low},e})$ of the primary component $a_{\text{low}}c_1 \cos(\theta_{\text{low}})$ of the first mode. Since c_1 is known, this estimate produces the estimate $a_{\text{low},e}\bar{y}(\theta_{\text{low},e})$ for the overtones of the lowest mode. To improve the accuracy of this estimate, in steps 12 and 13 the micro local KMD of Section 7.1 is iteratively applied to the residual signal $v_{\text{res}}^{(2)} \leftarrow v - a_{\text{low},e}\bar{y}(\theta_{\text{low},e})$, consisting of the signal v with the estimated overtones of the lowest mode removed. The rate parameter 1/2 in step 13 is to avoid overcorrecting the phase estimates, while the parameters ϵ_1 and ϵ_2 in steps 10 and 20 are pre-specified accuracy thresholds. The resulting estimated lowest mode is then removed from the signal to determine the first residual $v^{(2)} := v - a_{\text{low},e}y(\theta_{\text{low},e})$ in step 15.

Iterating this process, we can peel off an estimate $a_{i,e}y(\theta_{i,e})$ of the mode corresponding to the lowest instantaneous frequency of the residual $v^{(i)} := v - \sum_{j \leq i-1} a_{j,e}y(\theta_{j,e})$ of the signal v obtained in step 15, removing the interference of the first $i - 1$ modes, including their overtones, in our estimate of the instantaneous frequency and phase of the i -th mode. See Figure 28 for the evolution of the A_{low} sausage as these modes are peeled off. See sub-figures (3) and (5) of the top and bottom of Figure 26 for the results of peeling off the first two estimated modes of the signal v corresponding to both Figures 24 and 25 and sub-figures (4) and (6) for the results of the corresponding projections in (7.5). See sub-figures (3) and (4) of the top and bottom of Figure 27 for amplitude and its estimate of the results of peeling off the first estimated mode and sub-figures (5) and (6) corresponding to peeling of the first two estimated modes of the signal v corresponding to both Figures 24 and 25.

Once the amplitude/phase estimates $a_{i,e}, y(\theta_{i,e}), i \in \{1, \dots, m\}$ have been obtained in steps 1 to 17, steps 19 to 29 enable us to achieve even higher accuracies by iterating the micro local KMD of Section 7.1 on the residual signals $v_{i,\text{res}} \leftarrow v - a_{i,e}\bar{y}(\theta_{i,e}) - \sum_{j \neq i} a_{j,e}y(\theta_{j,e})$, consisting of the signal v with all the estimated modes $j \neq i$ and estimated overtones of the mode i removed.

The proposed algorithm can be further improved by (1) applying a Savitsky-Golay filter to locally smooth (de-noise) the curves corresponding to each estimate $\theta_{i,e}$ (which corresponds to refining our phase estimates through GPR filtering) (2) starting with a slightly larger α (to decrease interference from other modes/overtones) and slowly reducing its value in the final steps (to further localize our estimates after other components have been mostly eliminated).

7.4 Numerical experiments

Here we present results for both the triangle wave and EKG wave examples. As discussed in the previous section, these results are visually displayed in 26 and 27.

7.4.1 Triangle wave example

The base waveform is the triangle wave displayed in Figure 23. To avoid boundary artifacts we observe the signal v on a mesh spanning $[-3, 3]$ spaced at intervals of $\frac{1}{2000}$ and aim to recover each mode v_i on $[-1, 1]$. We slowly increased α from 10 to 15 in the loop corresponding to steps 1 to 17 and slowly decreased it to 6 in the final loop corresponding to steps 19 to 29. The amplitudes and frequencies of each of the modes are shown in Figure 24. The recovery errors of each mode as well as their amplitude and phase functions are displayed in Table 5. They were found to be on the order of 10^{-7} for the first signal component and approximately 10^{-6} for the higher two. A plot superimposing v_i and $v_{i,e}$ would visually appear to be one curve due to the negligible recovery errors.

Mode	$\frac{\ v_{i,e}-v_i\ _{L^2}}{\ v_i\ _{L^2}}$	$\frac{\ v_{i,e}-v_i\ _{L^\infty}}{\ v_i\ _{L^\infty}}$	$\frac{\ a_{i,e}-a_i\ _{L^2}}{\ a_i\ _{L^2}}$	$\ \theta_{i,e}-\theta_i\ _{L^2}$
$i = 1$	1.94×10^{-7}	3.65×10^{-7}	9.99×10^{-8}	1.50×10^{-7}
$i = 2$	3.71×10^{-6}	2.52×10^{-6}	5.68×10^{-7}	3.56×10^{-6}
$i = 3$	2.19×10^{-6}	3.89×10^{-6}	1.40×10^{-6}	1.51×10^{-6}

Table 5: Signal component recovery errors in the triangle base waveform example.

7.4.2 EKG wave example

The base waveform is the EKG wave displayed in Figure 23. We use the same discrete mesh as in the triangle case. Here, we slowly increased α from 20 to 30 in the loop corresponding to steps 1 to 17 and slowly decreased it to 10 in the final loop corresponding to steps 19 to 29. The amplitudes and frequencies of each of the modes are shown in Figure 25, while the recovery error of each mode as well as their amplitude and phase functions are shown in Table 6. Amplitude and phase relative errors are found to be on the order of 10^{-2} to 10^{-4} in this setting. Again, $v_{i,e}$ and v_i are visually indistinguishable due to the small recovery errors.

Mode	$\frac{\ v_{i,e}-v_i\ _{L^2}}{\ v_i\ _{L^2}}$	$\frac{\ v_{i,e}-v_i\ _{L^\infty}}{\ v_i\ _{L^\infty}}$	$\frac{\ a_{i,e}-a_i\ _{L^2}}{\ a_i\ _{L^2}}$	$\ \theta_{i,e}-\theta_i\ _{L^2}$
$i = 1$	2.72×10^{-3}	1.04×10^{-2}	9.11×10^{-4}	3.25×10^{-4}
$i = 2$	1.72×10^{-3}	4.30×10^{-3}	3.04×10^{-4}	2.31×10^{-4}
$i = 3$	5.28×10^{-3}	2.89×10^{-2}	1.02×10^{-3}	8.91×10^{-4}

Table 6: Signal component recovery errors in the EKG base waveform example.

8 Unknown base waveforms

We next consider the extension to the mode recovery problem to the case where the periodic base waveform of each mode may be unknown (and different across modes). In this context, our objective can be summarized as solving Problem 2. To avoid ambiguities caused by overtones when the waveforms y_i are not only non-trigonometric but also unknown, we will assume that the functions $(k\dot{\theta}_i)_{t \in [-1,1]}$ and $(k'\dot{\theta}_i)_{t \in [-1,1]}$ are distinct for $i \neq i'$ and $k, k' \in \mathbb{N}^*$ (those functions may be equal for some t but not for all t).

To describe the algorithm we write

$$y_i(t) = \cos(t) + \sum_{k=2}^{k_{\max}} c_{i,(k,c)} \cos(kt) + c_{i,(k,s)} \sin(kt) \quad (8.1)$$

for the Fourier representation of y_i , which, without loss of generality has been scaled, translated and truncated (k_{\max} can be arbitrarily large and in a discrete setting it is bounded by the inverse of the resolution of the discretization in time).

At the cost of some degree of forward referencing we will use the signal v and its corresponding modes v_1, v_2, v_3 displayed in Figure 30 to illustrate our approach. The waveforms y_1, y_2 and y_3 composing that signal are shown in Figure 31 and described in Section 8.3.

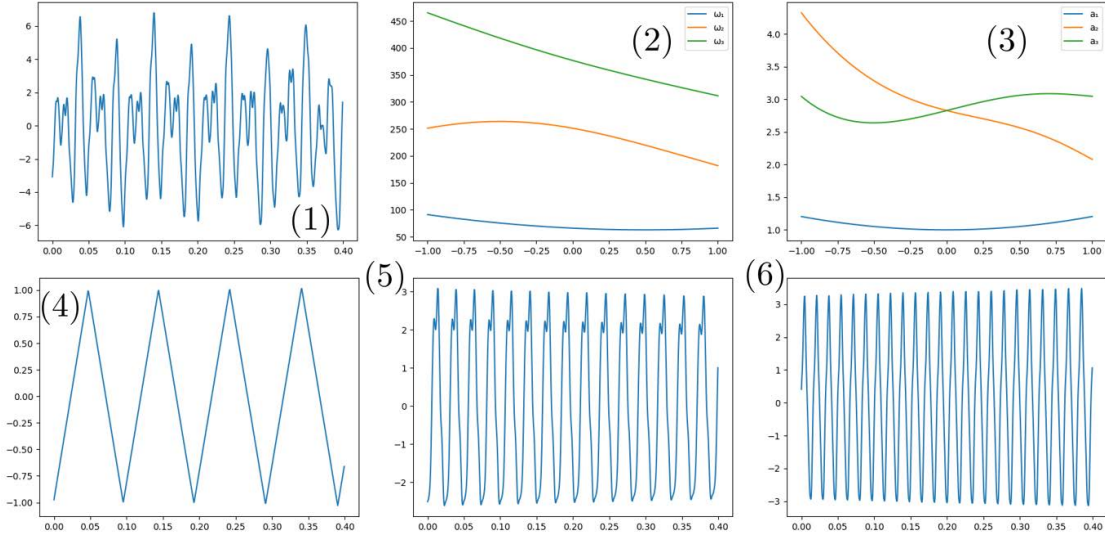


Figure 30: (1) Signal v (the signal is defined over $[-1, 1]$ but displayed over $[0, 0.4]$ for visibility) (2) Instantaneous frequencies $\omega_i := \dot{\theta}_i$ (3) Amplitudes a_i (4, 5, 6) Modes v_1, v_2, v_3 over $[0, 0.4]$ (mode plots have also been zoomed in for visibility).

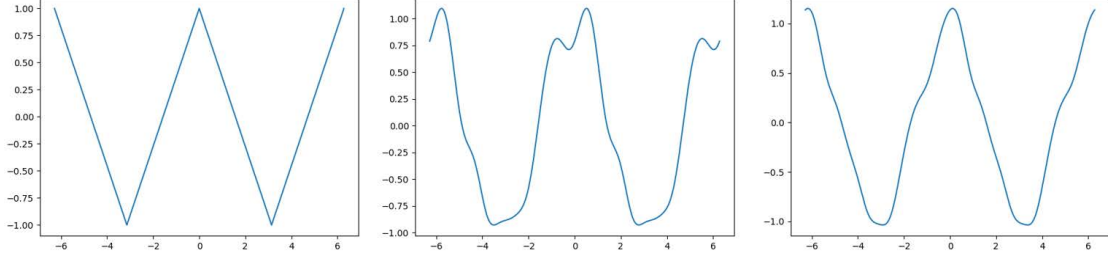


Figure 31: (1) y_1 (2) y_2 (3) y_3

8.1 Micro-local waveform KMD

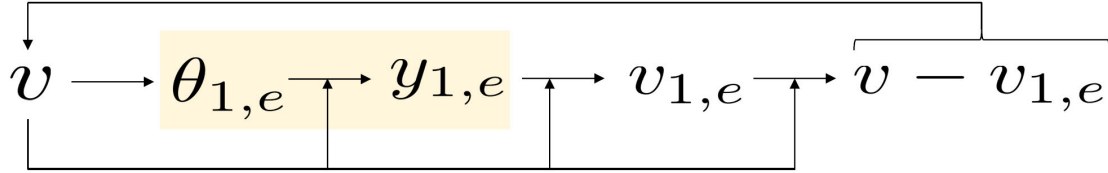


Figure 32: High level structure of the algorithm for the case when waveforms are unknown.

We now describe the micro-local *waveform* KMD, Algorithm 3, which takes as inputs a time τ , an estimated instantaneous amplitude and phase $t \rightarrow a(t), \theta(t)$, and a signal v , and outputs an estimate of the waveform $y(t)$ associated with the phase. The proposed approach is a direct extension of the one presented in Section 7.1 and the shaded part of Figure 32 shows the new block which will be added to Algorithm 2, the algorithm designed for the case when waveforms are non-trigonometric and known. As described below this new block produces an estimator $y_{i,e}$ of the waveform y_i from an estimate $\theta_{i,e}$ of the phase θ_i .

Given $\alpha > 0$, $\tau \in [-1, 1]$, and differentiable function $t \rightarrow \theta(t)$, define the following Gaussian process

$$\xi_{\tau,\theta}^y(t) = e^{-\left(\frac{\dot{\theta}(\tau)(t-\tau)}{\alpha}\right)^2} \left(X_{1,c}^y \cos(\theta(t)) + \sum_{k=2}^{k_{\max}} (X_{k,c}^y \cos(k\theta(t)) + X_{k,s}^y \sin(k\theta(t))) \right), \quad (8.2)$$

where $X_{1,c}^y$, $X_{k,c}^y$, and $X_{k,s}^y$ are independent $\mathcal{N}(0, 1)$ random variables. Let

$$v_{\tau,\theta}(t) := e^{-\left(\frac{\dot{\theta}(\tau)(t-\tau)}{\alpha}\right)^2} v(t), \quad \tau \in [-1, 1], \quad (8.3)$$

be the windowed signal, and define

$$Z_{k,j}^y(\tau, \theta, v) := \lim_{\sigma \downarrow 0} \mathbb{E}[X_{k,j}^y | \xi_{\tau,\theta}^y + \xi_\sigma = v_{\tau,\theta}], \quad (8.4)$$

and for $k \in \{2, \dots, k_{\max}\}$, $j \in \{c, s\}$, let

$$c_{k,j}(\tau, \theta, v) := \frac{Z_{k,j}^y(\tau, \theta, v)}{Z_{1,c}^y(\tau, \theta, v)}. \quad (8.5)$$

This yields an estimate of each Fourier coefficient of the waveform y expressed as in Problem 2 at time $t = \tau$. This waveform recovery is susceptible to error when there is interference in the overtone frequencies (that is for the values of τ at which $j_1 \dot{\theta}_{i_1} \approx j_2 \dot{\theta}_{i_2}$ for $i_1 < i_2$). To overcome this, we compute $c_{k,j}(\tau, \theta, v)$ at each time τ and take the most common approximate value over all τ . More specifically, let T be the finite set of values of τ used in the numerical discretization of the time axis. For an interval $I \subset \mathbb{R}$ let

$$T_I := \{\tau \in T | c_{k,j}(\tau, \theta, v) \in I\}. \quad (8.6)$$

and N_I for the number of elements of T_I . Let I_{\max} be a maximizer of N_I over intervals of fixed width L .

We then define our overall estimate $c_{k,j}(\theta, v)$ of the Fourier coefficient $c_{k,j}$ to be the average of the values of $c_{k,j}(\tau, \theta, v)$ over $\tau \in I_{\max} \cap T$, i.e.

$$c_{k,j}(\theta, v) := \begin{cases} \frac{1}{N_{I_{\max}}} \sum_{\tau \in T_{I_{\max}}} c_{k,j}(\tau, \theta, v) & \text{for } \frac{N_{I_{\max}}}{N} \geq 0.05 \\ 0 & \text{for } \frac{N_{I_{\max}}}{N} < 0.05 \end{cases}, \quad (8.7)$$

where N is the size of the time mesh, i.e. the number of elements of T . Figure 33 shows a zoomed-in histogram of the values of $c_{2,c}(\tau, \theta, v)$ associated with the waveform of the first mode and the plots of $\tau \rightarrow c_{1,(3,c)}, c_{1,(3,s)}$. The interpretation of the selection of the cutoff 0.05 is as follows: if $\frac{N_{I_{\max}}}{N}$ is small then there is interference in the overtones at all time $[-1, 1]$ and no information may be obtained about the corresponding Fourier coefficient.

On the interval width. The recovered modes and waveforms show little sensitivity to the specific value of L which has been set to be 0.002 in our numerical experiments (widths between 0.001 and 0.01 yield similar results). The rationale for the selection of the (rough) value of L is as follows. Suppose $v = \cos(\omega t)$ and $v' = v + \cos(1.5\omega t)$. Define the quantity

$$\max_{\tau} c_{2,c}(\tau, \theta, v') - c_{2,c}(\tau, \theta, v) \quad (8.8)$$

with the intuition of approximating the maximum corruption by the $\cos(1.5\omega t)$ term in the estimated first overtone. This quantity is mainly dependent on the selection of α and marginally on ω . For our selection of $\alpha = 10$, we numerically found its value to be approximately 0.002.

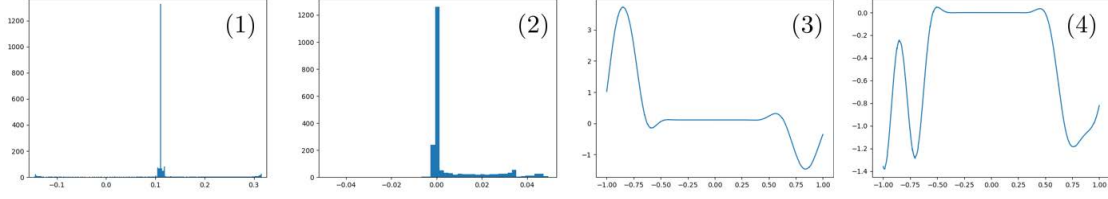


Figure 33: (1) A histogram (with cropped outliers) with bin width 0.002 of $c_{1,(3,c)}(\tau, \theta, v)$ values (the true value of $c_{1,(3,c)}$ is $1/9$ since y_1 is a triangle wave) (2) The analogous histogram of $c_{1,(3,s)}(\tau, \theta, v)$ values (the true coefficient of this overtone is 0) (3) $\tau \rightarrow c_{1,(3,c)}$ (4) $\tau \rightarrow c_{1,(3,s)}$.

8.2 Iterated micro-local KMD with unknown waveforms algorithm

Except for the steps discussed in Section 8.1 Algorithm 3 is identical to Algorithm 2. We first identify the lowest frequency of the cosine component of each mode (step 8) to obtain a refined⁴ estimate of $\theta_{i,e}$. Then the base waveform y_i recovery is estimated in steps 16-17. Finally, once each mode has been identified, we again apply waveform estimation in steps 27-28 (after nearly eliminating other modes and reducing interference in overtones for higher accuracies).

Mode	$\frac{\ v_{i,e} - v_i\ _{L^2}}{\ v_i\ _{L^2}}$	$\frac{\ v_{i,e} - v_i\ _{L^\infty}}{\ v_i\ _{L^\infty}}$	$\frac{\ a_{i,e} - a_i\ _{L^2}}{\ a_i\ _{L^2}}$	$\ \theta_{i,e} - \theta_i\ _{L^2}$	$\frac{\ y_{i,e} - y_i\ _{L^2}}{\ y_i\ _{L^2}}$
$i = 1$	6.59×10^{-3}	2.65×10^{-2}	1.52×10^{-5}	1.75×10^{-5}	6.65×10^{-3}
$i = 2$	2.62×10^{-4}	5.61×10^{-4}	8.12×10^{-5}	1.25×10^{-4}	2.15×10^{-4}
$i = 3$	6.55×10^{-4}	9.76×10^{-4}	3.99×10^{-4}	3.67×10^{-4}	3.43×10^{-4}

Table 7: Signal component recovery errors when the base waveforms are unknown

8.3 Numerical experiments

To illustrate this learning of the base waveform of each mode, we take $v(t) = \sum_{i=1}^3 a_i(t)y_i(\theta_i(t))$. We set the (unknown) waveform y_1 to be triangle as in Figure 23. For $i = 2, 3$, $k \in \{2, \dots, 7\}$ and $j \in \{c, s\}$ we set $y_{i,(k,j)}$ to be zero with probability 1/2 or to be a random sample from $\mathcal{N}(0, 1/k^4)$ with probability 1/2 (recall our convention that $y_{i,(0,c)} = 1$ and $y_{i,(0,s)} = 0$). The waveforms y_1, y_2, y_3 are illustrated in Figure 31. The modes v_1, v_2, v_3 , their amplitudes and instantaneous frequencies are shown in Figure 30.

We use the same mesh and the same value of α values as in Section 7.4.1. The main source of error for the recovery of the first mode's base waveform stems from the fact that a triangle wave has an infinite number of overtones, while in our implementation,

⁴unrefined estimates of $\theta_{i,e}$ in step 7 lead to poor recoveries of the y_i

Algorithm 3 Iterated micro-local KMD with unknown waveforms.

```
1:  $i \leftarrow 1$ 
2:  $v^{(1)} \leftarrow v$ 
3: while true do
4:   if  $\theta_{\text{low}}(v^{(i)}) = \emptyset$  then
5:     break loop
6:   else
7:      $\theta_{i,e} \leftarrow \theta_{\text{low}}(v^{(i)})$ 
8:      $y_{i,e} \leftarrow \cos(t)$ 
9:   end if
10:   $a_{i,e}(t) \leftarrow 0$ 
11:  while  $\sup_t |\delta\theta_{i,e}(t)| > \epsilon_1$  do
12:     $v_{\text{res}}^{(i)} \leftarrow v^{(i)} - a_{i,e} \bar{y}_{i,e}(\theta_{i,e})$ 
13:     $a_{i,e}(\tau) \leftarrow a(\tau, \theta_{i,e}, v_{\text{res}}^{(i)})$ 
14:     $\theta_{i,e}(\tau) \leftarrow \theta_{i,e}(\tau) + \frac{1}{2} \delta\theta(\tau, \theta_{i,e}, v_{\text{res}}^{(i)})$ 
15:  end while
16:   $c_{i,(k,j),e} \leftarrow c_{k,j}(\theta_{i,e}, v_{\text{res}}^{(i)})$ 
17:   $y_{i,e}(t) \leftarrow \cos(t) + \sum_{k=1}^{k_{\text{max}}} c_{i,(k,c),e} \cos(kt) + c_{i,(k,s),e} \sin(kt)$ 
18:   $v^{(i+1)} \leftarrow v^{(i)} - a_{i,e} y_{i,e}(\theta_{i,e})$ 
19:   $i \leftarrow i + 1$ 
20: end while
21:  $m \leftarrow i - 1$ 
22:  $i \leftarrow 1$ 
23: while  $\sup_{i,t} |\delta\theta_{i,e}(t)| > \epsilon_2$  do
24:   $v_{i,\text{res}} \leftarrow v - a_{i,e} \bar{y}_{i,e}(\theta_{i,e}) - \sum_{j \neq i} a_{j,e} y_{j,e}(\theta_{j,e})$ 
25:   $a_{i,e}(\tau) \leftarrow a(\tau, \theta_{i,e}, v_{i,\text{res}})$ 
26:   $\theta_{i,e}(\tau) \leftarrow \theta_{i,e}(\tau) + \frac{1}{2} \delta\theta(\tau, \theta_{i,e}, v_{i,\text{res}})$ 
27:   $c_{i,(k,j),e} \leftarrow c_{k,j}(\theta_{i,e}, v - \sum_{j \neq i} a_{j,e} y_{j,e}(\theta_{j,e}))$ 
28:   $y_{i,e}(t) \leftarrow \cos(t) + \sum_{k=1}^{k_{\text{max}}} c_{i,(k,c),e} \cos(kt) + c_{i,(k,s),e} \sin(kt)$ 
29:  if  $i < m$  then
30:     $i \leftarrow i + 1$ 
31:  else
32:     $i \leftarrow m$ 
33:  end if
34: end while
35: Return the modes  $v_{i,e} \leftarrow a_{i,e}(t) y(\theta_{i,e}(t))$  for  $i = 1, \dots, m$ 
```

we estimate only the first 15 overtones. Compared to the triangle wave truncated to the first 15 overtones, the L^2 -norm recovery error of the waveform is 2.09×10^{-3} . We omitted the plots of the $y_{i,e}$ as they are visually indistinguishable from those of the y_i . Recovery errors are presented in Table 7.

9 Proofs

9.1 Proof of Lemma 2.1

We first establish that $\Psi(v) = \Phi^-v$, where the Moore-Penrose inverse is defined by $\Phi^- := \Phi^T(\Phi\Phi^T)^{-1}$. To that end, let w^* be the solution of (2.5). Since $\Phi : \mathcal{B} \rightarrow V$ is surjective it follows that $\Phi : \text{Ker}^\perp(\Phi) \rightarrow V$ is a bijection and therefore

$$\{w : \Phi(w) = v\} = w_0 + \text{Ker}(\Phi)$$

for a unique $w_0 \in \text{Ker}^\perp(\Phi)$. Therefore, setting $w' := w - w_0$ we find that $(w')^* := w^* - w_0$ is a solution of

$$\begin{cases} \text{Minimize } \|w' + w_0\|_{\mathcal{B}} \\ \text{Subject to } w' \in \mathcal{B} \text{ and } \Phi(w') = 0, \end{cases} \quad (9.1)$$

so that by the projection theorem we have $(w')^* = P_{\text{Ker}(\Phi)}(-w_0)$ where $P_{\text{Ker}(\Phi)}$ is the orthogonal projection onto $\text{Ker}(\Phi)$. Therefore $w^* = w_0 + (w')^* = w_0 - P_{\text{Ker}(\Phi)}(w_0) = P_{\text{Ker}^\perp(\Phi)}w_0$, so that we obtain

$$w^* = P_{\text{Ker}^\perp(\Phi)}w_0.$$

Since Φ is surjective and continuous it follows from the closed range theorem, see e.g. Yosida [35, Pg. 208] that $\text{Im}(\Phi^T) = \text{Ker}^\perp(\Phi)$ and $\text{Ker}(\Phi^T) = \emptyset$, which implies that $\Phi\Phi^T : V \rightarrow V$ is invertible, so that the Moore-Penrose inverse $\Phi^- : V \rightarrow \mathcal{B}$ of Φ , is well-defined by

$$\Phi^- := \Phi^T(\Phi\Phi^T)^{-1}.$$

It follows that $P_{\text{Ker}^\perp(\Phi)} = \Phi^-\Phi$ and $\Phi\Phi^- = I_V$ so that

$$w^* = P_{\text{Ker}^\perp(\Phi)}w_0 = \Phi^-\Phi w_0 = \Phi^-v,$$

that is, we obtain the assertion $w^* = \Phi^-v$.

For the first assertion, suppose that $\text{Ker}\Phi = \emptyset$. Since it is surjective, it follows that Φ is a bijection. Then, the unique solution to the minmax problem is the only feasible one $w^* = \Phi^{-1}v = \Phi^-v$. When $\text{Ker}\Phi \neq \emptyset$, observe that since all u which satisfy $\Phi(u) = v$ have the representation $u = w_0 + u'$ for fixed $w_0 \in \text{Ker}^\perp(\Phi)$ and some $u' \in \text{Ker}(\Phi)$, it follows that the inner maximum satisfies

$$\begin{aligned} \max_{u \in \mathcal{B} | \Phi(u) = v} \frac{\|u - w\|_{\mathcal{B}}}{\|u\|_{\mathcal{B}}} &= \max_{u' \in \text{Ker}(\Phi)} \frac{\|u' + w_0 - w\|_{\mathcal{B}}}{\|u' + w_0\|_{\mathcal{B}}} \\ &= \max_{u' \in \text{Ker}(\Phi)} \max_{t \in \mathbb{R}} \frac{\|tu' + w_0 - w\|_{\mathcal{B}}}{\|tu' + w_0\|_{\mathcal{B}}} \\ &\geq 1 \end{aligned}$$

On the other hand, for $w := \Phi^{-1}v$, we have

$$\begin{aligned}
\max_{u \in \mathcal{B} | \Phi(u)=v} \frac{\|u - w\|_{\mathcal{B}}}{\|u\|_{\mathcal{B}}} &= \max_{u \in \mathcal{B} | \Phi(u)=v} \frac{\|u - \Phi^{-1}v\|_{\mathcal{B}}}{\|u\|_{\mathcal{B}}} \\
&= \max_{u \in \mathcal{B} | \Phi(u)=v} \frac{\|u - \Phi^{-1}\Phi(u)\|_{\mathcal{B}}}{\|u\|_{\mathcal{B}}} \\
&= \max_{u \in \mathcal{B} | \Phi(u)=v} \frac{\|u - P_{\text{Ker}^{\perp}(\Phi)}u\|_{\mathcal{B}}}{\|u\|_{\mathcal{B}}} \\
&\leq 1,
\end{aligned}$$

which implies that $w := \Phi^{-1}v$ is a minmax solution. To see that it is the unique optimal solution, observe that we have just established that

$$\max_{u \in \mathcal{B} | \Phi(u)=v} \frac{\|u - \Psi(v)\|_{\mathcal{B}}}{\|u\|_{\mathcal{B}}} = 1 \tag{9.2}$$

for any optimal $\Psi : V \rightarrow \mathcal{B}$. It then follows that

$$\max_{u \in \mathcal{B}} \frac{\|u - \Psi(\Phi(u))\|_{\mathcal{B}}}{\|u\|_{\mathcal{B}}} = 1$$

which implies that the map $I - \Psi \circ \Phi : \mathcal{B} \rightarrow \mathcal{B}$ is a contraction. Moreover, by selecting $u \in \text{Ker}(\Phi)$ tending to 0, it follows from (9.2) that $\Psi(0) = 0$. Since, by definition, $\Phi \circ \Psi = I_V$, we have

$$\begin{aligned}
(I - \Psi \circ \Phi)^2(u) &= (I - \Psi \circ \Phi)(u - \Psi \circ \Phi(u)) \\
&= u - \Psi \circ \Phi(u) - \Psi \circ \Phi(u - \Psi \circ \Phi(u)) \\
&= u - \Psi \circ \Phi(u) - \Psi(\Phi(u) - \Phi \circ \Psi \circ \Phi(u)) \\
&= u - \Psi \circ \Phi(u) - \Psi(\Phi(u) - \Phi(u)) \\
&= u - \Psi \circ \Phi(u) - \Psi(0) \\
&= u - \Psi \circ \Phi(u)
\end{aligned}$$

so that the map $I - \Psi \circ \Phi$ is a projection. Since $\Phi(u - \Psi \circ \Phi(u)) = \Phi(u) - \Phi \circ \Psi \circ \Phi(u) = 0$ it follows that $\text{Im}(I - \Psi \circ \Phi) \subset \text{Ker}(\Phi)$, but since for $b \in \text{Ker}(\Phi)$, we have $(I - \Psi \circ \Phi)(b) = b - \Psi \circ \Phi(b) = b$, we obtain the equality $\text{Im}(I - \Psi \circ \Phi) = \text{Ker}(\Phi)$.

To show that a projection of this form is necessarily linear, let us demonstrate that $\text{Im}(\Psi \circ \Phi) = \text{Ker}^{\perp}(\Phi)$. To that end, use the decomposition $\mathcal{B} = \text{Ker}(\Phi) \oplus \text{Ker}^{\perp}(\Phi)$ to write $u = u' + u''$ with $u' \in \text{Ker}(\Phi)$ and $u'' \in \text{Ker}^{\perp}(\Phi)$ and write the contractive condition $\|u - \Psi \circ \Phi(u)\|^2 \leq \|u\|^2$ as

$$\|u' + u'' - \Psi \circ \Phi(u' + u'')\|^2 \leq \|u' + u''\|^2,$$

which using the linearity of Φ and $u' \in \text{Ker}(\Phi)$ we obtain

$$\|u' + u'' - \Psi \circ \Phi(u'')\|^2 \leq \|u' + u''\|^2,$$

Suppose that $\Psi \circ \Phi(u'') = v' + v''$ with $v' \in \text{Ker}(\Phi)$ nontrivial. Then, selecting $u' = tv'$, with $t \in \mathbb{R}$, we obtain

$$\|(t-1)v' + u'' - v''|^2 \leq \|tv' + u''\|^2$$

which amounts to

$$(t-1)^2\|v'\|^2 + \|u'' - v''\|^2 \leq t^2\|v'\|^2 + \|u''\|^2$$

which amounts to

$$(1-2t)\|v'\|^2 + \|u'' - v''\|^2 \leq \|u''\|^2$$

which provides a contradiction for t large enough negative. Consequently, $v' = 0$ and $\text{Im}(\Psi \circ \Phi) \subset \text{Ker}^\perp(\Phi)$. Since $I = \Psi \circ \Phi + (I - \Psi \circ \Phi)$ with $\text{Im}(\Psi \circ \Phi) \subset \text{Ker}^\perp(\Phi)$ and $\text{Im}(I - \Psi \circ \Phi) \subset \text{Ker}(\Phi)$ it follows that $\text{Im}(\Psi \circ \Phi) = \text{Ker}^\perp(\Phi)$. Since $\Psi \circ \Phi$ is a projection it follows that

$$\Psi \circ \Phi(u'') = u'', \quad u'' \in \text{Ker}^\perp(\Phi).$$

Consequently, for two elements $u_1 = u'_1 + u''_1$ and $u_2 = u'_2 + u''_2$ with $u'_i \in \text{Ker}(\Phi)$ and $u''_i \in \text{Ker}^\perp(\Phi)$ for $i = 1, 2$ we have

$$\begin{aligned} (I - \Psi \circ \Phi)(u_1 + u_2) &= u_1 + u_2 - \Psi \circ \Phi(u_1 + u_2) \\ &= u'_1 + u'_2 + u''_1 + u''_2 - \Psi \circ \Phi(u''_1 + u''_2) \\ &= u'_1 + u'_2 \\ &= u'_1 + u'_1 - \Psi \circ \Phi(u''_1) + u'_2 + u'_2 - \Psi \circ \Phi(u''_2) \\ &= (I - \Psi \circ \Phi)(u_1) + (I - \Psi \circ \Phi)(u_2), \end{aligned}$$

and similarly, for $t \in \mathbb{R}$,

$$(I - \Psi \circ \Phi)(tu_1) = t(I - \Psi \circ \Phi)(u_1),$$

so we conclude that $I - \Psi \circ \Phi$ is linear.

Since according to Rao [31, Rem. 9, pg. 51], a contractive linear projection on a Hilbert space is an orthogonal projection, it follows that the map $I - \Psi \circ \Phi$ is an orthogonal projection, and therefore $\Psi \circ \Phi = P_{\text{Ker}^\perp(\Phi)}$. Since Φ^- is the Moore-Penrose inverse, it follows that $P_{\text{Ker}^\perp(\Phi)} = \Phi^- \Phi$ so that $\Psi \circ \Phi = \Phi^- \Phi$, and therefore the assertion $\Psi = \Phi^-$ follows by right multiplication by Ψ using the identity $\Phi \circ \Psi = I_V$.

9.2 Proof of Lemma 2.2

Let us write $\Phi : \mathcal{B} \rightarrow V$ as

$$\Phi(u) = \sum_{i \in \mathcal{I}} e_i u_i, \quad u = (u_i \in V_i)_{i \in \mathcal{I}},$$

where we now include the subspace injections $e_i : V_i \rightarrow V$ in its description. Let $\bar{e}_i : V_i \rightarrow \mathcal{B}$ denote the component injection $\bar{e}_i v_i := (0, \dots, 0, v_i, 0, \dots, 0)$ and let $\bar{e}_i^T : \mathcal{B} \rightarrow V_i$ denote the component projection. Using this notation, the norm (2.6) on \mathcal{B} becomes

$$\|u\|_{\mathcal{B}}^2 := \sum_{i \in \mathcal{I}} \|\bar{e}_i^T u\|_{V_i}^2, \quad u \in \mathcal{B}, \quad (9.3)$$

with inner product

$$\langle u_1, u_2 \rangle_{\mathcal{B}} := \sum_{i \in \mathcal{I}} \langle \bar{e}_i^T u_1, \bar{e}_i^T u_2 \rangle_{V_i}, \quad u_1, u_2 \in \mathcal{B}.$$

Clearly, $\bar{e}_j^T \bar{e}_i = 0, i \neq j$ and $\bar{e}_i^T \bar{e}_i = I_{V_i}$, so that

$$\begin{aligned} \langle \bar{e}_i^T u, v_i \rangle_{V_i} &= \langle \bar{e}_i^T u, \bar{e}_i^T \bar{e}_i v_i \rangle_{V_i} \\ &= \sum_{j \in \mathcal{I}} \langle \bar{e}_j^T u, \bar{e}_j^T \bar{e}_i v_i \rangle_{V_i} \\ &= \langle u, \bar{e}_i v_i \rangle_{\mathcal{B}}, \end{aligned}$$

implies that \bar{e}_i^T is indeed the adjoint of \bar{e}_i . Consequently we obtain

$$\Phi = \sum_{i \in \mathcal{I}} e_i \bar{e}_i^T$$

and therefore its Hilbert space adjoint $\Phi^T : V \rightarrow \mathcal{B}$ is

$$\Phi^T = \sum_{i \in \mathcal{I}} \bar{e}_i e_i^T,$$

where $e_i^T : V \rightarrow V_i$ is the Hilbert space adjoint of e_i . To compute it, use the Riesz isomorphism

$$\iota : V \rightarrow V^*$$

and the usual duality relationships to obtain

$$e_i^T = Q_i e_i^* \iota,$$

where $e_i^* : V^* \rightarrow V_i^*$ is the dual adjoint projection. Consequently we obtain

$$\begin{aligned} \Phi \Phi^T &= \sum_{j \in \mathcal{I}} e_j \bar{e}_j^T \sum_{i \in \mathcal{I}} \bar{e}_i e_i^T \\ &= \sum_{i, j \in \mathcal{I}} e_j \bar{e}_j^T \bar{e}_i e_i^T \\ &= \sum_{i \in \mathcal{I}} e_i e_i^T \\ &= \sum_{i \in \mathcal{I}} e_i Q_i e_i^* \iota, \end{aligned}$$

and therefore defining

$$S := \sum_{i \in \mathcal{I}} e_i Q_i e_i^*$$

it follows that

$$\Phi \Phi^T = S \iota.$$

Since $\Phi \Phi^T$ and ι are invertible, S is invertible. The invertibility of S implies both assertions regarding norms and their duality follows in a straightforward way from the definition of the dual norm. For the Hilbert space version see, e.g., [26, Prop. 11.4].

9.3 Proof of Theorem 2.3

We use the notations and results in the proof of Lemma 2.2. The assumption $V = \sum_i V_i$ implies that the information map $\Phi : \mathcal{B} \rightarrow V$ defined by

$$\Phi(u) = \sum_{i \in \mathcal{I}} u_i, \quad u = (u_i \in V_i)_{i \in \mathcal{I}},$$

is surjective. Consequently, Lemma 2.1 asserts that the minimizer of (2.5) is $w^* = \Psi(v) := \Phi^- v$, where the Moore-Penrose inverse $\Phi^- := \Phi^T(\Phi\Phi^T)^{-1}$ of Φ is well defined, with $\Phi^T : V \rightarrow \mathcal{B}$ being the Hilbert space adjoint to $\Phi : \mathcal{B} \rightarrow V$. The proof of Lemma 2.2 obtained $\Phi\Phi^T = S\iota$ where $S := \sum_{i \in \mathcal{I}} e_i Q_i e_i^*$ and $\iota : V \rightarrow V^*$ is the Riesz isomorphism, $e_i^T = Q_i e_i^* \iota$, where $e_i^T : V \rightarrow V_i$ is the Hilbert space adjoint of e_i and $e_i^* : V^* \rightarrow V_i^*$ is its dual space adjoint, and $\Phi^T = \sum_{i \in \mathcal{I}} \bar{e}_i e_i^T$, where $\bar{e}_i : V_i \rightarrow \mathcal{B}$ denotes the component injection $\bar{e}_i v_i := (0, \dots, 0, v_i, 0, \dots, 0)$.

Therefore, since $(\Phi\Phi^T)^{-1} = \iota^{-1} S^{-1}$, we obtain $\Phi^- = \sum_{i \in \mathcal{I}} \bar{e}_i Q_i e_i^* \iota^{-1} S^{-1}$, which amounts to

$$\Phi^- = \sum_{i \in \mathcal{I}} \bar{e}_i Q_i e_i^* S^{-1}, \quad (9.4)$$

or in coordinates

$$(\Phi^- v)_i = Q_i e_i^* S^{-1} v, \quad i \in \mathcal{I},$$

establishing the first assertion. The second follows from the general property $\Phi\Phi^- = \Phi\Phi^T(\Phi\Phi^T)^{-1} = I$ of the Moore-Penrose inverse. The first isometry assertion follows from

$$\begin{aligned} \|\Phi^- v\|_{\mathcal{B}}^2 &= \sum_{i \in \mathcal{I}} \|(\Phi^- v)_i\|_{V_i}^2 \\ &= \sum_{i \in \mathcal{I}} \|Q_i e_i^* S^{-1} v\|_{V_i}^2 \\ &= \sum_{i \in \mathcal{I}} [Q_i^{-1} Q_i e_i^* S^{-1} v, Q_i e_i^* S^{-1} v] \\ &= \sum_{i \in \mathcal{I}} [e_i^* S^{-1} v, Q_i e_i^* S^{-1} v] \\ &= \sum_{i \in \mathcal{I}} [S^{-1} v, e_i Q_i e_i^* S^{-1} v] \\ &= [S^{-1} v, \sum_{i \in \mathcal{I}} e_i Q_i e_i^* S^{-1} v] \\ &= [S^{-1} v, S S^{-1} v] \\ &= [S^{-1} v, v] \\ &= \|v\|_{S^{-1}}^2 \end{aligned}$$

for $v \in V$.

For the second, write $\Phi = \sum_{i \in \mathcal{I}} e_i \bar{e}_i^T$ and consider its dual space adjoint $\Phi : V^* \rightarrow \mathcal{B}^*$ defined by

$$\Phi^* = \sum_{i \in \mathcal{I}} \bar{e}_i^{T,*} e_i^*.$$

A straightforward calculation shows that $\bar{e}_i^{T,*} : V_i^* \rightarrow \mathcal{B}^*$ is the component injection into the product $\mathcal{B}^* = \prod_{i \in \mathcal{I}} V_i^*$. Consequently, we obtain

$$\bar{e}_i^T Q \bar{e}_j^{T,*} = \delta_{i,j} Q_j, \quad i, j \in \mathcal{I},$$

so that

$$\Phi Q \Phi^* = \sum_{i \in \mathcal{I}} e_i \bar{e}_i^T Q \sum_{j \in \mathcal{I}} \bar{e}_j^{T,*} e_j^* = \sum_{i,j \in \mathcal{I}} e_i \bar{e}_i^T Q \bar{e}_j^{T,*} e_j^* = \sum_{i \in \mathcal{I}} e_i Q_i e_i^* = S,$$

and since, for $\phi \in V^*$,

$$\|\Phi^* \phi\|_{\mathcal{B}^*}^2 = \langle \Phi^* \phi, \Phi^* \phi \rangle_{\mathcal{B}^*} = [\Phi^* \phi, Q \Phi^* \phi] = [\phi, \Phi Q \Phi^* \phi] = [\phi, S \phi] = \|\phi\|_S^2$$

it follows that Φ^* is an isometry.

9.4 Proof of Theorem 2.4

Use the Riesz isomorphism between V and V^* to represent the dual space adjoint $\Phi^* : V^* \rightarrow \mathcal{B}^*$ of $\Phi : \mathcal{B} \rightarrow V$ as $\Phi^* : V \rightarrow \mathcal{B}^*$. It follows from the definition of the Hilbert space adjoint $\Phi^T : V \rightarrow \mathcal{B}$ that

$$[\Phi^* v, b] = \langle v, \Phi b \rangle = \langle \Phi^T v, b \rangle_{\mathcal{B}}.$$

Since $Q : \mathcal{B}^* \rightarrow \mathcal{B}$ (2.11) defines the \mathcal{B} inner product through

$$\langle b_1, b_2 \rangle_{\mathcal{B}} = [Q^{-1} b_1, b_2], \quad b_1, b_2 \in \mathcal{B}$$

it follows that $[\Phi^* v, b] = \langle Q \Phi^* v, b \rangle_{\mathcal{B}}$ and therefore $\langle Q \Phi^* v, b \rangle_{\mathcal{B}} = \langle \Phi^T v, b \rangle_{\mathcal{B}}, v \in V, b \in \mathcal{B}$, so we conclude that

$$\Phi^T = Q \Phi^*.$$

Since Theorem 2.3 demonstrated that Ψ is the Moore-Penrose inverse Φ^- which implies that $\Psi \circ \Phi$ is the orthogonal projection onto $\text{Im}(\Phi^T)$ it follows that $\Psi \circ \Phi(u) \in \text{Im}(\Phi^T)$. However, the identity $\Phi^T = Q \Phi^*$ implies that $\text{Im}(\Phi^T) = Q \text{Im}(\Phi^*)$ so that we obtain the first part

$$\|u - \Psi(\Phi(u))\|_{\mathcal{B}} = \inf_{\phi \in V^*} \|u - Q \Phi^*(\phi)\|_{\mathcal{B}}$$

of the assertion. The second half follows from the definition (2.6) of $\|\cdot\|_{\mathcal{B}}$.

9.5 Proof of Proposition 3.1

Restating the assertion using the injections $e_i : V_i \rightarrow V$, our objective is establish that

$$E(i) = \text{Var}([\phi, e_i \xi_i]) = \text{Var}(\langle e_i \xi_i, v \rangle_{S^{-1}}).$$

Since $[\phi, e_i \xi_i] = [e_i^* \phi, \xi_i]$ it follows that $[\phi, e_i \xi_i] \sim \mathcal{N}(0, [e_i^* \phi, Q_i e_i^* \phi])$ so that $\text{Var}([\phi, e_i \xi_i]) = [e_i^* \phi, Q_i e_i^* \phi]$, which using $\phi = S^{-1}v$ becomes

$$\text{Var}([\phi, e_i \xi_i]) = [S^{-1}v, e_i Q_i e_i^* S^{-1}v].$$

On the other hand, the definitions (3.1) of $E(i)$, (2.7) of $\|\cdot\|_{V_i}$, and Theorem 2.3 imply that

$$\begin{aligned} E(i) &:= \|\Psi_i(v)\|_{V_i}^2 \\ &= [Q_i^{-1} \Psi_i(v), \Psi_i(v)] \\ &= [Q_i^{-1} Q_i e_i^* S^{-1}v, Q_i e_i^* S^{-1}v] \\ &= [e_i^* S^{-1}v, Q_i e_i^* S^{-1}v] \\ &= [S^{-1}v, e_i Q_i e_i^* S^{-1}v], \end{aligned}$$

so that we conclude the first part $E(i) = \text{Var}([\phi, e_i \xi_i])$ of the assertion. Since $[\phi, e_i \xi_i] = [S^{-1}v, e_i \xi_i] = \langle v, e_i \xi_i \rangle_{S^{-1}}$ we obtain the second.

9.6 Proof of Theorem 3.4

Fix $1 \leq k < r \leq q$. To apply Theorem 2.3, we select $\mathcal{B} := \mathcal{B}^{(k)}$ and $V := \mathcal{B}^{(r)}$ and endow them with the external direct sum vector space structure of products of vector spaces. Since the information operator $\Phi^{(r,k)} : \mathcal{B}^{(k)} \rightarrow \mathcal{B}^{(r)}$ defined in (3.9) is diagonal with components $\Phi_j^{(r,k)} : \mathcal{B}_j^{(k)} \rightarrow V_j^{(r)}, j \in \mathcal{I}^{(r)}$ and the norm on $\mathcal{B}^{(k)} = \prod_{i \in \mathcal{I}^{(r)}} \mathcal{B}_i^{(k)}$ is the product norm $\|u\|_{\prod_{i \in \mathcal{I}^{(r)}} \mathcal{B}_i^{(k)}}^2 = \sum_{i \in \mathcal{I}^{(r)}} \|u_i\|_{\mathcal{B}_i^{(k)}}^2, u = (u_i)_{i \in \mathcal{I}^{(r)}}$, it follows from the variational characterization of Lemma 2.1, the diagonal nature of the information map $\Phi^{(r,k)}$ and the product metric structure on $\mathcal{B}^{(k)}$ that the optimal recovery solution $\Psi^{(k,r)}$ is the diagonal operator with components the optimal solution operators corresponding to the component information maps $\Phi_j^{(r,k)} : \mathcal{B}_j^{(k)} \rightarrow V_j^{(r)}, j \in \mathcal{I}^{(r)}$. Since each component (3.8) of the observation operator is

$$\Phi_j^{(r,k)}(u) := \sum_{i \in j^{(k)}} u_i, \quad u \in \mathcal{B}_j^{(k)}$$

it follows that the appropriate subspaces of $V_j^{(r)}$ are

$$V_i^{(k)} \subset V_j^{(r)}, \quad i \in j^{(k)}.$$

Moreover, Condition 3.3 and the semigroup nature of the hierarchy of subspace embeddings implies that

$$e_{j,i}^{(k+2,k)} = \sum_{l \in j^{(k+1)}} e_{j,l}^{(k+2,k+1)} e_{l,i}^{(k+1,k)}, \quad i \in j^{(k)},$$

where the sum, despite its appearance, is over one term, and by induction we can establish that assumption (3.19) implies that

$$Q_j^{(r)} = \sum_{i \in j^{(k)}} e_{j,i}^{(r,k)} Q_i^{(k)} e_{i,j}^{(k,r)}, \quad j \in \mathcal{I}^{(r)}. \quad (9.5)$$

Utilizing the adjoint $e_{i,j}^{(k,r)} : V_j^{(r),*} \rightarrow V_i^{(k),*}$ (3.13) to the subspace embedding $e_{j,i}^{(r,k)} : V_i^{(k)} \rightarrow V_j^{(r)}$, it now follows from Theorem 2.3 and (9.5) that these component optimal solution maps $\Psi_j^{(k,r)} : V_j^{(r)} \rightarrow \mathcal{B}_j^{(k)}$ are those assumed in the theorem in (3.14) and (3.15) as

$$\Psi_j^{(k,r)}(v_j) := (Q_i^{(k)} e_{i,j}^{(k,r)} Q_j^{(r),-1} v_j)_{i \in j^{(k)}}, \quad v_j \in V_j^{(r)}. \quad (9.6)$$

The first three assertions for each component j then follow from Theorem 2.3, thus establishing the first three assertions in full.

For the semigroup assertions, Condition 3.3 implies that, for $k < r < s$ and $l \in \mathcal{I}^{(s)}$, there is a one to one relationship between $\{j \in l^{(r)}, i \in j^{(k)}\}$ and $\{i \in l^{(k)}\}$. Consequently, the definition (3.9) of $\Phi^{(r,k)}$ implies

$$\Phi^{(s,r)} \circ \Phi^{(r,k)}(u) = \left(\sum_{j \in l^{(r)}} \left(\sum_{i \in j^{(k)}} u_i \right) \right)_{l \in \mathcal{I}^{(s)}} = \left(\sum_{i \in l^{(k)}} u_i \right)_{l \in \mathcal{I}^{(s)}} = \Phi^{(s,k)}(u),$$

establishing the fourth assertion $\Phi^{(s,k)} = \Phi^{(s,r)} \circ \Phi^{(r,k)}$.

For the fifth, the definition (3.16) of $\Psi^{(k,r)}$ implies that

$$\begin{aligned} \Psi^{(k,r)} \circ \Psi^{(r,s)}(v) &= (Q_i^{(k)} e_{i,j}^{(k,r)} Q_j^{(r),-1} \Psi_j^{(r,s)}(v))_{i \in j^{(k)}} \\ &= (Q_i^{(k)} e_{i,j}^{(k,r)} Q_j^{(r),-1} Q_j^{(r)} e_{j,l}^{(r,s)} Q_l^{(s),-1} v_l)_{i \in j^{(k)}} \\ &= (Q_i^{(k)} e_{i,j}^{(k,r)} e_{j,l}^{(r,s)} Q_l^{(s),-1} v_l)_{i \in j^{(k)}} \\ &= (Q_i^{(k)} e_{i,l}^{(k,s)} Q_l^{(s),-1} v_l)_{i \in l^{(k)}} \\ &= \Psi^{(k,s)}(v), \end{aligned}$$

establishing $\Psi^{(k,s)} = \Psi^{(k,r)} \circ \Psi^{(r,s)}$.

The last assertion follows directly from the second and the fifth.

9.7 Proof of Theorem 3.6

Since $\xi^{(k)} : \mathcal{B}^{(k),*} \rightarrow \mathbf{H}$ is an isometry to a Gaussian space of real variables we can abuse notation and write $\xi^{(k)}(b^*) = [b^*, \xi^{(k)}]$ which emphasizes the interpretation of $\xi^{(k)}$ as a weak $\mathcal{B}^{(k)}$ -valued random variable. Since, by Theorem 3.4

$$\Phi^{(k,1),*} : (\mathcal{B}^{(k),*}, \|\cdot\|_{\mathcal{B}^{(k),*}}) \rightarrow (\mathcal{B}^{(1),*}, \|\cdot\|_{\mathcal{B}^{(1),*}}) \text{ is an isometry} \quad (9.7)$$

and $\xi^{(1)} : \mathcal{B}^{(1),*} \rightarrow \mathbf{H}$ is an isometry, it follows that

$$\Phi^{(k,1)}\xi^{(1)} := \xi^{(1)} \circ \Phi^{(k,1),*} : \mathcal{B}^{(k),*} \rightarrow \mathbf{H}$$

is an isometry, and therefore a Gaussian field on $\mathcal{B}^{(k)}$. Since Gaussian fields transform like Gaussian measures with respect to continuous linear transformations, we obtain that $\xi^{(1)} \sim \mathcal{N}(0, Q^1)$ implies that

$$\Phi^{(k,1)}\xi^{(1)} \sim \mathcal{N}(0, \Phi^{(k,1)}Q^1\Phi^{(k,1),*}),$$

but the isometric nature (9.7) of $\Phi^{(k,1),*}$ implies that

$$\Phi^{(k,1)}Q^{(1)}\Phi^{(k,1),*} = Q^{(k)},$$

so we conclude that

$$\Phi^{(k,1)}\xi^{(1)} \sim \mathcal{N}(0, Q^k)$$

thus establishing the assertion that $\xi^{(k)}$ is distributed as $\Phi^{(k,1)}\xi^{(1)}$.

The conditional expectation $\mathbb{E}[\xi^{(k)} \mid \Phi^{(r,k)}(\xi^{(k)})]$ is uniquely characterized by its field of conditional expectations $\mathbb{E}[[b^*, \xi^{(k)}] \mid \Phi^{(r,k)}(\xi^{(k)})], b^* \in \mathcal{B}^{(k),*}$ which because of the linearity of conditional expectation of Gaussian random variables appears as

$$\mathbb{E}[[b^*, \xi^{(k)}] \mid \Phi^{(r,k)}(\xi^{(k)})] = [A_{b^*}, \Phi^{(r,k)}(\xi^{(k)})]$$

for some $A_{b^*} \in V^*$. Furthermore, the Gaussian conditioning also implies that the dependence of A_{b^*} on b^* is linear so we write $A_{b^*} = Ab^*$ for some $A : \mathcal{B}^* \rightarrow V^*$, thereby obtaining

$$\mathbb{E}[[b^*, \xi^{(k)}] \mid \Phi^{(r,k)}(\xi^{(k)})] = [Ab^*, \Phi^{(r,k)}(\xi^{(k)})], \quad b^* \in \mathcal{B}^{(k),*}. \quad (9.8)$$

Using the well-known fact, see e.g. Dudley [5, Thm. 10.2.9], that the conditional expectation of a square integrable random variable on a probability space (Ω, Σ', P) with respect to a sub- σ -algebra $\Sigma' \subset \Sigma$ is the orthogonal projection onto the closed subspace $L^2(\Omega, \Sigma', P) \subset L^2(\Omega, \Sigma, P)$, it follows that the conditional expectation satisfies

$$\mathbb{E}([(b^*, \xi^{(k)}) - [Ab^*, \Phi^{(r,k)}(\xi^{(k)})][v^*, \Phi^{(r,k)}(\xi^{(k)})]) = 0, \quad b^* \in \mathcal{B}^{(k),*}, v^* \in V^{(k),*}.$$

Rewriting this as

$$\mathbb{E}([(b^*, \xi^{(k)}) - [\Phi^{(r,k),*}Ab^*, \xi^{(k)}]][\Phi^{(r,k),*}v^*, \xi^{(k)}]) = 0, \quad b^* \in \mathcal{B}^{(k),*}, v^* \in V^{(k),*},$$

we obtain

$$\begin{aligned} [b^*, Q^{(k)}\Phi^{(r,k),*}v^*] &= [\Phi^{(r,k),*}Ab^*, Q^{(k)}\Phi^{(r,k),*}v^*] \\ &= [b^*, A^*\Phi^{(r,k)}Q^{(k)}\Phi^{(r,k),*}v^*] \end{aligned}$$

for all $b^* \in \mathcal{B}^{(k),*}$ and $v^* \in V^{(k),*}$, and so conclude that

$$A^*\Phi^{(r,k)}Q^{(k)}\Phi^{(r,k),*}v^* = Q^{(k)}\Phi^{(r,k),*}v^*, \quad b^* \in \mathcal{B}^{(k),*}, v^* \in V^{(k),*}$$

which implies that

$$A^* \Phi^{(r,k)} b = b, \quad b \in \text{Im}(Q^{(k)} \Phi^{(r,k),*}). \quad (9.9)$$

Since

$$\begin{aligned} \langle \Phi^{(r,k),T} b^{(r)}, b^{(k)} \rangle_{\mathcal{B}^{(k)}} &= \langle b^{(r)}, \Phi^{(r,k)} b^{(k)} \rangle_{\mathcal{B}^{(k)}} \\ &= [Q^{(k),-1} b^{(r)}, \Phi^{(r,k)} b^{(k)}] \\ &= [\Phi^{(r,k),*} Q^{(k),-1} b^{(r)}, b^{(k)}] \\ &= [Q^{(r),-1} Q^{(r)} \Phi^{(r,k),*} Q^{(k),-1} b^{(r)}, b^{(k)}] \\ &= \langle Q^{(r)} \Phi^{(r,k),*} Q^{(k),-1} b^{(r)}, b^{(k)} \rangle_{\mathcal{B}^{(r)}}, \end{aligned}$$

we conclude that

$$\Phi^{(r,k),T} = Q^{(r)} \Phi^{(r,k),*} Q^{(k),-1},$$

and therefore

$$\text{Im}(Q^{(r)} \Phi^{(r,k),*}) = \text{Im}(\Phi^{(r,k),T}).$$

Consequently, (9.9) now reads

$$A^* \Phi^{(r,k)} b = b, \quad b \in \text{Im}(\Phi^{(r,k),T}). \quad (9.10)$$

Since clearly

$$A^* \Phi^{(r,k)} b = 0, \quad b \in \text{Ker}(\Phi^{(r,k)})$$

it follows that

$$A^* \Phi^{(r,k)} = P_{\text{Im}(\Phi^{(r,k),T})}$$

Since $P_{\text{Im}(\Phi^{(r,k),T})} = (\Phi^{(r,k)})^- \Phi^{(r,k)}$, the identity $\Phi^{(r,k)} (\Phi^{(r,k)})^- = I$ establishes that

$$A^* = (\Phi^{(r,k)})^-$$

Since (9.8) implies that

$$\mathbb{E}[[b^*, \xi^{(k)}] | \Phi^{(r,k)}(\xi^{(k)})] = [b^*, A^* \Phi^{(r,k)}(\xi^{(k)})], \quad b^* \in \mathcal{B}^{(k),*},$$

which in turn implies that

$$\mathbb{E}[\xi^{(k)} | \Phi^{(r,k)}(\xi^{(k)})] = A^* \Phi^{(r,k)}(\xi^{(k)}),$$

we obtain

$$\mathbb{E}[\xi^{(k)} | \Phi^{(r,k)}(\xi^{(k)})] = (\Phi^{(r,k)})^- \Phi^{(r,k)}(\xi^{(k)}).$$

Since Theorem 2.3 established that the optimal solution operator $\Psi^{(k,r)}$ corresponding to the information map $\Phi^{(r,k)}$ was the Moore-Penrose inverse $\Psi^{(k,r)} = (\Phi^{(r,k)})^-$ we obtain

$$\mathbb{E}[\xi^{(k)} | \Phi^{(r,k)}(\xi^{(k)})] = \Psi^{(k,r)} \circ \Phi^{(r,k)}(\xi^{(k)}), \quad (9.11)$$

so that

$$\mathbb{E}[\xi^{(k)} | \Phi^{(r,k)}(\xi^{(k)}) = v] = \Psi^{(k,r)}(v),$$

thus establishing the final assertion. To establish the martingale property, let us define $\hat{\xi}^{(1)} := \xi^{(1)}$ and

$$\hat{\xi}^{(k)} := \mathbb{E}[\xi^{(1)} \mid \Phi^{(k,1)}(\xi^{(1)})], \quad k = 2, \dots$$

as a sequence of Gaussian fields all on the same space $\mathcal{B}^{(1)}$. (9.11) implies that

$$\hat{\xi}^{(k)} = \Psi^{(1,k)} \circ \Phi^{(k,1)}(\xi^{(1)}), \quad (9.12)$$

so that, the identities $\Phi^{(r,1)} = \Phi^{(r,k)} \circ \Phi^{(k,1)}$ and $\Phi^{(k,1)} \circ \Psi^{(1,k)} = I_{\mathcal{B}^{(1)}}$ from Theorem 3.4

$$\begin{aligned} \mathbb{E}[\hat{\xi}^{(k)} \mid \Phi^{(r,1)}(\hat{\xi}^{(k)})] &= \mathbb{E}[\Psi^{(1,k)} \circ \Phi^{(k,1)}(\hat{\xi}^{(1)}) \mid \Phi^{(r,1)} \circ \Psi^{(1,k)} \circ \Phi^{(k,1)}(\hat{\xi}^{(1)})] \\ &= \mathbb{E}[\Psi^{(1,k)} \circ \Phi^{(k,1)}(\hat{\xi}^{(1)}) \mid \Phi^{(r,k)} \circ \Phi^{(k,1)} \circ \Psi^{(1,k)} \circ \Phi^{(k,1)}(\hat{\xi}^{(1)})] \\ &= \mathbb{E}[\Psi^{(1,k)} \circ \Phi^{(k,1)}(\hat{\xi}^{(1)}) \mid \Phi^{(r,k)} \circ \Phi^{(k,1)}(\hat{\xi}^{(1)})] \\ &= \mathbb{E}[\Psi^{(1,k)} \circ \Phi^{(k,1)}(\hat{\xi}^{(1)}) \mid \Phi^{(r,1)}(\hat{\xi}^{(1)})] \\ &= \Psi^{(1,k)} \circ \Phi^{(k,1)} \mathbb{E}[\hat{\xi}^{(1)} \mid \Phi^{(r,1)}(\hat{\xi}^{(1)})] \\ &= \Psi^{(1,k)} \circ \Phi^{(k,1)} \hat{\xi}^{(r)} \\ &= \Psi^{(1,k)} \circ \Phi^{(k,1)} \Psi^{(1,r)} \circ \Phi^{(r,1)} \hat{\xi}^{(1)} \\ &= \Psi^{(1,k)} \circ \Phi^{(k,1)} \Psi^{(1,k)} \Psi^{(k,r)} \circ \Phi^{(r,1)} \hat{\xi}^{(1)} \\ &= \Psi^{(1,k)} \circ \Psi^{(k,r)} \circ \Phi^{(r,1)} \hat{\xi}^{(1)} \\ &= \Psi^{(1,r)} \circ \Phi^{(r,1)} \hat{\xi}^{(1)} \\ &= \hat{\xi}^{(r)}, \end{aligned}$$

that is $\hat{\xi}^{(k)}$ is a reverse martingale.

9.8 Proof of Theorem 5.1

Let us simplify for the moment and define a scaled wavelet

$$\bar{\chi}_{\tau,\omega,\theta}(t) := \omega^{\frac{1-\beta}{2}} \cos(\omega(t-\tau) + \theta) e^{-\frac{\omega^2(t-\tau)^2}{\alpha^2}}, \quad t \in \mathbb{R}, \quad (9.13)$$

so that at $\beta = 0$ we have

$$\chi_{\tau,\omega,\theta} = \left(\frac{2}{\pi^3 \alpha^2} \right)^{\frac{1}{4}} \bar{\chi}_{\tau,\omega,\theta}. \quad (9.14)$$

Since

$$\begin{aligned} K(s, t) &:= \int_{-\pi}^{\pi} \int_{\mathbb{R}_+} \int_{\mathbb{R}} \bar{\chi}_{\tau,\omega,\theta}(s) \bar{\chi}_{\tau,\omega,\theta}(t) d\tau d\omega d\theta \\ &= \int_{-\pi}^{\pi} \int_{\mathbb{R}_+} \int_{\mathbb{R}} \cos(\omega(s-\tau) + \theta) e^{-\frac{\omega^2(s-\tau)^2}{\alpha^2}} \cos(\omega(t-\tau) + \theta) e^{-\frac{\omega^2(t-\tau)^2}{\alpha^2}} d\tau \omega^{1-\beta} d\omega d\theta \\ &= \int_{-\pi}^{\pi} \int_{\mathbb{R}_+} \int_{\mathbb{R}} \cos(\omega(s-\tau) + \theta) \cos(\omega(t-\tau) + \theta) e^{-\frac{\omega^2(s-\tau)^2}{\alpha^2}} e^{-\frac{\omega^2(t-\tau)^2}{\alpha^2}} d\tau \omega^{1-\beta} d\omega d\theta \end{aligned}$$

the trigonometric identity

$$\begin{aligned} & \cos(\omega(s-\tau) + \theta) \cos(\omega(t-\tau) + \theta) \\ = & \left(\cos(\omega(s-\tau)) \cos \theta - \sin(\omega(s-\tau)) \sin \theta \right) \left(\cos(\omega(t-\tau)) \cos \theta - \sin(\omega(t-\tau)) \sin \theta \right) \end{aligned}$$

and the integral identities $\int_{-\pi}^{\pi} \cos^2 \theta d\theta = \int_{-\pi}^{\pi} \sin^2 \theta d\theta = \pi$ and $\int_{-\pi}^{\pi} \cos \theta \sin \theta d\theta = 0$ imply that

$$K(s, t) = \pi \int_{\mathbb{R}_+} \int_{\mathbb{R}} \left(\cos(\omega(s-\tau)) \cos(\omega(t-\tau)) + \sin(\omega(s-\tau)) \sin(\omega(t-\tau)) \right) e^{-\frac{\omega^2(s-\tau)^2}{\alpha^2}} e^{-\frac{\omega^2(t-\tau)^2}{\alpha^2}} d\tau \omega^{1-\beta} d\omega$$

so that the trigonometric identity $\cos(a-b) = \cos a \cos b + \sin a \sin b$ implies

$$K(s, t) = \pi \int_{\mathbb{R}_+} \int_{\mathbb{R}} \cos(\omega(s-t)) e^{-\frac{\omega^2(s-\tau)^2}{\alpha^2}} e^{-\frac{\omega^2(t-\tau)^2}{\alpha^2}} d\tau \omega^{1-\beta} d\omega$$

which amounts to

$$K(s, t) = \pi \Re \int_{\mathbb{R}_+} \int_{\mathbb{R}} e^{i\omega(s-t)} e^{-\frac{\omega^2(s-\tau)^2}{\alpha^2}} e^{-\frac{\omega^2(t-\tau)^2}{\alpha^2}} d\tau \omega^{1-\beta} d\omega. \quad (9.15)$$

Using the identity

$$e^{-\frac{\omega^2|s-\tau|^2}{\alpha^2}} e^{-\frac{\omega^2|t-\tau|^2}{\alpha^2}} = e^{-\frac{\omega^2}{\alpha^2}(2\tau^2 - 2(s+t)\tau)} e^{-\frac{\omega^2}{\alpha^2}(s^2+t^2)}$$

and the integral identity

$$\int e^{-a\tau^2 - 2b\tau} d\tau = \sqrt{\frac{\pi}{a}} e^{\frac{b^2}{a}}, \quad a > 0, b \in \mathbb{C}, \quad (9.16)$$

with the choice $a := \frac{2\omega^2}{\alpha^2}$ and $b := -\frac{\omega^2}{\alpha^2}(s+t)$, so that $b^2/a = \frac{\omega^2}{2\alpha^2}(s+t)^2$, we can evaluate the integral

$$\int e^{-\frac{\omega^2}{\alpha^2}(2\tau^2 - 2(s+t)\tau)} d\tau = \frac{\alpha}{\omega} \sqrt{\frac{\pi}{2}} e^{\frac{\omega^2}{2\alpha^2}(s+t)^2}.$$

Consequently,

$$\begin{aligned} K(s, t) &= \pi \Re \int e^{i\omega(s-t)} e^{-\frac{\omega^2|s-\tau|^2}{\alpha^2}} e^{-\frac{\omega^2|t-\tau|^2}{\alpha^2}} d\tau \omega^{1-\beta} d\omega \\ &= \pi \Re \int e^{i\omega(s-t)} e^{-\frac{\omega^2}{\alpha^2}(s^2+t^2)} e^{-\frac{\omega^2}{\alpha^2}(2\tau^2 - 2(s+t)\tau)} d\tau \omega^{1-\beta} d\omega \\ &= \pi \Re \int e^{i\omega(s-t)} e^{-\frac{\omega^2}{\alpha^2}(s^2+t^2)} \left(\int e^{-\frac{\omega^2}{\alpha^2}(2\tau^2 - 2(s+t)\tau)} d\tau \right) \omega^{1-\beta} d\omega \\ &= \alpha \sqrt{\frac{\pi^3}{2}} \Re \int e^{i\omega(s-t)} e^{-\frac{\omega^2}{\alpha^2}(s^2+t^2)} e^{\frac{\omega^2}{2\alpha^2}(s+t)^2} \omega^{-\beta} d\omega \\ &= \alpha \sqrt{\frac{\pi^3}{2}} \Re \int e^{i\omega(s-t)} e^{-\frac{\omega^2}{2\alpha^2}(s-t)^2} \omega^{-\beta} d\omega \\ &= \alpha \sqrt{\frac{\pi^3}{2}} \int \cos(\omega(s-t)) e^{-\frac{\omega^2}{2\alpha^2}(s-t)^2} \omega^{-\beta} d\omega, \end{aligned}$$

that is,

$$K(s, t) = \alpha \sqrt{\frac{\pi^3}{2}} \int \cos(\omega(s-t)) e^{-\frac{\omega^2}{2\alpha^2}(s-t)^2} \omega^{-\beta} d\omega. \quad (9.17)$$

Utilizing the integral identity

$$\int_0^\infty x^{\mu-1} e^{-p^2 x^2} \cos(ax) dx = \frac{1}{2} p^{-\mu} \Gamma\left(\frac{\mu}{2}\right) e^{-\frac{a^2}{4p^2}} {}_1F_1\left(-\frac{\mu}{2} + \frac{1}{2}, \frac{1}{2}; \frac{a^2}{4p^2}\right), \quad a > 0, \mu > 0, \quad (9.18)$$

from Gradshteyn and Ryzhik [10, 3.952:8], with

$$\frac{a^2}{4p^2} = \frac{\alpha^2}{2},$$

$p^2 = \frac{|s-t|^2}{2\alpha^2}$, $a := |s-t|$ and $\mu := 1-\beta$, we obtain

$$K(s, t) = \alpha \sqrt{\frac{\pi^3}{2}} \frac{1}{2} (\sqrt{2}\alpha)^{1-\beta} |s-t|^{\beta-1} \Gamma\left(\frac{1-\beta}{2}\right) e^{-\frac{\alpha^2}{2}} {}_1F_1\left(\frac{\beta}{2}, \frac{1}{2}; \frac{\alpha^2}{2}\right).$$

Consequently, reintroducing the scaling (9.14) obtains $K_u(s, t) = \left(\frac{2}{\pi^3 \alpha^2}\right)^{\frac{1}{2}} K(s, t)$ when $\beta = 0$. To indicate the dependence on β , we define

$$K_\beta(s, t) = \frac{1}{2} (\sqrt{2}\alpha)^{1-\beta} |s-t|^{\beta-1} \Gamma\left(\frac{1-\beta}{2}\right) e^{-\frac{\alpha^2}{2}} {}_1F_1\left(\frac{\beta}{2}, \frac{1}{2}; \frac{\alpha^2}{2}\right), \quad (9.19)$$

so that $K_u = K_0$. For fixed α , at the limit $\beta = 0$, we have, recalling that $\Gamma\left(\frac{1}{2}\right) = \sqrt{\pi}$,

$$K_0(s, t) = \frac{\sqrt{2\pi}}{2} \alpha |s-t|^{-1} e^{-\frac{\alpha^2}{2}} {}_1F_1\left(0, \frac{1}{2}; \frac{\alpha^2}{2}\right)$$

and since

$${}_1F_1\left(0, \frac{1}{2}; \frac{\alpha^2}{2}\right) = 1$$

we obtain

$$K_0(s, t) = \frac{\sqrt{2\pi}}{2} \alpha |s-t|^{-1} e^{-\frac{\alpha^2}{2}}.$$

The scaling constant $H(\beta)$ defined in the theorem satisfies

$$H(\beta) := \frac{1}{2} (\sqrt{2}\alpha)^{1-\beta} \Gamma\left(1 - \frac{\beta}{2}\right) e^{-\frac{\alpha^2}{2}} {}_1F_1\left(\frac{\beta}{2}, \frac{1}{2}; \frac{\alpha^2}{2}\right) \bar{H}(\beta)$$

with

$$\bar{H}(\beta) := 2^\beta \pi^{\frac{1}{2}} \frac{\Gamma\left(\frac{\beta}{2}\right)}{\Gamma\left(1 - \frac{\beta}{2}\right)}, \quad (9.20)$$

so that, by (9.19) we have

$$\frac{1}{H(\beta)} K_\beta(s, t) = \frac{|s - t|^{\beta-1}}{\bar{H}(\beta)}.$$

Therefore, if we let \mathcal{K}_β denote the integral operator

$$(\mathcal{K}_\beta f)(s) := \frac{1}{H(\beta)} \int_{\mathbb{R}} K_\beta(s, t) f(t) dt$$

associated to the kernel K_β scaled by $H(\beta)$, it follows that

$$(\mathcal{K}_\beta f)(s) : \frac{1}{\bar{H}(\beta)} \int_{\mathbb{R}} |s - t|^{\beta-1} f(t) dt,$$

namely that it is a scaled version of the integral operator $f \mapsto \int_{\mathbb{R}} |s - t|^{\beta-1} f(t) dt$ corresponding to the Riesz potential $|s - t|^{\beta-1}$. Consequently, according to Helgason [12, Lem. 5.4 & Prop. 5.5], this scaling of the Riesz potential by $\bar{H}(\beta)$ implies the assertions of the theorem.

9.9 Proof of Lemma 6.1

The outer most integral in the definition (6.1) of K_β is

$$\begin{aligned} \int_{-\pi}^{\pi} y(\omega(s - \tau) + \theta) y^*(\omega(t - \tau) + \theta) d\theta &= \int_{-\pi}^{\pi} \sum_{-N}^N c_n e^{in(\omega(s - \tau) + \theta)} \sum_{-N}^N c_m^* e^{-im(\omega(t - \tau) + \theta)} d\theta \\ &= \sum_{n=-N}^N \sum_{m=-N}^N e^{in\omega(s - \tau)} e^{-im\omega(t - \tau)} c_n c_m^* \int_{-\pi}^{\pi} e^{i(n - m)\theta} d\theta \\ &= 2\pi \sum_{n=-N}^N e^{in\omega(s - \tau)} e^{-in\omega(t - \tau)} |c_n|^2 \\ &= 2\pi \sum_{n=-N}^N e^{in\omega(s - t)} |c_n|^2 \end{aligned}$$

so that

$$K_\beta(s, t) = 2\pi \sum_{n=-N}^N K_n(s, t) |c_n|^2$$

where

$$\begin{aligned}
K_n(s, t) &= \Re \int e^{in\omega(s-t)} e^{-\frac{\omega^2|s-\tau|^2}{\alpha^2}} e^{-\frac{\omega^2|t-\tau|^2}{\alpha^2}} d\tau \omega^{1-\beta} d\omega \\
&= \Re \int e^{in\omega(s-t)} e^{-\frac{\omega^2}{\alpha^2}(s^2+t^2)} e^{-\frac{\omega^2}{\alpha^2}(2\tau^2-2(s+t)\tau)} d\tau \omega^{1-\beta} d\omega \\
&= \Re \int e^{in\omega(s-t)} e^{-\frac{\omega^2}{\alpha^2}(s^2+t^2)} \left(\int e^{-\frac{\omega^2}{\alpha^2}(2\tau^2-2(s+t)\tau)} d\tau \right) \omega^{1-\beta} d\omega \\
&= \alpha \sqrt{\frac{\pi}{2}} \Re \int e^{in\omega(s-t)} e^{-\frac{\omega^2}{\alpha^2}(s^2+t^2)} e^{\frac{\omega^2}{2\alpha^2}(s+t)^2} \omega^{-\beta} d\omega \\
&= \alpha \sqrt{\frac{\pi}{2}} \Re \int e^{in\omega(s-t)} e^{-\frac{\omega^2}{2\alpha^2}(s-t)^2} \omega^{-\beta} d\omega \\
&= \alpha \sqrt{\frac{\pi}{2}} \int \cos(n\omega(s-t)) e^{-\frac{\omega^2}{2\alpha^2}(s-t)^2} \omega^{-\beta} d\omega.
\end{aligned}$$

Consequently, using the integral identity (9.18) with $a = |n||s-t|$, $\mu = 1 - \beta$, $p^2 = \frac{|s-t|^2}{2\alpha^2}$, and therefore $\frac{a^2}{4p^2} = \frac{|n|\alpha^2}{2}$ and $p = \frac{|s-t|}{\sqrt{2}\alpha}$ we conclude that

$$K_n(s, t) = \frac{\alpha\sqrt{\pi}}{2\sqrt{2}} (\sqrt{2}\alpha)^{1-\beta} |s-t|^{\beta-1} \Gamma\left(\frac{1-\beta}{2}\right) e^{-\frac{|n|\alpha^2}{2}} {}_1F_1\left(\frac{\beta}{2}; \frac{1}{2}; \frac{|n|\alpha^2}{2}\right),$$

which does not appear to have a nice dependency on n , except for $\beta = 0$, where

$${}_1F_1\left(0; \frac{1}{2}; \frac{|n|\alpha^2}{2}\right) = 1$$

and $\Gamma(\frac{1}{2}) = \sqrt{\pi}$, so that

$$K_n(s, t) = \frac{1}{2} \alpha^2 \pi e^{-\frac{|n|\alpha^2}{2}} |s-t|^{-1}$$

and therefore

$$K_0(s, t) = \alpha^2 \pi^2 \|y\|^2 |s-t|^{-1},$$

when written in terms of the norm $\|y\|^2 := \sum_{n=-N}^N e^{-\frac{|n|\alpha^2}{2}} |c_n|^2$.

9.10 Proof of Lemma 6.2

For $\gamma > 0$, let us evaluate the function

$$\phi(s) := \sum_{n=-\infty}^{\infty} e^{-|n|\gamma} e^{ins} \tag{9.21}$$

with Fourier coefficients $\hat{\phi}(n) = e^{-|n|\gamma}$. Since

$$\begin{aligned}
\phi(s) &= \sum_{n=-\infty}^{\infty} e^{-|n|\gamma} e^{ins} \\
&= \sum_{n=1}^{\infty} e^{-n\gamma} e^{ins} + 1 + \sum_{n=-\infty}^{-1} e^{n\gamma} e^{ins} \\
&= \sum_{n=1}^{\infty} e^{-n\gamma} e^{ins} + 1 + \sum_{n=1}^{\infty} e^{-n\gamma} e^{-ins} \\
&= 1 + 2 \sum_{n=1}^{\infty} e^{-n\gamma} \cos(ns),
\end{aligned}$$

the identity

$$1 + 2 \sum_{n=1}^{\infty} e^{-n\gamma} \cos ns = \frac{\sinh(\gamma)}{\cosh(\gamma) - \cos(s)} \quad (9.22)$$

of Gradshteyn and Ryzhik [10, 1.461:2] implies that

$$\phi(s) = \frac{\sinh(\gamma)}{\cosh(\gamma) - \cos(s)}.$$

Consequently, with the choice $\gamma := \frac{\alpha^2}{4}$ in (9.21), that is for

$$\phi(s) := \sum_{n=-\infty}^{\infty} e^{-|n|\frac{\alpha^2}{4}} e^{ins}$$

we find that

$$\phi(s) = \frac{\sinh(\frac{\alpha^2}{4})}{\cosh(\frac{\alpha^2}{4}) - \cos(s)}. \quad (9.23)$$

We will need two basic facts about the Fourier transform of 2π -periodic functions, see e.g. Katznelson [18, Sec. I]. If we denote the Fourier transform by $\hat{f}(n) := \frac{1}{2\pi} \int_{-\pi}^{\pi} f(s) e^{-ins}$, $\forall n$, the convolution theorem states that for periodic functions $f, g \in L^1[-\pi, \pi]$ that the convolution $(f \star g)(s) := \frac{1}{2\pi} \int_{-\pi}^{\pi} f(s-t)g(t)dt$ is a well defined periodic function in $L^1[-\pi, \pi]$ and that $(f \hat{\star} g)(n) = \hat{f}(n)\hat{g}(n)$, $\forall n$. Moreover, for square integrable 2π -periodic functions in $L^2[-\pi, \pi]$, the Parseval identity is $\sum_{n=-\infty}^{\infty} |\hat{f}(n)|^2 = \frac{1}{2\pi} \int_0^{2\pi} |f(s)|^2$.

Consequently, observing that $c_n = 0$, $n < -N, n > N$, the Parseval identity and the

convolution formula imply that

$$\begin{aligned}
\|y\|^2 &= \sum_{n=-N}^N e^{-\frac{|n|\alpha^2}{2}} |c_n|^2 \\
&= \|(e^{-\frac{|n|\alpha^2}{4}} c_n)_{n=-\infty}^{\infty}\|_{\ell^2}^2 \\
&= \|(\hat{\phi}\hat{y})_{n=-\infty}^{\infty}\|_{\ell^2}^2 \\
&= \|(\phi \star \hat{y})_{n=-\infty}^{\infty}\|_{\ell^2}^2 \\
&= \|\phi \star y\|_{L^2[-\pi,\pi]}^2 \\
&= \int |\phi \star y|^2 \\
&= \int \left| \int \phi(s-t)y(t)dt \right|^2 ds \\
&= \int \left(\int \phi(s-t)y(t)dt \int \phi(s-t')y^*(t')dt' \right) ds \\
&= \int \int \phi(s-t)y(t)\phi(s-t')y^*(t')dt dt' ds \\
&= \int G(t,t')y(t)y^*(t')dt dt',
\end{aligned}$$

that is,

$$\|y\|^2 = \int G(t,t')y(t)y^*(t')dt dt'$$

where

$$G(t,t') := \int \phi(s-t)\phi(s-t')ds \quad (9.24)$$

with

$$\phi(s) = \frac{\sinh(\frac{\alpha^2}{4})}{\cosh(\frac{\alpha^2}{4}) - \cos(s)}. \quad (9.25)$$

We can evaluate G using the identity (9.22) as follows: Since

$$\begin{aligned}
G(t,t') &= \int \phi(s-t)\phi(s-t')ds \\
&= \int \left(1 + 2 \sum_{n=1}^{\infty} e^{-n\frac{\alpha^2}{4}} \cos n(s-t)\right) \left(1 + 2 \sum_{n'=1}^{\infty} e^{-n'\frac{\alpha^2}{4}} \cos n'(s-t')\right) ds,
\end{aligned}$$

and, for each product, we have

$$\begin{aligned}
&\int \cos n(s-t) \cos n'(s-t')ds \\
&= \int (\cos ns \cos nt - \sin ns \sin nt) (\cos n's \cos n't' - \sin n's \sin n't') ds \\
&= \delta_{n,n'} \int (\cos ns \cos nt - \sin ns \sin nt) (\cos ns \cos nt' - \sin ns \sin nt') ds,
\end{aligned}$$

using the L^2 -orthogonality of the cosines and the sines and the identities $\int \cos^2 ns = \pi$ and $\int \sin^2 ns = \pi$, we conclude that

$$\begin{aligned} \int (\cos ns \cos nt - \sin ns \sin nt) (\cos ns \cos nt' - \sin ns \sin nt') ds &= \pi (\cos nt \cos nt' + \sin nt \sin nt') \\ &= \pi \cos n(t - t') \end{aligned}$$

and therefore

$$\int \cos n(s - t) \cos n'(s - t') ds = \pi \delta_{n,n'} \cos n(t - t'). \quad (9.26)$$

Consequently, we obtain

$$\begin{aligned} G(t, t') &= \int \left(1 + 2 \sum_{n=1}^{\infty} e^{-n \frac{\alpha^2}{4}} \cos n(s - t)\right) \left(1 + 2 \sum_{n'=1}^{\infty} e^{-n' \frac{\alpha^2}{4}} \cos n'(s - t')\right) ds \\ &= \int \left(1 + 4 \sum_{n=1}^{\infty} e^{-n \frac{\alpha^2}{2}} \cos n(s - t) \cos n(s - t')\right) ds \\ &= 2\pi + 4\pi \sum_{n=1}^{\infty} e^{-n \frac{\alpha^2}{2}} \cos n(t - t') \end{aligned}$$

and therefore, using the identity (9.22) again, we conclude

$$G(t, t') = 2\pi \frac{\sinh(\frac{\alpha^2}{2})}{\cosh(\frac{\alpha^2}{2}) - \cos(t - t')}.$$

Acknowledgments The authors gratefully acknowledge support by the Air Force Office of Scientific Research under award number FA9550-18-1-0271 (Games for Computation and Learning).

References

- [1] V. Adam, J. Hensman, and M. Sahani. Scalable transformed additive signal decomposition by non-conjugate Gaussian process inference. In *2016 IEEE 26th International Workshop on Machine Learning for Signal Processing (MLSP)*, pages 1–6. IEEE, 2016.
- [2] J. C. A. Barata and M. S. Hussein. The Moore–Penrose pseudoinverse: A tutorial review of the theory. *Brazilian Journal of Physics*, 42(1-2):146–165, 2012.
- [3] I. Daubechies, J. Lu, and H.-T. Wu. Synchrosqueezed wavelet transforms: An empirical mode decomposition-like tool. *Applied and Computational Harmonic Analysis*, 30(2):243–261, 2011.
- [4] K. Dragomiretskiy and D. Zosso. Variational mode decomposition. *IEEE Transactions on Signal Processing*, 62(3):531–544, 2014.

- [5] R. M. Dudley. *Real Analysis and Probability*, volume 74 of *Cambridge Studies in Advanced Mathematics*. Cambridge University Press, Cambridge, 2002. Revised reprint of the 1989 original.
- [6] N. Durrande, D. Ginsbourger, and O. Roustant. Additive covariance kernels for high-dimensional Gaussian process modeling. In *Annales de la Faculté des sciences de Toulouse: Mathématiques*, volume 21, pages 481–499, 2012.
- [7] N. Durrande, J. Hensman, M. Rattray, and N. D. Lawrence. Gaussian process models for periodicity detection. *PeerJ Computer Science*, 2016.
- [8] D. K. Duvenaud, H. Nickisch, and C. E. Rasmussen. Additive Gaussian processes. In *Advances in Neural Information Processing Systems*, pages 226–234, 2011.
- [9] D. Gabor. Theory of communication. part 1: The analysis of information. *Journal of the Institution of Electrical Engineers-Part III: Radio and Communication Engineering*, 93(26):429–441, 1946.
- [10] I. S. Gradshteyn and I. M. Ryzhik. *Table of Integrals, Series, and Products 6th edn* (San Diego, CA: Academic). 2000.
- [11] T. J. Hastie and R. J. Tibshirani. *Generalized Additive Models*, volume 43 of *Monographs on Statistics and Applied Probability*. Chapman and Hall, Ltd., London, 1990.
- [12] S. Helgason. *The Radon Transform*, volume 2. Springer, 1999.
- [13] T. Y. Hou and Z. Shi. Adaptive data analysis via sparse time-frequency representation. *Advances in Adaptive Data Analysis*, 3(01n02):1–28, 2011.
- [14] T. Y. Hou, Z. Shi, and P. Tavallali. Sparse time frequency representations and dynamical systems. *Communications in Mathematical Sciences*, 13(3):673–694, 2015.
- [15] N. E. Huang. *Hilbert-Huang Transform and its Applications*, volume 16. World Scientific, 2014.
- [16] N. E. Huang, Z. Shen, S. R. Long, M. C. Wu, H. H. Shih, Q. Zheng, N.-C. Yen, C. C. Tung, and H. H. Liu. The empirical mode decomposition and the Hilbert spectrum for nonlinear and non-stationary time series analysis. *Proceedings of the Royal Society of London. Series A: Mathematical, Physical and Engineering Sciences*, 454(1971):903–995, 1998.
- [17] M. Hutson. AI researchers allege that machine learning is alchemy. *Science*, 360(6388):861, 2018.
- [18] Y. Katznelson. *An Introduction to Harmonic Analysis*. Cambridge University Press, 2004.

- [19] Y. LeCun, Y. Bengio, and G. Hinton. Deep learning. *Nature*, 521(7553):436–444, 2015.
- [20] C.-Y. Lin, L. Su, and H.-T. Wu. Wave-shape function analysis. *Journal of Fourier Analysis and Applications*, 24(2):451–505, 2018.
- [21] A. Liutkus, R. Badeau, and G. Richard. Gaussian processes for underdetermined source separation. *IEEE Transactions on Signal Processing*, 59(7):3155–3167, 2011.
- [22] S. Maji, A. C. Berg, and J. Malik. Efficient classification for additive kernel SVMs. *IEEE Transactions on Pattern Analysis and Machine Intelligence*, 35:66–77, 2013.
- [23] G. J. McLachlan, S. X. Lee, and S. I. Rathnayake. Finite mixture models. *Annual Review of Statistics and its Application*, 6:355–378, 2019.
- [24] C. A. Micchelli and T. J. Rivlin. A survey of optimal recovery. In *Optimal Estimation in Approximation Theory*, pages 1–54. Springer, 1977.
- [25] H. Owhadi. Multigrid with rough coefficients and multiresolution operator decomposition from hierarchical information games. *SIAM Review*, 59(1):99–149, 2017.
- [26] H. Owhadi and C. Scovel. *Operator Adapted Wavelets, Fast Solvers, and Numerical Homogenization, from a game theoretic approach to numerical approximation and algorithm design*. Cambridge Monographs on Applied and Computational Mathematics. Cambridge University Press, 2019.
- [27] H. Owhadi, C. Scovel, and F. Schäfer. Statistical numerical approximation. *Notices of the AMS*, 2019.
- [28] S. Park and S. Choi. Gaussian processes for source separation. In *2008 IEEE International Conference on Acoustics, Speech and Signal Processing*, pages 1909–1912. IEEE, 2008.
- [29] A. B. Patel, M. T. Nguyen, and R. Baraniuk. A probabilistic framework for deep learning. In *Advances in Neural Information Processing Systems*, pages 2558–2566, 2016.
- [30] T. A. Plate. Accuracy versus interpretability in flexible modeling: Implementing a tradeoff using gaussian process models. *Behaviormetrika*, 26(1):29–50, 1999.
- [31] M. M. Rao. *Foundations of Stochastic Analysis*. Academic Press, 1981.
- [32] F. Schäfer, T. J. Sullivan, and H. Owhadi. Compression, inversion, and approximate PCA of dense kernel matrices at near-linear computational complexity. *arXiv:1706.02205*, 2017.
- [33] I. Steinwart and A. Christmann. *Support Vector Machines*. Springer Science & Business Media, 2008.

- [34] C. J. Stone. Additive regression and other nonparametric models. *The Annals of Statistics*, 13(2):689–705, 1985.
- [35] K. Yosida. *Functional Analysis*. Springer-Verlag, Berlin, 5th edition, 1978.